

# TABLE OF CONTENTS

<b>DECLARATION OF ORIGINALITY</b>	<b>iii</b>
<b>DEDICATION</b>	<b>v</b>
<b>ABSTRACT</b>	<b>vii</b>
<b>ACKNOWLEDGEMENTS</b>	<b>ix</b>
<b>TABLE OF CONTENTS</b>	<b>xi</b>
<b>LIST OF FIGURES</b>	<b>xiv</b>
<b>LIST OF TABLES</b>	<b>xvi</b>
<b>LIST OF ABBREVIATIONS AND SYMBOLS</b>	<b>xvii</b>
<b>CHAPTER 1: INTRODUCTION</b>	<b>1</b>
<b>CHAPTER 2: LITERATURE REVIEW</b>	<b>5</b>
<b>2.1 Interaction between lasers and human tissue</b>	<b>5</b>
<b>2.2 Human skin</b>	<b>6</b>
2.2.1 Epidermis	7
2.2.1.1 Stratum corneum	7
2.2.1.2 Living epidermis	7
2.2.1.2.1 Melanin	8
2.2.1.2.2 Fitzpatrick skin tone classification	9
2.2.2 Dermis	10
<b>2.3 Optical properties</b>	<b>10</b>
2.3.1 Descriptions and definitions	11
2.3.1.1 Refractive index	12
2.3.1.2 Reflection and refraction at an interface	12
2.3.1.3 Absorption	13
2.3.1.4 Scattering	14
2.3.1.5 Anisotropy	15
2.3.1.6 Reduced scattering coefficient	16
2.3.2 Values for the optical properties of skin	17
<b>2.4 Measurement techniques</b>	<b>19</b>
2.4.1 Integrating sphere	19

2.4.2	Diffuse reflectance probe	20
<b>2.5</b>	<b>Skin simulating phantoms</b>	<b>21</b>
2.5.1	Liquid phantoms	22
2.5.2	Solid phantoms	22
<b>2.6</b>	<b>Light propagation models</b>	<b>23</b>
2.6.1	Radiative Transport equation	23
2.6.1.1	Diffusion approximation	24
2.6.1.2	Monte Carlo simulations	24
2.6.2	Raytracing models	26
<b>2.7</b>	<b>Cancer and photodynamic therapy</b>	<b>27</b>
2.7.1	Photodynamic therapy (PDT)	27
2.7.1.1	Photodynamic interaction mechanism	28
<b>2.8</b>	<b>Synthesis</b>	<b>29</b>
 <b>CHAPTER 3: DEVELOPMENT OF A LASER FLUENCE RATE PREDICTION MODEL</b>		 <b>33</b>
<b>3.1</b>	<b>ASAP raytracing software</b>	<b>33</b>
<b>3.2</b>	<b>Layered skin model</b>	<b>34</b>
3.2.1	Geometrical layout	34
3.2.2	Light source	35
3.2.3	Ray tracing - Monte Carlo approach	35
3.2.4	Henye-Greenstein approximation	36
3.2.5	Evaluations	36
<b>3.3</b>	<b>Non-planar epidermal/dermal interface</b>	<b>38</b>
<b>3.4</b>	<b>Experimental verification and validation of the computer model</b>	<b>39</b>
<b>3.5</b>	<b>Paper on the experimental validation of the computer model</b>	<b>41</b>
<b>3.6</b>	<b>Contribution of the computer model to the work</b>	<b>51</b>
 <b>CHAPTER 4: THE ROLE OF EPIDERMAL ABSORPTION COEFFICIENTS APPLICABLE TO THE SOUTH AFRICAN POPULATION</b>		 <b>53</b>
<b>4.1</b>	<b>Diffuse reflectance theory and model development</b>	<b>53</b>
<b>4.2</b>	<b>Probe calibration</b>	<b>58</b>
4.2.1	Paper on Reflectance probe calibration	60
<b>4.3</b>	<b>Contribution of the diffuse reflectance probe calibration to the work</b>	<b>71</b>
<b>4.4</b>	<b><i>In vivo</i> tests</b>	<b>71</b>
4.4.1	Paper on <i>in vivo</i> tests	74

4.5	Value of the diffuse reflectance probe measurements	85
<b>CHAPTER 5: EFFECT OF THE OPTICAL PROPERTIES OF THE EPIDERMIS ON LASER TREATMENT PARAMETERS</b>		<b>87</b>
5.1	Paper on the Effect of the epidermis on laser treatment parameters	89
5.2	Value of the epidermal absorption work	98
<b>CHAPTER 6: CONCLUSIONS AND WAY FORWARD</b>		<b>99</b>
6.1	Brief summary of the major findings and contributions of the work in the thesis	99
6.2	Objectives set out and their achievement	99
6.2.1	Objective 1: To develop a computer model that can predict the laser fluence rate some distance into skin.	100
6.2.2	Objective 2: To develop a non-invasive optical measurement technique to determine the epidermal absorption coefficient of an individual.	100
6.2.3	Objective 3: To determine the effect of skin phototype on the absorption of laser light in the epidermis.	100
6.3	Limitations of the work	101
6.4	Further investigations identified	102
6.5	Contributions of the work to the scientific community and the wider public	102
6.5.1	Contribution to the scientific community	102
6.5.2	Contribution to the wider public	103
6.6	Conclusions	103
<b>REFERENCES</b>		<b>105</b>
<b>APPENDIX 1: ETHICS CLEARANCE - CSIR</b>		<b>113</b>
<b>APPENDIX II: ETHICS CLEARANCE - UNIVERSITY OF PRETORIA</b>		<b>114</b>
<b>APPENDIX III: SOURCE CODE FOR THE ASAP COMPUTER MODEL</b>		<b>115</b>

# LIST OF FIGURES

Figure 2.1: Relation between total exposure and exposure time for different modes of laser-tissue interaction (with permission from (Peng Q, 2008)).	6
Figure 2.2: Relation between fluence rate and exposure time for different modes of laser-tissue interaction (with permission from (Peng Q, 2008)).	6
Figure 2.3: Structure of the human skin.	7
Figure 2.4: Extinction coefficient as a function of wavelength for both of eumelanin and pheomelanin (data from (Jacques S, 2001)).	9
Figure 2.5: Fitzpatrick skin tone colour card.	10
Figure 2.6: Absorption coefficient as a function of wavelength for oxyhaemoglobin and deoxyhaemoglobin (data from (Prahl S, 1999)).	11
Figure 2.7: Snell's law.	12
Figure 2.8: Wavelength dependence of the major biological absorbers (from tabulated data (Jacques SL, 1998(a)), (Prahl S, 1999)).	14
Figure 2.9: Scattering from typical cellular structures (as adapted from (Jacques SL, 1998(a))).	15
Figure 2.10: Similarity principle where photons taking different paths arrive at the same end point.	17
Figure 2.11: Integrating sphere system for reflection (R) and transmission (T) measurements.	19
Figure 2.12: Absorption and scattering in skin.	21
Figure 2.13: Schematics of an experimental setup for the diffuse reflectance probe measurements.	21
Figure 2.14: Random walk of 15 photons.	25
Figure 2.15: Random walk of 3.1 million photons.	25
Figure 2.16: Energy level diagram for a Type 2 photosensitiser.	28
Figure 3.1: Layered structure of the computer model with the laser beam entering the outer layer.	35
Figure 3.2: Schematic of the computer model with the detectors and the different layers.	37
Figure 3.3: Typical OCT image of skin recorded at the NLC with a Thorlabs OCT system.	38
Figure 3.4: Wavy epidermis/dermis interface 0.12 mm into the skin with a wave amplitude of 0.05 mm and length of 0.6 mm.	38
Figure 3.5: Transmission through the resin without the addition of absorbers and scatterers.	40
Figure 3.6: Absorption spectrum of the black ink used in the experiments.	40
Figure 3.7: Schematic of the cuvettes for the Intralapid phantoms.	44
Figure 3.8: Integrating sphere system for reflection and transmission measurements.	45
Figure 3.9: Side view of the computer model of a two-layered solid phantom. The semi-sphere back reflector detector as well as the circular detector plate is visible.	46
Figure 3.10: Experimental setup: S (Sample), L (Lens $f=150\text{mm}$ , $D=50.8\text{mm}$ ), CCD (Camera), PC (Computer), $u$ (Object distance = 450 mm), $v$ (Image distance = 225 mm), F= filters, $M(v/u)=0.5$ , HeNe Laser power = 9 mW.	48
Figure 3.11(a): Fluence rate contour plots from the CCD images of the back surface of the liquid phantoms.	49
Figure 3.11(b): Fluence rate contour plots from the calculated fluence rate through the last layer in the IL phantom model.	49
Figure 4.1: Diffuse reflected light.	54
Figure 4.2: Comparing the two different melanin models for three volunteers each representing a different skin phototype. Model A2 only uses a single melanin parameter and model D2 uses both eumelanin and pheomelanin. Solid lines (—) represent the experimental data and the dashed lines (---) the fitted curve.	57
Figure 4.3: Comparison of input values to the fitted values for two different test cases. Solid lines (—) represent the input data and the dashed lines (---) the fitted curve.	57

Figure 4.4: Experimental setup for calibration and <i>in vivo</i> tests. ....	59
Figure 4.5: Absorption and scattering in skin. ....	62
Figure 4.6: Experimental setup. ....	62
Figure 4.7(a): Calibration data - Absorbance as function of the wavelength for the different OD filters. ....	67
Figure 4.7(b): Calibration data - $\mu_a$ values extracted from the DRP measurements compared to the true $\mu_a$ values (measured using the beer Lambert law) of the ink phantoms. ....	67
Figure 4.8(a): Reflectance probe measurement as a function of $\mu'_s$ at $\lambda=676$ nm when only IL was used ( $\mu_a = 0$ ). ....	68
Figure 4.8(b): Reflectance probe measurement as a function of $\mu_a$ at a $\lambda=676$ nm for three different $\mu'_s$ solutions. ....	68
Figure 4.9(a): Reflectance probe measurements on three individuals with skin phototype II, IV and V. Three measurements were taken on both the lower outer arm (sun exposed) and the inner upper arm (not sun exposed). ....	69
Figure 4.9(b): Absorption coefficient values calculated from the reflection probe measurements for three different skin phototypes at wavelengths 633 nm and 676 nm on sun exposed (E) and non- exposed (N) parts of the arm. ....	69
Figure 4.10: Fitzpatrick skin tone colour card. ....	71
Figure 4.11: Absorption spectra of eumelanin and pheomelanin (data from (Jacques S, 2001)). ....	72
Figure 4.12: Reflectance measurements for two different skin phototypes. ....	74
Figure 4.13: Experimental setup with the main system components (Karsten A, 2012(b)). ....	76
Figure 4.14: Reflectance probe measurements on the inner arm as a function of wavelength for all volunteers. Line styles were used to group graphs with similar trends. ....	79
Figure 4.15(a): Absorption coefficients ( $\text{mm}^{-1}$ ) as calculated at a wavelength of 633 nm, for volunteers of skin phototypes I-III. The volunteer numbers are displayed on the X-axis. Sun-exposed value ( $0.084 \text{ mm}^{-1}$ ) for volunteer 18 is excluded from the graph for scaling purposes. ....	80
Figure 4.15(b): Absorption coefficients ( $\text{mm}^{-1}$ ) as calculated at a wavelength of 633 nm, for volunteers of skin phototypes IV-V. The volunteer numbers are displayed on the X-axis. The not exposed value ( $0.0075 \text{ mm}^{-1}$ ) for volunteer 15 is barely visible. ....	80
Figure 4.16 (a): Absorption coefficient as a function of wavelength for the lower absorbance volunteers. Measurements were done on the outer arm (sun-exposed). ....	81
Figure 4.16(b): Absorption coefficient as a function of wavelength for the higher absorbance volunteers. Measurements were done on the outer arm (sun-exposed). ....	81
Figure 5.1(a): Schematic of the computer model with the detectors and the different layers. ....	93
Figure 5.1(b): Structure of the un-even epidermis-dermis interface. ....	93
Figure 5.2 (a): Absorption of light in the first 100 $\mu\text{m}$ through the NBCC model for the different epidermal thicknesses. ....	94
Figure 5.2(b): Absorption of light in the first 100 $\mu\text{m}$ through the SCC model for the different epidermal thicknesses. ....	94
Figure 5.3(a): Fluence rate transmitted through the first 100 $\mu\text{m}$ of the NBCC model for the different epidermal thicknesses. ....	94
Figure 5.3(b): Fluence rate transmitted through the first 100 $\mu\text{m}$ of the SCC model for the different epidermal thicknesses. ....	94
Figure 5.4(a): Reflection measured on the reflection detector of the model for different epidermal thicknesses and a NBCC tumour. ....	95
Figure 5.4(b): Reflection measured on the reflection detector of the model for different epidermal thicknesses and a SCC tumour. ....	95

# LIST OF TABLES

Table 2.1: Fundamental optical properties of tissue. ....	11
Table 2.2: Transport properties. ....	11
Table 2.3: Comparison of optical properties measured in various laboratories. Note: most authors publish the data in units of $\text{cm}^{-1}$ and therefore this table uses $\text{cm}^{-1}$ but in the rest of this work units of $\text{mm}^{-1}$ are used (Table adapted from (Tuchin V, 2007)). ....	18
Table 3.1: Optical parameters used in the sawtooth model. ....	38
Table 3.2: Percentage of reflected light collected on the back reflection detector for the different sawtooth parameters described in Table 3.1 and the planar skin model with an epidermal thickness of 0.09 mm. ....	39
Table 3.3: Geometric parameters for the IL phantoms. ....	46
Table 3.4: Optical parameters for the IL phantoms used in the model. ....	46
Table 3.5: Optical parameters for the solid phantoms. Parameters for the A and B samples are given. Sample C used the $\mu_a$ and $\mu_s$ values from A and B respectively for the 2 layers in the phantom. ....	47
Table 3.6: Optimisation results showing the total absorption through the phantom, absorption in the last layer, the transmitted power and the standard deviation (Stdev) of the data. ....	47
Table 3.7: Comparisons between the model and measured values for the solid phantoms. ....	48
Table 3.8: Comparisons between the model and measured values for the liquid phantoms. ....	48
Table 4.1: Fitted parameters as compared to the input parameters into the algorithm. ....	57
Table 4.2: IL concentrations and corresponding $\mu'_s$ values at $\lambda = 632$ and $676$ nm. ....	65
Table 4.3: Ink sample and the $\mu'_s$ values calculated with the Beer-Lambert law using the transmission measurements. ....	65
Table 4.4: Comparison between the different methods to calculate $\mu_a$ for the neutral density absorbing filters at a wavelength of $676$ nm. ....	66
Table 4.5: Geometrical parameters ( $k_1$ and $k_2$ ), calculated from the reflectance measurements of the IL+ ink phantoms in Figures 4.8(a) and 4.8(b). ....	68
Table 4.6: Absorption coefficients calculated using the mean $k_1$ and $k_2$ values for the different skin types at wavelengths of $633$ nm and $676$ nm. ....	68
Table 4.7: Minimum and maximum $\mu_a$ and $\mu'_s$ values at wavelengths, $561$ , $633$ and $676$ nm. ....	81
Table 4.8: Absorption coefficients from literature using similar diffuse reflectance techniques (Reflectance) as well as an integrating sphere (IS). ....	82
Table 5.1: Geometrical dimensions for the planar surfaces and optical properties of the different layers in the skin model. ....	93
Table 5.2: % Light reflected from the model for the different wave interface parameters described above. ....	94
Table 5.3: Fraction of power reaching $100 \mu\text{m}$ into the skin, just entering the dermis for the SCC tumour. ....	95
Table 5.4: Fraction of power reaching the SCC tumour at a depth of $200 \mu\text{m}$ into the skin and the resulting treatment time to deliver a light dose of $4.5 \text{ J/cm}^2$ onto the tumour. The laser beam diameter is $1.3 \text{ cm}$ at the tumour depth. ....	96

## LIST OF ABBREVIATIONS AND SYMBOLS

ASAP	Advanced Systems Analysis Program
BCC	Basal Cell Carcinoma
$c$	Speed of light in vacuum
$c_d$	Scatter size parameter
$c_{Hb}$	Deoxyhaemoglobin concentration
$c_{HbO_2}$	Oxyhaemoglobin concentration
$c_{mel}$	Melanin concentration
$c_{Pheo}$	Pheomelanin concentration
$c_{Eu}$	Eumelanin concentration
CANSA	Cancer Association of South Africa
CW	Continuous Wave
$d, l$	Optical path length through the medium
$d_s$	Effective scatter size
DRP	Diffuse Reflectance Probe
$g$	Anisotropy
$I$	Laser intensity
$I_0$	Laser intensity before sample (initial laser intensity)
IL	Intralipid
IR	Infrared
IS	Integrating Sphere
MC	Monte Carlo
$n$	Refractive index
OCT	Optical Coherence Tomography
$p$	Henye-Greenstein scattering phase function
PCG	Preconditioned Conjugate Gradients
PDT	Photodynamic therapy
PS	Photosensitiser
$R_p$	Reflectance probe measurement
RSM	Realistic Skin Model
RTE	Radiative Transport Equation
SCC	Squamous Cell Carcinoma

$R_t$	Total diffuse reflection
$T_p$	Probability of ‘survival’ of a photon after a path length $l$
UV	Ultraviolet
$\alpha$	Oxygen saturation
$\epsilon_{HbO_2}$	Extinction coefficient for oxyhaemoglobin
$\epsilon_{Eu}$	Extinction coefficient for eumelanin
$\epsilon_{mel}$	Extinction coefficient for melanin
$\epsilon_{Pheo}$	Extinction coefficient for pheomelanin
$\lambda$	Wavelength
$\mu_a$	Absorption coefficient
$\mu_s$	Scattering coefficient
$\mu'_s$ with $\mu'_s = (1 - g)\mu_s$	Reduced scattering coefficient
$\mu_t$ with $\mu_t = \mu_s + \mu_a$	Total attenuation
$v$	Speed of light in medium
$\xi$	Random number between 0 and 1
$\rho_a$	Volume density of absorbers
$\rho_s$	Volume density of scatterers
$\sigma_a$	Effective absorption cross-sectional area
$\sigma_s$	Effective scattering cross-sectional area
$\phi$	Fluence rate

## CHAPTER 1: INTRODUCTION

For effective skin related treatment and diagnosis with lasers, the decline in laser fluence rate (due to scattering and absorption in the skin) needs to be quantified and compensated for. In the work presented here a simple multi-layer computer model was developed to predict the fluence rate at any pre-determined depth in the skin. The model was validated with experimental measurements on skin simulating phantoms.

Melanin in the epidermal layer of the skin is a major absorber of light in the visible and near infrared region. Due to the lack of data available on the epidermal absorption for different skin phototypes, measurements were done on 30 South African volunteers to establish the expected range of absorption coefficients for the South African population. The reduction in laser fluence rate due to the difference in absorption for the different skin phototypes was evaluated with the multi-layer computer model.

The discipline of biophotonics is an area where sub-fields of physics and biology meet. Biophotonics has become the term for techniques that deal with the interaction between photons and biological media (Vo-Dinh T, 2003) (p1-2). Photons are used to image, detect and manipulate biological materials. The applications of biophotonics allow researchers to see, measure, analyse and manipulate living tissues in ways that have not been possible before for both cellular and bulk tissue (IEEE, 2004), (Peng Q, 2008).

Human skin is considered to be a highly scattering (or turbid) medium for light in the visible and near infrared wavelength regions. Light dosimetry, the study of the irradiation of tissue for treatment purposes, is not yet as well understood as in the case of radiation therapy (Star WM, 1997). The optical properties of human skin and the laser light propagation within skin have been investigated by numerous researchers, (Whitton JT, 1973), (Anderson RR, 1981) (van Gemert MJC, 1989), (Graaff R, 1993), (Jacques S, 2001), (González FJ, 2010), (Doronin A, 2011). These properties are important as they determine the reduction in the laser fluence rate as it propagates through the tissue.

The optimal use of lasers as a treatment modality requires an understanding of the parameters involved in the process. Some of the primary parameters are the penetration depth of the laser light (determined by the optical properties of the tissue), the initial laser power and beam profile. In laser treatment, it is important to determine the fluence rate reaching a certain depth into the organ being treated in order to provide the correct laser irradiance dose ( $J/cm^2$ ). *In vivo* measurements to determine the fluence rate are seldom

practical. Computer modelling is one of the methods that provide a capability to predict the fluence rate at any given penetration depth into the tissue.

This work focuses on the way that laser light interacts with tissue and the absorption and scattering of the photons as they propagate through the tissue. Photodynamic therapy (PDT) has been used as an application for the computer model developed, to illustrate the effect of the epidermal absorption on the laser transmission through the skin. PDT is a cancer therapy where a photosensitiser (PS) is administered to a patient. The PS accumulates in the tumour and after a period of time the cancerous tumour is irradiated with a laser (Sekkat N, 2012). In order to deliver a therapeutically appropriate amount of laser power to a tumour embedded in the skin, it is important to understand the interaction of laser light with the tissue. In the literature review in Chapter 2, PDT will be discussed in more detail as an example to illustrate the practical application of the work.

The South African population consists of individuals of different ethnicity with a wide range in the skin colours or skin tones. In literature this is referred to as skin type or skin phototype and the standard classification used is the Fitzpatrick skin scale (Fitzpatrick TB, 1988). This scale classifies skin based on its reaction to sun (UV) exposure from skin phototype I (the lightest skin that will always burn due to sun exposure and only turn red and not turn brown) to skin phototype VI (the darkest skin that does not appear to be affected by sun exposure). The range of epidermal absorption coefficients for the different skin phototypes usually present in the South African population is not available in the literature. Measurements were done to determine the absorption coefficient of a small sample of the South African population to establish the typical range of absorption coefficients that may be expected in clinical settings in South Africa. Detailed measurements on a larger sample of the South African population should be conducted but this falls outside the scope of this work.

The continuous increase in medical applications of lasers both for treatment and diagnostic purposes (Peng Q, 2008), (Overton G, 2011) necessitate the ability to model the laser-tissue interaction mechanisms. A computer model was developed to predict the loss of laser light through some tissue layers in order to determine the fluence rate reaching the treatment site. The model was used to predict the fluence rate reaching a tumour 200  $\mu\text{m}$  into the skin for different skin phototypes.

The following objectives were set in this thesis:

1. To develop a computer model that can predict the laser fluence rate some distance into skin.

2. To develop a non-invasive optical measurement technique to determine the epidermal absorption coefficient of an individual.
3. To determine the effect of skin phototype on the absorption of laser light in the epidermis.

The remainder of the thesis is divided into six chapters:

- Chapter 2 - the literature review that addresses the background information required for this work.
- Chapters 3-5 are based on papers published on different aspects of the work. Each chapter consists of a short introduction and information additional to the paper, followed by the paper itself, as published.
  - Chapter 3 - the development of the computer model followed by the paper on the verification of the computer model and validation against optical parameters measured on skin simulating phantoms.
  - Chapter 4 - deals with the determination of the optical properties of human skin. This led to the development and calibration of a diffuse reflectance probe system and software to determine the epidermal absorption coefficient for the different South African skin phototypes. For this work ethics permission was obtained from both the CSIR (Ref 17/2011, Appendix I) and the University of Pretoria (EC110830-060, Appendix II) to do measurements on 30 volunteers.
  - Chapter 5 - the application of the computer model to the various South African skin phototypes. This chapter deals with the effect of both melanin concentration (different skin phototypes) and epidermal thickness on the loss of laser fluence rate through the outer skin layers in PDT treatment for skin cancer.
- Chapter 6 contains the conclusions and possible future work.
- Appendix I and II: Copies of the Ethics approvals.
- Appendix III: Source code of the laser-tissue interaction computer model.

## CHAPTER 2: LITERATURE REVIEW

The relevant aspects pertinent as background information will be discussed in this literature review which starts with a discussion of interaction modes of laser light with human tissue and in particular with human skin. Only the relevant skin layers are discussed. This is followed by optical properties applicable to the computer model. Some optical properties were not available in literature. Measurement techniques to determine them are discussed in subsequent sections. A computer model was developed to model the interaction of laser light with human skin. Several light propagation models are discussed briefly before the introduction of the computer model to predict laser fluence rate in the skin. The final section of this chapter provides a very brief summary of an application of the model, which is photodynamic treatment of cancer.

### 2.1 INTERACTION BETWEEN LASERS AND HUMAN TISSUE

In dealing with the interaction between laser light and human tissue the amount of laser light reaching the target area is of primary importance. The rate of energy delivered per unit area at a specific position is called the fluence rate ( $\text{W}/\text{cm}^2$ ) (Welch A, 2011) (p29) and is sometimes referred to as the exposure rate.

It should be noted that all the work in this thesis is based on continuous wave (CW) lasers and that the work concentrates on the macroscopic interaction of light with bulk tissue and does not focus on the cellular interaction.

Laser applications are often portrayed in the popular media as contradictory treatments e.g. enhancing wound healing versus surgical cutting of tissue or as a means of stimulating hair growth versus the removal of unwanted hair. These seemingly conflicting applications of the same technology are possible because of the variety of lasers which are available with a large range of wavelengths, output power or energy and appropriate choices of treatment time (Peng Q, 2008). The interaction of laser light with tissue can be broadly divided into six categories or interaction modes listed in order of increasing treatment times (Peng Q, 2008):

- Electro-mechanical (photochemical or photodisruptive) mode
- Ablation
- Vaporisation
- Coagulation or photothermal processes

- Photochemical (photodynamic) reactions
- Biostimulation and wound healing

The six interaction modes are illustrated in Figures 2.1 and 2.2 (Peng Q, 2008). In Figure 2.2 the fluence rate decreases as a function of increasing interaction time with the tissue and cells. In the high fluence rate applications, the treatment time is very short due to the high intensity of the laser light and the processes are usually destructive/disruptive in nature. For the longer exposure treatments, the fluence rate is much lower to prevent damage to the cells.

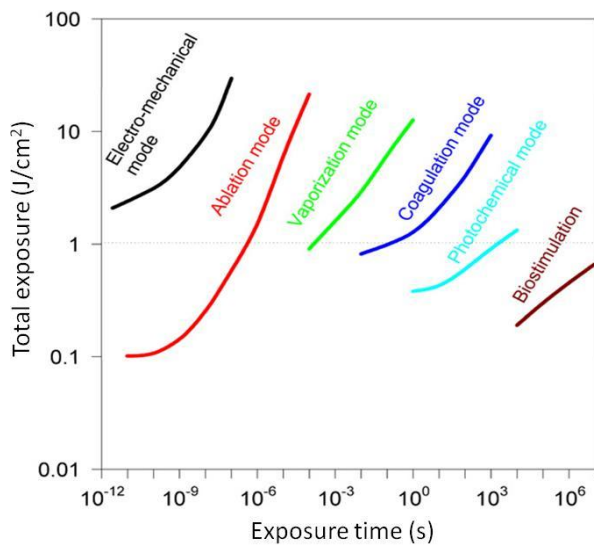


Figure 2.1: Relation between total exposure and exposure time for different modes of laser-tissue interaction (with permission from (Peng Q, 2008)).

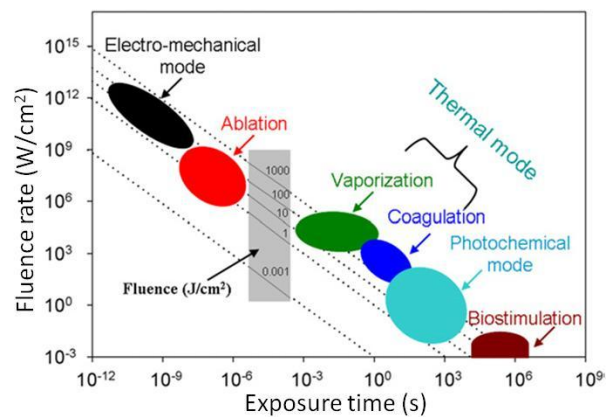


Figure 2.2: Relation between fluence rate and exposure time for different modes of laser-tissue interaction (with permission from (Peng Q, 2008)).

The last two interaction modes, namely photochemical reactions (with PDT as an example) and biostimulation (where penetration into tissue is required), are applicable for this thesis.

## 2.2 HUMAN SKIN

Human skin is the largest organ of the body, both in terms of volume and surface. The surface area of skin for the average adult is  $1.8 \text{ m}^2$  and the weight of the skin is on average 5 kg for males and 4.3 kg for females (Agache P, 2004). The human skin is a complex, heterogeneous medium with blood and pigment spatially distributed in the skin. (Bashkatov AN, 2005).

Skin is generally described as consisting of three main layers (as shown in Figure 2.3):

- The epidermis that is approximately  $100 \mu\text{m}$  thick and is blood free.

- The dermis that has blood vessels and is between 1 and 4 mm thick.
- The hypodermis which is a fatty layer consisting of subcutaneous fat and is between 1 and 6 mm thick.

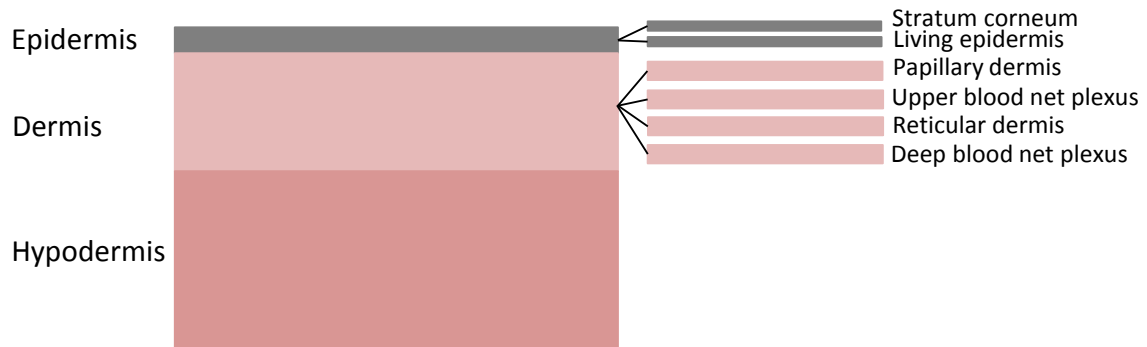


Figure 2.3: Structure of the human skin.

The aim of this thesis is to evaluate the effect of skin phototype on the transmission of light through skin. Only the epidermis has an influence on the skin phototype (see section 2.2.1.2.1 below) and therefore only the epidermis and the next layer, the dermis, will be discussed in more detail.

## 2.2.1 Epidermis

The epidermis can be divided into two sublayers (Bashkatov AN, 2005), the stratum corneum and the living epidermis.

### 2.2.1.1 Stratum corneum

The outer layer of the skin is the non-living epidermis, also called the stratum corneum, and is about 10-20  $\mu\text{m}$  thick with a refractive index of 1.55. It consists of dead squamous cells (Bashkatov AN, 2005), (Kollias N, 1995). These cells are highly keratinised with a high lipid and protein content but low water content (Bashkatov AN, 2005).

### 2.2.1.2 Living epidermis

The second layer is the living epidermis, hereafter referred to as the epidermis. This layer is about 100  $\mu\text{m}$  thick (approximately 10 cell layers) consisting of keratinocytes, melanocytes and Langerhans cells. This layer contains most of the skin pigmentation (i.e. melanin that is produced by the melanocytes) (Kollias N, 1995), (Bashkatov AN, 2005). According to Kollias (Kollias N, 1995) melanin is the major absorbing chromophore in the visible range. The refractive index of the epidermis is close to that of water (nominally 1.33 in the visible

wavelength range), therefore, only weak reflections is expected from the interface between the stratum corneum and the epidermis (Kollias N, 1995). Melanin in the epidermal layer is responsible for the skin colour or skin tone of an individual and impacts on the optical properties of the skin as discussed in section 2.3.

#### **2.2.1.2.1 Melanin**

Epidermal melanin can be broadly divided into two families, sulphur poor eumelanin (black-brown colour) and sulphur rich pheomelanin (yellow-reddish colour) (Yoon T, 2003), (Liu Y, 2005), (Costin GE, 2007). Darker coloured skins do not necessarily have more melanocytes than lighter coloured skins, but the melanocytes are more productive and produce more melanin (Störing M, 2004). Melanin in the skin is located in the melanosomes and consists of solid absorbing particles with a diameter between 20 and 40 nm. It is an optically dense material which absorbs light in the visible wavelength region. Melanin is not a single pigment, but consists of various chromophores each with their own optical and physical properties (Alaluf S, 2001). Both eumelanin and pheomelanin are forms of melanin that are synthesized within the melanosomes inside the melanocytes, located in the basal layer (or bottom layer) of the epidermis. The mature melanosomes get transferred via dendrites to the keratinocytes in the epidermis where they are responsible for skin pigmentation and photo-protection (Costin GE, 2007), (Fu D, 2008). A typical 'epidermal unit' consists of one melanocyte that is in contact with about 35-40 neighbouring keratinocytes. It is keratinocytes and fibroblast cells that actively regulate the melanocyte function with respect to cell growth, cell morphology and pigmentation (Yoon T, 2003). The typical extinction coefficients of the eumelanin and pheomelanin as a function of wavelength are shown in Figure 2.4.

The concentration of eumelanin and pheomelanin in an individual depends on both genetic and environmental factors (e.g. sun or UV light exposure). Sun exposed areas yield higher absorption coefficients than areas that are not usually exposed to sunlight.

Eumelanin provides better protection against solar radiation than pheomelanin (Agache P, 2004) (p475). In healthy, photo-exposed skin, the distribution of melanin depends on the exposure of the skin to UVA (315-400 nm) or UVB (290-315 nm) radiation. Exposure to UVB radiation increases the production of melanin and the transfer into keratinocytes. This leads to an increase in the concentration of melanin in the epidermis. UVA exposure increase the melanin in melanocytes and keratinocytes of the basal layer, but the melanin concentration in the rest of the epidermis remains unchanged (Agache P, 2004) (p473-474).

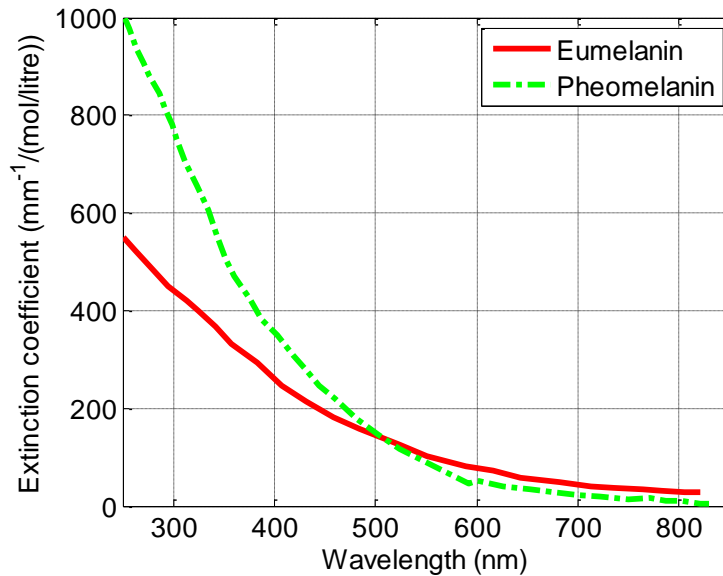


Figure 2.4: Extinction coefficient as a function of wavelength for both of eumelanin and pheomelanin (data from (Jacques S, 2001)).

It is generally believed that one of the major functions of melanin pigmentations is to shield the skin from harmful ultraviolet (UV) radiation (Fu D, 2008). In skin phototypes III to VI (see section 2.2.1.2.2 for the Fitzpatrick scale), the “melanosomes appear to be extensively melanised with solid melanin that has a high molecular weight” (Szabo G, 1969). The refractive index of the melanin is 1.65 (Kurtz SK, 1986), substantially higher than the refractive index of the surrounding medium typically between 1.4 and 1.5, and it is anticipated that the melanin granules may also be strong scatterers of light (Kollias N, 1995) resulting in a higher scattering coefficient. The relationship between melanin and skin absorbance remains a topic of research (Kollias N, 1995), (Alaluf S, 2002(b)), (Lanigan S, 2003), (Lepselter J, 2004), (Liu Y, 2005), (González FJ, 2010).

Even though not all the issues regarding melanin are well understood, it is clear that the melanin concentration impacts on the absorption of laser light in the epidermis and therefore influences the fluence rate available for treatment as will be discussed in Chapters 4 and 5.

### 2.2.1.2.2 Fitzpatrick skin tone classification

The standard classification for skin tone or skin phototype is the Fitzpatrick skin scale (Fitzpatrick TB, 1988). It is a scale that consists of only six colours to identify the phototype of an individual. This scale classifies skin based on its reaction to sun (UV) exposure and range from skin phototype I (the lightest skin that will always burn due to sun exposure and only turn red and not turn brown) to skin phototype VI (the darkest skin that does not appear

to be affected by sun exposure). A typical Fitzpatrick colour card is shown in Figure 2.5 (Baxamua BN, 2012).



Figure 2.5: Fitzpatrick skin tone colour card.

### 2.2.2 Dermis

According to Bashkatov (Bashkatov AN, 2005), the dermis can be subdivided into four layers:

- The papillary dermis (150  $\mu\text{m}$  thick).
- The upper blood net plexus (100  $\mu\text{m}$  thick).
- The reticular dermis (1-4 mm thick).
- The deep blood net plexus (100  $\mu\text{m}$  thick).

Even though the dermis can be subdivided into four layers the dermis will be treated as a single layer for the modelling work done later. This is a necessary assumption in order to simplify the model described later in Chapter 3.

The dermis is a vascularised layer with haemoglobin (blood), carotene and bilirubin the main absorbers in the visible region of the light spectrum (Bashkatov AN, 2005). Dermal collagen fibres are the major scatterers of visible light in the dermis, having a refractive index different from that of the surrounding dermis (Scheuplein RJ, 1964), (Kollias N, 1995).

Haemoglobin is the dominant chromophore in the dermis. It exists as either oxyhaemoglobin or deoxyhaemoglobin. In the visible wavelengths, the absorption spectra (Figure 2.6) of both states have characteristic maxima. Haemoglobin is confined to the blood vessels. The perceived redness of the skin is caused by the absorption of light by the haemoglobin in the capillaries and the upper superficial arteriolar and venular plexi. Therefore *ex vivo*, bloodless dermis appears very white (Kollias N, 1995).

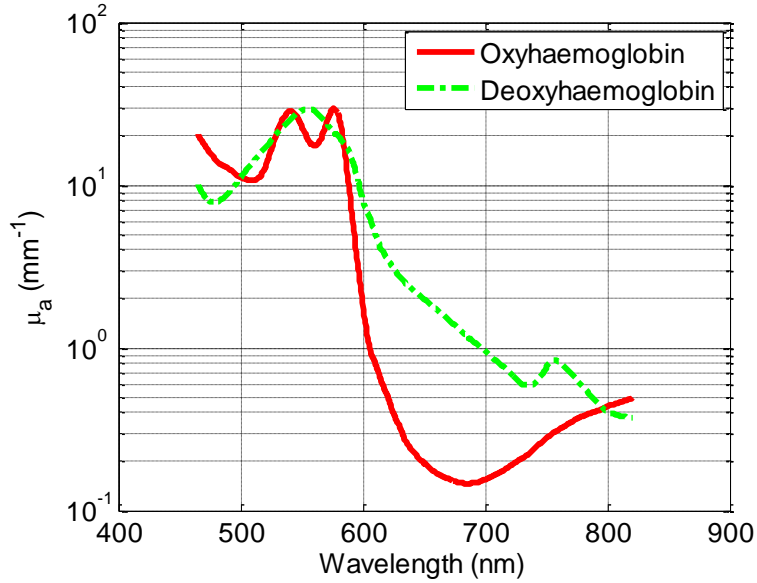


Figure 2.6: Absorption coefficient as a function of wavelength for oxyhaemoglobin and deoxyhaemoglobin (data from (Prahl S, 1999)).

## 2.3 OPTICAL PROPERTIES

In this section the optical properties of importance for this work will be introduced briefly.

### 2.3.1 Descriptions and definitions

In discussing the optical properties of tissue it is important to distinguish between the fundamental optical properties and the transport properties used in the modelling work (Jacques S, 2008(b)). The properties of the two groups are listed in Tables 2.1 and 2.2.

Table 2.1: Fundamental optical properties of tissue.

Quantity	Symbol	Units
Refractive index	$n$	dimensionless
Absorption coefficient	$\mu_a$	$\text{cm}^{-1}$
Scattering coefficient	$\mu_s$	$\text{cm}^{-1}$
Anisotropy of scatter	$g$	dimensionless

Table 2.2: Transport properties.

Quantity	Symbol	Units
Reduced scattering coefficient	$\mu'_s = (1 - g)\mu_s$	$\text{cm}^{-1}$
Transport mean free path	$MFP' = 1/(\mu_a + \mu'_s)$	cm

For this work it is assumed that the media under investigation are isotropic. This assumption simplifies the description of the fundamental properties without compromising the essential features of the phenomena. Three photo-physical properties are important to describe the propagation of light in biological tissue: refraction, scattering and absorption (Vo-Dinh T, 2003).

### 2.3.1.1 Refractive index

Refractive index is a fundamental property of homogenous media (Vo-Dinh T, 2003). In a homogeneous medium, the refractive index describes the linear optical properties of the medium. The ratio of the speed of an electromagnetic wave in vacuum to that in a specific medium is known as the absolute refractive index,  $n$ , for that medium and is given by (Hecht E, 1974) (p38):

$$n = \frac{c}{v} \quad (2.1)$$

with

$c$  = speed of light in vacuum

$v$  = speed of light in medium

Both the phase speed and the wavelength of the light depend on the refractive index, but the wave frequency and its photon energy ( $E = hv$ ) are always the same as in vacuum.

### 2.3.1.2 Reflection and refraction at an interface

Light propagates in a material/medium until it encounters a boundary with another material (or medium) with a different refractive index. At this point the direction of the light is changed. It will be partially reflected from the surface and refracted when entering the second medium. Snell's law (Eq. 2.2 and Figure 2.7) describes the relation between the incidence angle and the refraction angle (Vo-Dinh T, 2003).

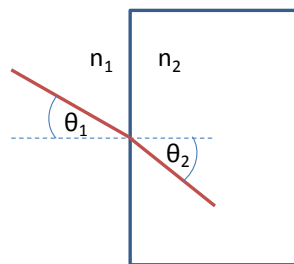


Figure 2.7: Snell's law.

$$n_1 \sin \theta_1 = n_2 \sin \theta_2 \quad (2.2)$$

with

$n_1$  = refractive index of medium 1

$n_2$  = refractive index of medium 2

For normal incidence onto a planar boundary, the fraction ( $T$ ) of the incident energy that is transmitted across the interface is given by:

$$T = \frac{4n_1n_2}{(n_1 + n_2)^2} \quad (2.3)$$

The fraction ( $R$ ) of the incident energy reflected from the surface (also known as Fresnell reflection) is given by:

$$R = 1 - T = \frac{(n_1 - n_2)^2}{(n_1 + n_2)^2} \quad (2.4)$$

The refractive index of the skin is important due to the changes in refractive index for the different skin layers. Mismatch of the refractive index at the surface of the tissue gives rise to specular reflection of the incident beam (Wilson BC, 1990). The photons that are specularly reflected do not enter the tissue to ‘probe’ the tissue but only provide information regarding the surface roughness and refractive index of the tissue (skin) (Wilson BC, 1990). Diffuse reflected photons that entered the skin provide information regarding the sub-surface skin layers as applied in the diffuse reflectance probe measurements discussed in Chapter 4.

### 2.3.1.3 Absorption

The major absorbing chromophores in skin are the blood, melanin and water. The absorption coefficient,  $\mu_a$ , of a medium containing many chromophores with a volume density,  $\rho_a$ , and an effective cross-sectional area,  $\sigma_a$ , is defined as (Jacques SL, 1998(a)), (Dam JS, 2000(b)):

$$\mu_a = \rho_a \sigma_a \quad (2.5)$$

[cm<sup>-1</sup>] [cm<sup>-3</sup>] [cm<sup>2</sup>]

The measurement unit of  $\mu_a$  usually used is cm<sup>-1</sup>, which is not an SI unit but quite practical. The probability of ‘survival’ of a photon ( $T_p$ ) after a path length,  $d$ , (or the transmission of a photon for a distance  $d$ ) is given by (Jacques SL, 1998(a)):

$$T_p = e^{-\mu_a d} \quad (2.6)$$

This expression is true regardless of whether the photon path is a straight line (ballistic photon) or if the photon was scattered numerous times in an optically turbid medium.

When a photon is detected at a specific position in the skin (or skin surface) it is not possible to determine which path the photon took to the end point. It could have moved to the position with one or two scattering events or in numerous scattering events. This is the so-called similarity principle and is illustrated later in Figure 2.10 in section 2.3.1.6.

Figure 2.8 shows the wavelength dependence of some of the major biological absorbers. The best penetration in skin is for wavelengths where the blood and melanin absorption are a

minimum and the absorption due to the water is still low. This gave rise to the term ‘optical and diagnostic window’ for the wavelength band between 600 and 1000 nm.

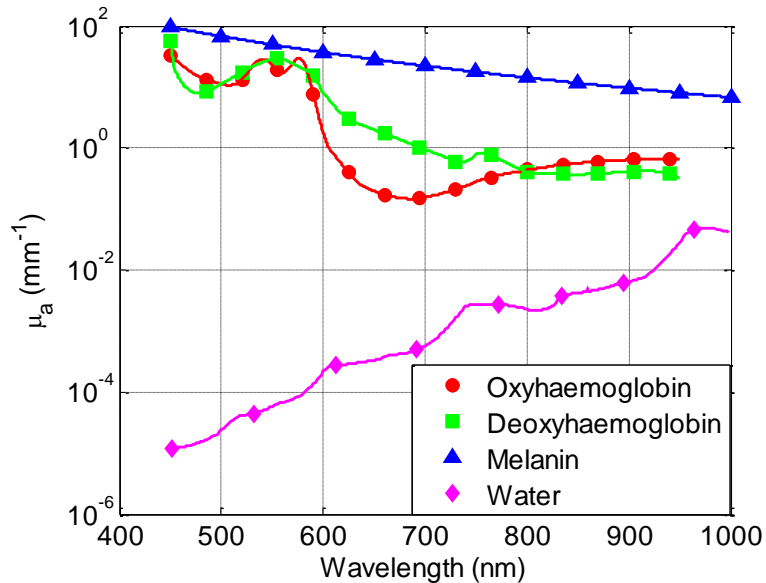


Figure 2.8: Wavelength dependence of the major biological absorbers (from tabulated data (Jacques SL, 1998(a)), (Prahl S, 1999)).

The Beer-Lambert law relates the transmission of light through a medium with the optical properties of the medium and can be written as:

$$I = I_0 e^{-\mu_a d} \quad (2.7)$$

with:

$I$  = measured laser intensity after the sample

$I_0$  = initial laser intensity

$d$  = optical path length through the medium

$\mu_a$  = absorption coefficient

### 2.3.1.4 Scattering

In biomedical optics, scattering processes are very important in both diagnostic and therapeutic applications. Scattering depends on the size, morphology and structure of the components in tissue (Vo-Dinh T, 2003). Mie theory describes the scattering of light by structures that are of the same size as the wavelength of the photon. Rayleigh scattering describes the scattering of light by structures that are much smaller than the photon wavelength. Figure 2.9 illustrates Mie and Rayleigh scattering of visible and infrared light by tissue structures. Most laser treatments are done in the visible and near infrared part of the light spectrum where the sub-cellular components scatter the light.

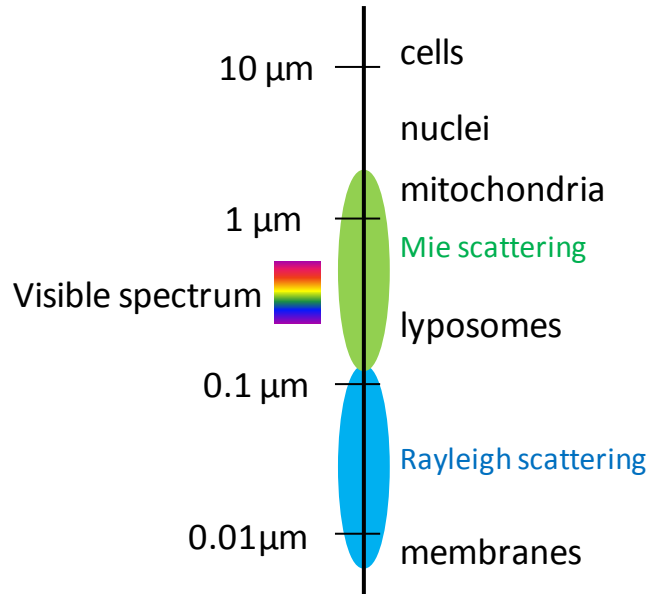


Figure 2.9: Scattering from typical cellular structures (as adapted from (Jacques SL, 1998(a))).

Scattering in tissue is generally caused by morphological variations in the tissue density and the refractive index (Welch A, 2011) (p46). Due to the scattering the light fluence rate  $\phi$  [ $\text{W}/\text{cm}^2$ ] just under the skin surface can be higher than the incident irradiance  $E_0$  [ $\text{W}/\text{cm}^2$ ] (Welch A, 2011) (p46). The increase in the fluence rate relative to the irradiance may in some cases be as high as a factor of five (Welch A, 2011).

Analogous to the absorption coefficient, the scattering coefficient ( $\mu_s$ ) can be defined as (Jacques SL, 1998(a)), (Dam JS, 2000(b)):

$$\mu_s = \rho_s \sigma_s \quad (2.8)$$

$[\text{cm}^{-1}] \quad [\text{cm}^{-3}] \quad [\text{cm}^2]$

with:

$\rho_s$  = volume density of scatterers

$\sigma_s$  = effective cross-sectional area of the scatterers

### 2.3.1.5 Anisotropy

The anisotropy,  $g$ , is a measure of the amount of forward direction retained by a photon after a single scattering event. When a photon is scattered by a particle so that its trajectory is deflected by a deflection angle  $\theta$ , then the component of the new trajectory which is aligned in the forward direction is  $\cos \theta$ . The average deflection angle or the mean value of the cosine of the scattering angle,  $\langle \cos \theta \rangle$ , is defined as the anisotropy (Dam JS, 2000(b)). This is a dimensionless parameter that varies between -1 and 1 (backscatter to forward scatter). For

isotropic scattering,  $g = 0$ , there is a uniform distribution at all angles, but as  $g$  approaches 1, the distribution becomes highly peaked in the forward direction.

The Henyey-Greenstein model can be used to describe the angular distribution of light scattered by small particles. This model has been applied to numerous situations, ranging from the scattering of light by biological tissue to scattering by interstellar dust clouds (Henyey L, 1941). In this work the Henyey-Greenstein model is used to describe the angular distribution of light scattered from the subcellular particles in the skin:

$$\rho(\theta) = \frac{1}{4\pi} \frac{1 - g^2}{[1 + g^2 - 2g \cos \theta]^{3/2}} \quad (2.9)$$

### 2.3.1.6 Reduced scattering coefficient

In highly scattering media (e.g. skin) the photons propagate through the medium in consecutive steps which are random in length and direction (the so-called random walk). Each step commences with a scattering event that is equally likely to scatter the photon in any direction. The reduced scattering coefficient,  $\mu'_s$ , describes isotropic scattering which is related to the (anisotropic) scattering coefficient,  $\mu_s$ , through (Vo-Dinh T, 2003):

$$\mu'_s = (1 - g)\mu_s \quad (2.10)$$

For  $g = 0.75$ , an average of 4 scattering events is required for a population of photons to disperse isotropically. In tissue the value of  $g$  may vary from 0.4 to 0.99. This means that the photons are isotropically dispersed after anything from 2 to 100 scattering events (Vo-Dinh T, 2003) (p 2-25).

As noted in section 2.3.1.3, if a photon is detected at a specific point in or on the surface of the tissue, it is not possible to distinguish the path the photon took. In a medium with a specific reduced scattering coefficient, two photons may be detected at the same point after taking two completely different paths as illustrated in Figure 2.10 and Eq 2.11 (Dam JS, 2000(b)).

$$\mu'_s = (1 - g_1)\mu_{s1} = (1 - g_2)\mu_{s2} \quad (2.11)$$

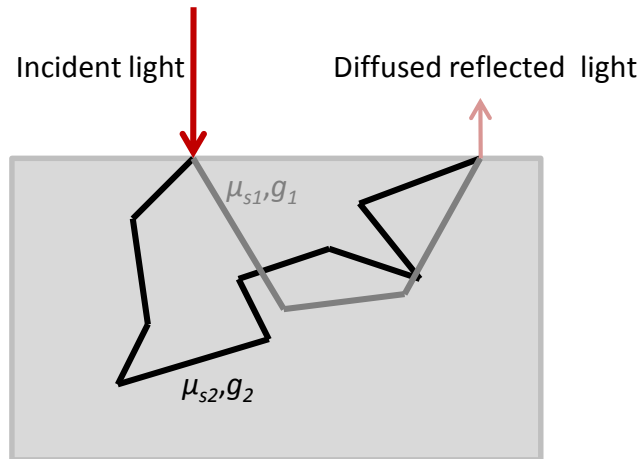


Figure 2.10: Similarity principle where photons taking different paths arrive at the same end point.

### 2.3.2 Values for the optical properties of skin

The optical properties of skin determine the fluence rate reaching deeper parts in the skin. During the past three decades, several researchers have measured the optical properties of different tissue types (Cheong WF, 1990), (Jacques SL, 1998(a)), (Simpson R, 1998(a)), (Salomatina E, 2006), (Tuchin V, 2007), (Tseng S, 2009). Comparing the published values for skin, it became apparent that the different authors did not report the same values for a variety of reasons. Table 2.3 is a summary of some of the published data for the optical properties of skin. Apart from the variance between different researchers, the optical properties of human skin also exhibit great variation between individuals and even from site to site on the body of the same patient (Zhang R, 2005).

Few references refer to the epidermal absorption coefficient for the different skin phototypes. There are some references (Zonios G, 2001), (Alaluf S, 2002(a)), (Alaluf S, 2002(b)), (Tseng S, 2009) but they mostly refer to a quantity known as the ‘melanin index’, for which the relation to the actual absorption coefficient is not particularly clear. Alaluf et.al. (Alaluf S, 2002(a)) reported on melanin concentration for the different skin phototypes (typically South African). Their findings were that the ‘African’ skin had about double the epidermal melanin concentration of the ‘European’ skin. This was true for both the sun-exposed and non-exposed skin samples retrieved from 4 mm punch biopsies. It is not a straight forward process to convert the melanin concentrations measured from the skin biopsies to the corresponding absorption coefficients. It is also reported that for the darker skin phototypes the melanin particle sizes are usually larger than for the lighter skin phototypes (Alaluf S, 2002(a)).

Table 2.3: Comparison of optical properties measured in various laboratories. Note: most authors publish the data in units of  $\text{cm}^{-1}$  and therefore this table uses  $\text{cm}^{-1}$  but in the rest of this work units of  $\text{mm}^{-1}$  are used (Table adapted from (Tuchin V, 2007)).

Tissue	$\lambda$ (nm)	$\mu_a$ ( $\text{cm}^{-1}$ )	$\mu_s$ ( $\text{cm}^{-1}$ )	$\mu'_s$ ( $\text{cm}^{-1}$ )	$g$	Reference
Epidermis	600	19	460	-	0.80	(van Gemert MJC, 1989)
Epidermis	633	35	450	88	0.80	(van Gemert MJC, 1989)
Epidermis	633	2.6	-	47.6	0.80	(Salomatina E, 2006)
Epidermis (caucasian)	633	0.35	-	27.5	-	(Simpson R, 1998(a))
Epidermis (negroid)	633	2.6	-	32.5	-	(Simpson R, 1998(a))
Epidermis (type I-II)	633	0.63	-	22.4	-	(Tseng S, 2009)
Epidermis (type III-IV)	633	0.66	-	22.3	-	(Tseng S, 2009)
Epidermis (type V-VI)	633	0.73	-	22.1	-	(Tseng S, 2009)
Epidermis	800	40	420	62	0.85	(van Gemert MJC, 1989)
Epidermis	820	1.5	-	36	0.80	(Salomatina E, 2006)
Dermis	600	2.2	200	-	0.80	(van Gemert MJC, 1989)
Dermis	633	2.7	187.5	37	0.80	(van Gemert MJC, 1989)
Dermis	633	1.9	-	23.8	-	(Tuchin V, 2007)
Dermis	633	<10	-	11.64	0.97	(Tuchin V, 2007)
Dermis	633	1.5	-	50.2	-	(Tuchin V, 2007)
Dermis	633	1.5	-	29.9	0.80	(Salomatina E, 2006)
Dermis	800	2.3	175	30	0.85	(van Gemert MJC, 1989)
Dermis	820	1.1	-	21.8	0.80	(Salomatina E, 2006)
Skin (negroid)	633	2.41	-	32.2	-	(Simpson R, 1998(b))
Skin (caucasian)	633	0.33	-	27.3	-	(Simpson R, 1998(b))

Skin damage (including blistering) has been reported during laser hair removal procedures on darker skin phototypes (Lanigan S, 2003), (Battle E, 2004). This underlines the importance of determining the absorption coefficient of the skin before laser treatment commences.

It is important to note that there are differences in optical properties depending on whether the measurements were done *in vivo* or *in vitro*. In general *in vivo* measured values of  $\mu'_s$  and  $\mu_s$  are two to ten times smaller than *in vitro* measured values (Tuchin V, 2000) (p37).

The wide range in reported  $\mu_a$  values for the epidermis made it difficult to extract the required  $\mu_a$  values from the published literature. This work is aimed at the *applicability of laser based treatment to the South African population*. The lack of consistency in reported  $\mu_a$  values prompted the author to investigate techniques that can be used to determine the optical properties of tissue, specifically the epidermis, non-invasively. This will be discussed in the next section.

## 2.4 MEASUREMENT TECHNIQUES

To the knowledge of the author, there is no established technique that can be used to directly measure the optical properties of tissue. All the techniques rely on inverse methods to determine the optical properties. The two methods used in this work are an integrating sphere (IS) and a diffuse reflectance probe (DRP). In both methods, the optical properties are calculated from the average properties in the sampled (illuminated) area. These average values are later used in the computer model that requires an average value of the optical properties for each layer.

### 2.4.1 Integrating sphere

An integrating sphere (IS) can be described as a hollow sphere with a few ports (entrance, exit and detector). The inside of the sphere is coated with a highly reflective material. In the visible and near infrared wavelength regions (400-1500 nm), the coating is usually Spectralon with a reflectivity of more than 98% (Labsphere, 2012). An IS system integrates the radiant flux spatially and can be used to measure optical radiation (Labsphere, 2012).

IS systems are widely used to measure the optical properties of various materials, including human tissue (Pickering JW, 1993), (Nilsson AM, 1998), (Dam JS, 2000(b)), (Bashkatov AN, 2005), (Salomatina E, 2006), (Singh A, 2009), (Singh A, 2011). This method uses one or two Integrating Spheres to measure the reflectance from a sample and the transmission through the sample as shown in Figure 2.11. For these measurements, the underlying assumption is that the sample is homogeneous.

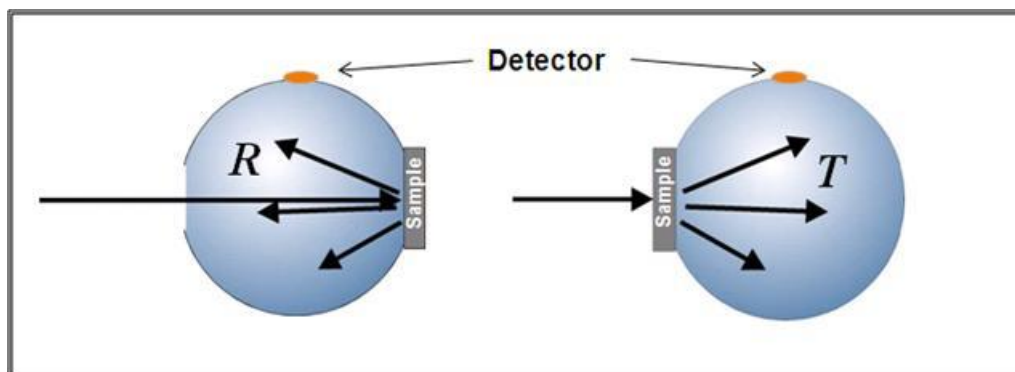


Figure 2.11: Integrating sphere system for reflection (R) and transmission (T) measurements.

For a single sphere the sample is moved from the port closest to the light source to the opposite port to measure either the transmitted or reflected light. The light beam for the IS is usually about 2-4 mm in diameter. For the efficient use of the IS, samples need to have a

diameter of  $> 15$  mm. This means that the same area is not necessarily sampled during the measurements when the samples are moved from the one port to the other.

In a double IS system, two spheres are put next to each other with only the sample holder between the two spheres. In this configuration the same area is sampled for both the transmission and reflection measurements. In the double IS system cross-talk between the spheres may influence the data (Nilsson AM, 1998), (Dam JS, 2000(b)), (Salomatina E, 2006).

The IS system needs to be calibrated with a set of phantoms with known absorption and scattering coefficients. The optical properties of the sample under investigation are then determined from the measurements using the calibration model to extract the values using a multiple polynomial regression method (Dam JS, 2000(a)), (Dam JS, 2000(b)). The method involves fitting different order polynomial functions of  $\mu_a$  and  $\mu'_s$  to the measured data and then predicting  $\mu_a$  and  $\mu'_s$  for the particular sample using a Newton-Raphson algorithm.

The IS system is not suitable to measure optical properties of skin *in vivo*. In order to use the IS system to measure the optical properties of skin, samples must be acquired either through skin biopsies or excess skin from surgical procedures. This is an invasive process. A less invasive measurement technique using diffuse reflectance is discussed in the following section.

#### **2.4.2 Diffuse reflectance probe**

In the recent decade numerous papers have been published where the optical properties of skin were measured, non-invasively, with a diffuse reflectance probe (Dam JS, 2000(b)), (Johns M, 2005), (Zonios G, 2006), (Reif R, 2007), (González FJ, 2010). Light entering skin can be scattered directly from the surface of the skin and a portion of the light may enter the skin and be reflected/scattered from deeper lying structures as indicated in Figure 2.12. It is this diffusely reflected light that is detected with a diffuse reflectance probe (DRP). A typical layout for a DRP experiment is shown in Figure 2.13.

The scattered light that exits the skin sample can be collected by a detector placed some distance from the light source. By measuring the diffusely reflected light as a function of wavelength (usually with a spectrometer) the values of  $\mu_a$  and  $\mu'_s$  can be calculated. Some systems use a probe with a single detection fibre and a single or multiple emitting fibres (Johns M, 2005), (Zonios G, 2006), (Reif R, 2008) while others use multiple detection fibres which are placed at different distances from the source (Dam JS, 2000(b)), (Meglinski IV, 2002), (Wang Q, 2008). Using different distances between the light emitting fibre and the

detecting fibres allow the user to probe different depths into the skin because the further the distance between the emitting and collection fibres, the ‘deeper’ the light can travel into the skin and still be detected by the collecting fibre (Meglinsky IV, 2001), (Doronin A, 2011). The probe system used in this work had a fixed light delivery-detector distance and only the outer layers of the skin could be sampled.

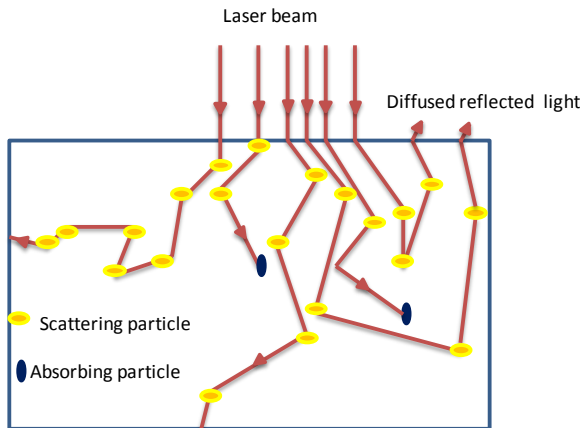


Figure 2.12: Absorption and scattering in skin.

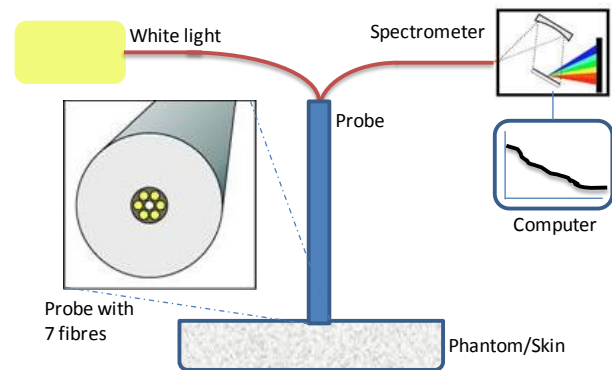


Figure 2.13: Schematics of an experimental setup for the diffuse reflectance probe measurements.

## 2.5 SKIN SIMULATING PHANTOMS

Due to the difficulties in handling human tissue, phantoms are used to simulate the properties of tissue/skin. Over the years skin simulating phantoms have been developed in order to test and calibrate bio-optical instrumentation and techniques. Skin simulating phantoms can be broadly divided into three categories: liquid, gel and solid phantoms (Pogue B W, 2006). Liquid phantoms, usually prepared from biological materials e.g. intralipid (IL), have the advantage that they are easy and quick to prepare but do not usually have a long shelf life. They are usually used to calibrate systems e.g. IS or reflectance probe systems, but are not used as long term reference standards. Gel based phantoms provide more flexibility, but also have a limited shelf life and must be stored correctly, usually in a liquid, which in itself has an effect on the measured optical properties. Solid phantoms are generally more cumbersome to prepare, but are stable over longer periods of time and can be used as a calibration standard for systems. Phantoms usually consist of a host material (or matrix) with both absorbers and scatterers added to the matrix. In this work only liquid and solid phantoms were used. Both liquid and solid phantoms were used to validate the computer model discussed in Chapter 3.

When scattering and absorbing particles are used in phantoms to mimic skin behaviour, it is assumed that the scattering particles do not absorb light at the investigating wavelength (assume  $\mu_a = 0$ ). Similarly it is assumed that the absorbing particles do not scatter the light.

### 2.5.1 Liquid phantoms

Intralipid (IL) is a known simulant for scattering in human skin. It is a white, fat based emulsion with spherical particles (mean diameter of 0.4  $\mu\text{m}$ ) (Das BB, 1997). It is usually supplied in a concentration of 20% volume IL/total volume in a mixture consisting of the IL and distilled water. The IL is mixed with an equal volume of an absorbing mixture consisting of distilled water and absorbing particles (black ink or carbon black particles). The optical properties of IL (diluted to a concentration of 10% IL in distilled water) are well documented for HeNe lasers ( $\lambda = 632.8 \text{ nm}$ ) (van Staveren HJ, 1991), (Flock S, 1992), (Michielsen K, 1998), (Choukeife JE, 1999). At this wavelength  $\mu'_s$  and  $\mu_a$  for IL is given by (van Staveren HJ, 1991):

$$\mu'_{s(\lambda=632.8 \text{ nm})} = 1.104 \text{ mm}^{-1} \times (\text{IL concentration}) \quad (2.12)$$

and

$$\mu_{a(\lambda=632.8 \text{ nm})} = 0.15 \times 10^{-2} \text{ mm}^{-1} \times (\text{IL concentration}) \quad (2.13)$$

The value of  $\mu_a$  for IL is about  $10^3$  smaller than  $\mu'_s$  and is generally disregarded for the 10% IL. The anisotropy can be calculated by (van Staveren HJ, 1991):

$$g = 1.1 - 0.58\lambda \quad (2.14)$$

with  $\lambda$  between 0.4 and 1.1  $\mu\text{m}$  (with the units of  $\lambda$  in  $\mu\text{m}$ ).

To calculate the  $\mu_a$  of the ink sample, the intensity of the laser ( $I_0$ ) without the ink and with the ink ( $I$ ) is measured as well as the path length ( $d$ ) though the sample (cuvette). The Beer-Lambert law discussed in section 2.3.1.3 is then used to calculate the  $\mu_a$  at the required wavelength.

$$\mu_a = \frac{1}{d} \ln \frac{I_0}{I} \quad (2.15)$$

### 2.5.2 Solid phantoms

Solid phantoms are usually prepared by using a resin (with a high transmission and low absorbance at the required wavelength) as base material (or matrix) with added scatterers (TiO) and absorbing particles (carbon black). The optical properties of the solid phantoms are determined by the concentration of the TiO and carbon black added to the matrix.

## 2.6 LIGHT PROPAGATION MODELS

A continuing increase in medical applications of lasers both for treatment and diagnostic purposes (Peng Q, 2008), (Overton G, 2011) necessitates the ability to model the laser-tissue interaction mechanisms. The purpose of computer model simulations is to predict the fluence rate as a function of depth inside the tissue (Cheong WF, 1990). The accuracy of these predictions is dependent on how well the model simulates the tissue and the validity of the values of the optical properties used in the model.

The focus of this work is on the implementation of a computer model developed in a commercially available software environment and therefore only a brief overview is given of the major models predicting light propagation through tissue. More extensive formulations can be found in (Splinter R, 2007), (Martelli F, 2010), (Welch A, 2011).

A fundamental theory of light propagation in multiple scattering media has been developed by applying Maxwell's equations (Dam JS, 2000(b)), (Martelli F, 2010). This theory preserves the wave properties of the light and is able to account for all the effects of multiple scattering, diffraction and interference. The complexity of this rigorous mathematical formalism is overwhelming and even with fast computers and computing techniques no practical models for general use in multi-scattering media is available as yet (Cheong WF, 1990), (Dam JS, 2000(b)), (Martelli F, 2010) .

For practical applications one has to resort to numerical models based on the solution of the radiative transport equation. (Dam JS, 2000(b)).

### 2.6.1 Radiative Transport equation

The radiative transport equation (RTE) describes the transport of energy through a scattering medium phenomenologically (Ishimaru A, 1989), (Martelli F, 2010). In the electromagnetic theory (Maxwell's equations) the propagation of light is described by the superposition of electromagnetic fields while the transport theory depends on the superposition of energy fluxes (Dam JS, 2000(b)), (Jacques S, 2008(b)). Even though the radiative transport theory lacks the rigorous mathematical formulation of the Maxwell's equation approach, it is able to account for all the physical effects involved in light propagation (Martelli F, 2010).

Multiple scattering is associated with de-coherence of the light and therefore in turbid media the wave nature of light is suppressed (Vo-Dinh T, 2003). Most of the laser-tissue interaction models are based on the RTE (Cheong WF, 1990), (Jacques SL, 1998(b)). The

RTE does not have exact closed form analytical solutions which are relevant in most practical applications.

Two of the most common methods used to solve the RTE are the diffusion approximation and the Monte Carlo simulation (or probabilistic) method.

### 2.6.1.1 Diffusion approximation

This approximation provides useful solutions when certain restrictions are taken into account. In the diffusion theory, the photon migration is modelled as a gradient-driven diffusion of energy or energy flux (Dam JS, 2000(b)), (Jacques S, 2008(b)). A restriction in the diffusion approximation is that a photon must undergo several scattering events before it is absorbed.

In the diffusion approximation it is assumed that the radiant energy does not travel in a preferential direction. When a laser or collimated beam is directed onto skin, the photons have a specific direction of movement (Mustafa FH, 2011). During the scattering process in the skin, they lose their directionality and the diffusion approximation can be implemented (Jacques S, 2008(b)). One of the assumptions of the diffusion theory is that the photons take part in a random walk. For this to happen, a photon must undergo several scattering events before it is absorbed. The commonly cited rule of thumb is that  $\mu'_s/\mu_a > 10$  (Star WM, 1988), (Dam JS, 2000(b)), (Jacques S, 2008(b)), (Martelli F, 2010). With enough scattering events, the average photon propagation depends on the product  $(\mu_s(1 - g))$  rather than on the specific values of  $\mu_s$  and  $g$  (Star WM, 1988), (Jacques S, 2008(b)).

For modelling light transport in skin and especially the epidermis with high absorption coefficients, the diffusion approximation condition ( $\mu'_s/\mu_a > 10$ ) is not always met. The Monte Carlo process is an alternative light transport model used in the skin when the diffusion approximation assumption is too stringent.

### 2.6.1.2 Monte Carlo simulations

Monte Carlo (MC) simulations can be used as an alternative modelling technique to solve the radiative transport equation (Vo-Dinh T, 2003), (Martelli F, 2010), (Welch A, 2011). It is a stochastic or randomised approach. In this method the trajectories of photons are traced through the model, making use of the particle nature of the photons. MC methods are used to simulate the photon path of a great number of photons (more than 1 million). The path of each photon is traced as it undergoes scattering and absorption. It is a purely stochastic approach and models light as discrete photons bouncing around in the scattering medium

(Dam JS, 2000(b)). The assumption is also made that the media are homogeneous. MC simulations are not constrained by the condition that the absorption coefficient should be smaller than the reduced scattering coefficient (diffusion approximation). The only requirement is to define the turbid medium using its scattering and absorption coefficients as well as the anisotropy (Private communication with Breault Research, vendor of the ASAP software).

### *The Monte Carlo process*

The MC process consists of a number of steps

- MC process is a statistical process and therefore a large number of photons are launched into the medium (typically more than 1 million). The effect of a few photons compared to that of 3.1 million photons is illustrated in Figures 2.14 and 2.15.

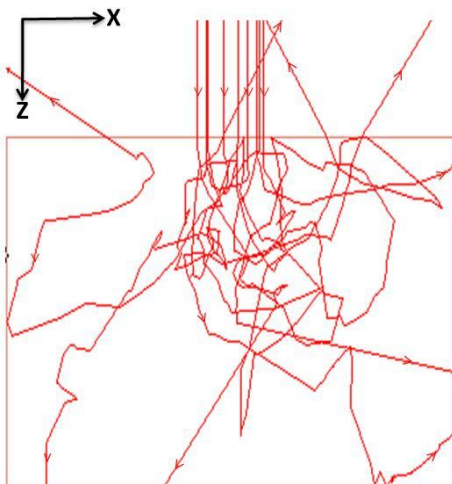


Figure 2.14: Random walk of 15 photons.

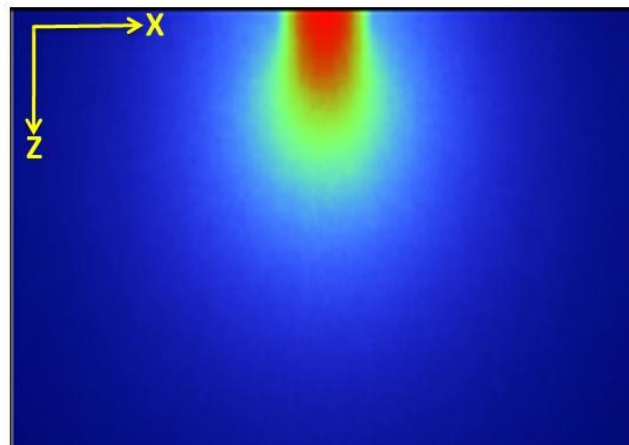


Figure 2.15: Random walk of 3.1 million photons.

- Each photon performs a random walk in the skin. The path of a photon is decided by a number of iterative decisions along the path of the photon:
  - The distance a photon travels before an interaction occurs.
  - The direction in which the photon proceeds after the interaction.
- The macroscopic optical properties,  $\mu_a$  and  $\mu_s$ , determine the path length of a photon between interactions and the anisotropy,  $g$ , determines the direction of travel in the random process.
- The step size or path length of a photon between photon-tissue interaction sites is given by

$$l = \frac{-\ln(\xi)}{(\mu_a + \mu_s)} \quad (2.16)$$

with  $\xi$  a uniformly distributed random number between 0 and 1.

- A photon ‘loses’ part of its energy after each step by an amount of (1- albedo), where

$$albedo = \frac{\mu_s}{(\mu_a + \mu_s)} \quad (2.17)$$

## 2.6.2 Raytracing models

In this work the Monte Carlo approach was used because the radiative transport equation requirement,  $\mu'_s/\mu_a > 10$ , is too stringent when applied to visible light interaction with the epidermal layer.

Raytracing has been used for many decades to design optical systems (Stevenson M, 2006). Free software is available online (e.g MCML – Monte-Carlo Modelling of Light transport (Jacques SL, 1998(b))), or commercially (e.g. ASAP from Breault Research Organization). The online software assumes symmetry around the light source (Jacques SL, 1998(b)), but this is not always desirable.

The ASAP (Advanced Systems Analysis Program) software from Breault Research Organization (Tucson, Arizona in the USA) is capable of performing non-sequential raytracing where rays (or photons) can interact with objects as they are encountered. The rays are not restricted to the order in which the objects were defined in the model as is the case in sequential raytracing (Michel B, 2005), (Breault Research, 2006). ASAP does not assume symmetry and allows for any geometrical shape to be used.

The following were taken into account on the decision to use ASAP:

Advantages of ASAP:

- Any shape of form can be modeled, irregular shapes can be used and predefined or measured shapes can be imported through computer aided design (CAD) software. Some tumors may have irregular shapes.
- Geometrical changes are relatively easy to implement.
- The system is a raytracing software package and as such in is applicable for more than just laser tissue interaction modeling.

Disadvantages of ASAP:

- The software is expensive.
- It has not been widely applied in peer-reviewed articles.

The verified model developed in the ASAP environment is described in more detail in Chapter 3. The model was applied to a cancer therapy which is described in the next section.

## **2.7 CANCER AND PHOTODYNAMIC THERAPY**

According to the latest statistics available from the Cancer Association of South Africa (CANSA), non-melanoma skin cancer (consisting of basal cell carcinoma (BCC) and squamous cell carcinoma (SCC)) is the most common type of cancer in South Africa with about 20 000 new cases reported each year. Australia and South Africa have the highest incidence of skin cancer in the world (Mqoqi N, 2004).

“Basal cell carcinoma accounts for more than 90% of all skin cancers. Basal cell cancer grows slowly and does not usually spread to other parts of the body. However, if left untreated, it can spread to nearby areas and invade bone and other tissues under the skin. Squamous cell carcinoma (SCC) is much less common than BCC but can be more aggressive than BCC and is also more likely to grow deep below the skin and spread to distant parts of the body. When squamous or basal cell skin cancers are found early, there is nearly a 100 % chance for cure” (MD Anderson Cancer Centre, 2009). Both BCC and SCC may potentially be treated with photodynamic therapy.

### **2.7.1 Photodynamic therapy (PDT)**

Photodynamic therapy (PDT) is one of the newer cancer treatments under investigation worldwide (Schuitmaker J, 1996), (Hopper C, 2000), (Brown SB, 2004), (Robertson CA, 2009), (Sekkat N, 2012). PDT is usually defined as the administration of a non-toxic drug or dye (sometimes called photosensitiser (PS)) either systemically, locally or topically to the patient with a tumour. After some delay allowing for the PS to accumulate in the tumour, the tumour is irradiated with light where the wavelength has been tuned to an absorption peak of the PS. In the presence of oxygen toxic species are formed that lead to cell death and tissue destruction in the tumour. The PS preferentially accumulates in tumour cells rather than normal cells. One of the major features of PDT as a treatment modality is its dual selectivity, both light and the PS must be present for the destruction of the cells. Collateral damage to normal tissue can be minimised by delivering the light only to the affected area that requires treatment. Tumours can be destroyed rapidly and any damage to healthy tissue usually heals within a few weeks (Brown SB, 2004).

The more recent use of PDT in oncology dates back to the early 1970's when Dr. Thomas J. Dougherty started his investigations into the mechanisms and clinical use of

hematoporphyrin derivatives (HpD). Since then PDT has been approved in numerous countries (Mang TS, 2004). A list of some of the photosensitisers (PS's) and their potential therapeutic applications can be found in (Sekkat N, 2012).

### 2.7.1.1 Photodynamic interaction mechanism

“Light absorption and energy transfer is at the heart of PDT. The ground state PS has two electrons with opposite spins in the low energy molecular orbital. After the absorption of photons, one of these electrons is excited to a high energy orbital, but keeps its spin (first excited singlet state)” (Castano AP, 2004). The electron stays in this excited state for only a few nanoseconds before losing its energy through fluorescence, internal heat conversion or intersystem crossings as illustrated in Figure 2.16 (Castano AP, 2004), (Zhu TC, 2006). The fluorescence has some added benefits as it can be used to quantify the amount of PS in the cells or tissue or as *in vivo* fluorescence imaging to follow the distribution of the PS.

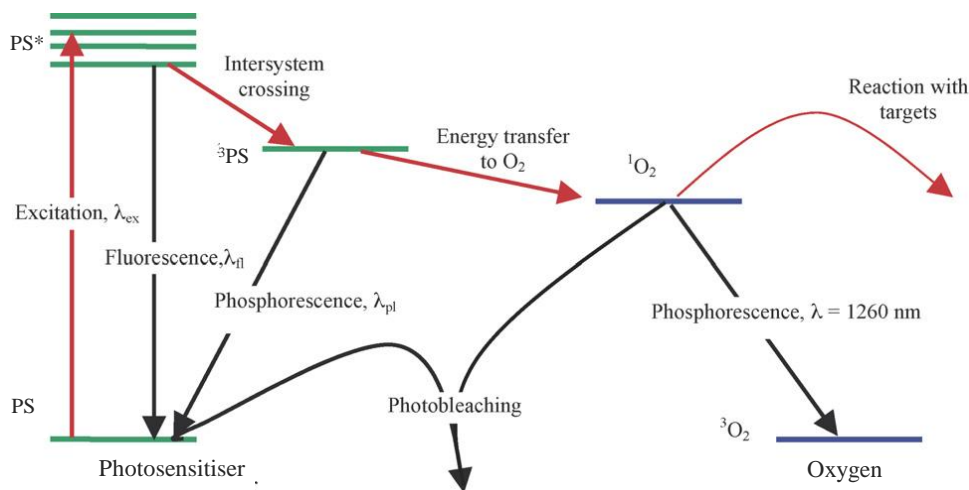


Figure 2.16: Energy level diagram for a Type 2 photosensitiser.

A relatively long-lived (in the order of microseconds) excited triplet state is formed during the intersystem crossing. From the excited triplet state the PS can follow two paths or reactions to induce cell death. (Castano AP, 2004), (Zhu TC, 2006) (p235 – 236).

- Type 1 reaction:
  - Direct interaction with a cell membrane or a molecule. This interaction may generate cytotoxic free radicals.
  - Further reactions of the free radicals with oxygen may produce reactive oxygen species.

- Type 2 reaction:
  - In this reaction, excited state singlet oxygen is formed directly by the transfer of energy from the PS in the triplet state.

It is possible for both type 1 and 2 reactions to occur simultaneously. In this case the ratio between the two processes depends on various factors (i.e. the type of PS used, the concentration of the PS in the tissue and the oxygen levels in the tissue). The majority of the newer PS compounds available for PDT utilise the Type 2 process (Zhu TC, 2006). The energy levels in Figure 2.16 explain some of the underlying physical processes during in a Type 2 PDT process. Highly reactive singlet oxygen ( $^1\text{O}_2$ ) is formed and the PS returns to its ground state. During this process the PS is not ‘consumed’ and can create another singlet oxygen molecule.

Singlet oxygen has a short half-life and is highly reactive. Therefore only molecules and structures that are close to the PS are directly affected by PDT (Castano AP, 2004). In cells the typical half-life of singlet oxygen is less than 40 ns. The singlet oxygen is only active in a radius of the order of 20 nm (Castano AP, 2004).

An effective PDT process is dependent on the absorption of light by the PS. As such it is important to ensure that the required fluence rate reach the PS in the tumour. The term light dose or treatment dose ( $\text{J}/\text{cm}^2$ ) is often used in PDT treatment. When a continuous wave laser is used, this dose term will combine the fluence rate and treatment time (energy = power  $\times$  treatment time).

Optical properties of tissue, and particularly in skin, are important in laser applications such as PDT and biostimulation. Epidermal absorption of the light reduces the fluence rate reaching the intended treatment site. The layered structure of skin, combined with the optical properties of the different layers, can be used in a computer model to predict the laser fluence rate at the treatment site.

## 2.8 SYNTHESIS

The absorption of light in the epidermal layer of the skin is a factor that is not usually considered during laser skin treatments. Epidermal absorption is dependent on the skin phototype and if not taken into account, may result in unwanted skin damage (Lanigan S, 2003), (Lepselter J, 2004), (Lim SRP, 2006).

With the information discussed in this chapter, it has become apparent that a computer model may be a useful tool to predict the fluence rate at any depth into the skin. Depending

on the skin site, there may be a large variation in the absorption of light in the epidermal layer of the skin. This influences the transmission of light through the epidermis and as a result influences the fluence rate available for treatment deeper into the skin. A predictive computer model may enable a clinician to adapt the treatment parameters to the specific treatment site at the required depth of treatment for the patient.

Computer models that can trace light through tissue do exist (Jacques SL, 1998(b)), (Breault Research, 2006). Modifying software developed by other authors to accommodate one's own specific application requirements is not always practical. Investigation into existing software led to the decision to acquire the commercially available ASAP software package from Breault Research Inc. While their Realistic Skin Model (RSM) is a useful tool, it is too complex to be validated with skin simulating phantoms that can be prepared in a research laboratory where a simpler model is required to test the influence of specific parameters on the fluence rate at a specific depth into the skin. The major influencing factors under investigation are the epidermal absorption (absorption coefficient for the individual to be treated) and the thickness of the epidermal layer (body site to be treated). The development of such a simpler model in the ASAP environment and the experimental validation is discussed in the next chapter (Chapter 3).

The second 'stumbling block' in the prediction of the fluence rate in the skin is the lack of data on the absorption coefficient for the different skin phototypes (see section 2.3.2). Due to the importance of this parameter for the computer model, the absorption coefficient had to be measured on a sample that is representative of the South African population. The most appropriate non-invasive technique that could be identified was the diffuse reflectance probe (DRP) technique described by Zonios (Zonios G, 2006). The development of this technique, the accompanying software as well as the *in vivo* test on 30 volunteers is described in Chapter 4. This DRP technique is a fast, cost effective, non-invasive and portable technique that has the potential to be implemented at "point-of-care" in South Africa.

The final implementation of the computer model for different skin phototypes as well as different epidermal thicknesses is discussed in Chapter 5.

The discussion in this review chapter led to the following conclusions that are important for this work:

- The optical properties influence light transmission through skin and as such the fluence rate reaching deeper into the skin.

- Basic optical ray tracing models are not sufficient due to the multi-scattering in tissue.
- Layered structured computer models are available commercially and online.
- The online software (MCML, (Jacques SL, 1998(b))) is cumbersome to use and geometry changes are not easy to implement.
- Change in geometry is important in a fluence rate prediction model. The ASAP software allows for this.
- Both models (ASAP and MCML) are based on the Monte Carlo simulation process where vast numbers of photons are traced through the model.
- Data on the expected range of absorption coefficients for the South African population is not available. Data is scarce for the absorption coefficient of the different skin phototypes. For the implementation of the model in the South African environment, this data is necessary.

This led to the conclusions that:

- A computer model (with flexibility to add structures in the model, e.g. tumours) must be developed to predict the fluence rate at any pre-determined depth into skin.
- The extent of the epidermal absorption coefficient spread for the South African skin phototypes needs to be measured. A diffuse reflectance probe provides the capability to do that.
- The influence of the epidermal absorption influences the fluence rate that is available for treatment some distance into the skin. This needs to be quantified for the South African population.

In the next chapters the development of the computer model is discussed as well as the development of a diffuse reflectance probe measurement protocol and data extraction with the introduction of representative absorption coefficients into the computer model. The computer model is then used to give an indication of the treatment time adjustments required for different skin phototypes present in the South African population.

The next chapter will be devoted to the development, verification and validation of the layered structure computer model to simulate skin.

## **CHAPTER 3: DEVELOPMENT OF A LASER FLUENCE RATE PREDICTION MODEL**

Light can be described as an electromagnetic wave or a stream of photons. Wave theory allows for the description of light as it propagates and is affected by optical elements like mirrors and lenses. The particle nature of light allows for the quantum understanding of light (Welch A, 2011) (p14).

Human tissue is considered highly scattering in the visible to near infrared wavelengths (400-1200 nm). The average photon will travel between 0.01 and 0.2 mm between scattering events (Welch A, 2011) (p28). For real tissue, such as skin, “creating a precise representation in the form of a phantom or computer model is formidable if not totally impossible” (Welch A, 2011) (p28). Skin is therefore presented as a bulk material with scatterers randomly distributed in the volume. It is assumed that the skin can be described as an isotropic and homogenous medium even though that is not a true representation of the actual skin (Welch A, 2011) (p28).

### **3.1 ASAP RAYTRACING SOFTWARE**

Advanced Systems Analysis Program (ASAP) is a flexible optical system modelling tool which simulates the interaction of light with optical and mechanical (or biological) structures. Monte Carlo raytracing techniques are used in a single, global, three-dimensional coordinate system (Breault Research, 2006). The software does not assume symmetry. ASAP performs simulations based on the way light behaves in the ‘real world’ and rays are allowed to split into reflected, refracted, diffracted, polarized, and scattered components as they propagate through the system (Breault Research, 2006). Each ray propagates independently from the other rays, following physically realisable paths. A ray can encounter objects (optical or mechanical) in any order as it propagates through the system.

The Realistic Skin Model (RSM) is a module in the ASAP software package specially designed to simulate the light propagation through human skin. At the start of this project the RSM model had not been used in any peer reviewed papers and therefore it was important to develop a model that could be verified and validated with optical measurements as discussed in the paper in section 3.5 (Karsten AE, 2012(a)). The RSM model can be used to model the effect of hair on the skin surface as well as blood vessels specified by the user. It is however difficult to verify and validate a model with such complexity. In a recent study (Mustafa FH,

2011) it was shown that hair on the skin surface reduces the fluence rate entering the epidermis by a maximum of 7% and it was decided not to include hair in the model.

The RSM model was not used in this work, but a much simpler model was developed in the ASAP environment that could be directly validated with optical measurements. The focus of the modelling work was on the effect of the different melanin concentrations and the epidermal thickness on the transmission of light up to a pre-defined depth into the tissue. Therefore an uncomplicated model with only the required layers was used. The skin was modelled as a layered structure with planar surfaces. As discussed in section 3.3, a wavy interface between the epidermal layer and the dermal layer was also considered, but the influence was minimal and only planar surfaces were used in the work. In future work for clinical applications, it would be valuable to introduce an ‘advanced’ model that includes hair, blood and a wavy outer layer for the epidermis.

## 3.2 LAYERED SKIN MODEL

Defining a computer model of the light propagation through skin in the ASAP environment is a four step process as described below:

- Define and verify the geometry of the system and allocate the optical properties of each component or layer.
- Define the light/laser source.
- Trace the rays through the system.
- Perform the analysis to determine the fluence rate at different layers in the system.

Each of the steps indicated above is described in more detail in the next sections.

### 3.2.1 Geometrical layout

A three layered skin model (Figure 3.1) has been developed to mimic the layered structure of skin. Each layer is described as a rectangular slab with known dimensions and known optical properties, i.e. absorption coefficient ( $\mu_a$ ), scattering coefficient ( $\mu_s$ ), anisotropy ( $g$ ) and refractive index ( $n$ ). Each layer is considered to be homogenous hence the optical properties are the same everywhere in the layer. In practice the values used represent an average of values in the more complex ‘real’ skin and is a necessary assumption for Monte Carlo raytracing as discussed in section 2.6.1.2.

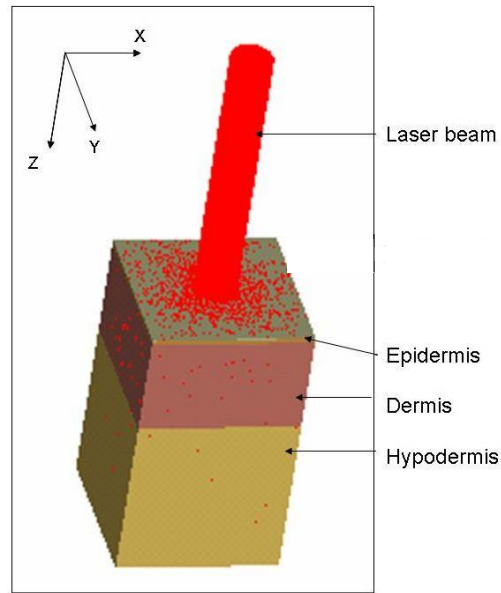


Figure 3.1: Layered structure of the computer model with the laser beam entering the outer layer.

The thickness of the different layers can be adapted according to the application. In the first application, the skin model consisted of three layers, the first and last layers are glass with the liquid phantom (second layer) in-between the glass. In the case of the solid phantoms simulations, the skin model consisted of one or two layers (see section 3.4). For the PDT treatment simulations the skin model consisted of two layers and a tumour embedded in the dermis.

### 3.2.2 Light source

A Gaussian profile light beam with a diameter of 10 mm and an output power of 1 mW was traced through the model. The laser power at any point in the model can then be expressed as a fraction of the incident power. This allows for the results to be easily scaled up when higher input power is required.

### 3.2.3 Ray tracing - Monte Carlo approach

In the ASAP software, the Monte Carlo approach is used because it is a rigorous, yet flexible approach to photon transport in random media. The random migration of each photon is traced until it is absorbed or leaves the boundaries of the model. Because the Monte Carlo approach is a stochastic method, a vast number of photons need to be traced to achieve statistical relevant data. In this computer model about 3.1 million rays or photons were traced through the system as described in the optimisation process in section 3.5.

During the propagation of a photon through the bulk media the following rules are followed/employed:

- The path length ( $l$ ) that photon undertakes between each interaction with the tissue (scattering or absorbing) is given by:

$$l = \frac{-\ln(\xi)}{(\mu_a + \mu_s)} \quad (3.1)$$

with  $\xi$  a uniformly distributed random number between 0 and 1.

- A photon ‘loses’ part of its energy after each step by an amount of  $(1-\textit{albedo})$ , where the scattering albedo is defined as:

$$\textit{albedo} = \frac{\mu_s}{(\mu_a + \mu_s)} \quad (3.2)$$

### 3.2.4 Henyey-Greenstein approximation

ASAP implemented a simplified model that uses the bulk absorption and scattering properties of the media in combination with the Henyey-Greenstein scattering profile or scattering phase function (Henyey L, 1941). This phase function is a reasonable estimate of the forward scattering nature of biological media such as skin. Even though it not an exact representation of the forward scattering of the tissue, experiments showed that it is a good approximation that is practical to use (Welch A, 2011) (49-51). One of the advantages of this phase function is that it only depends on one parameter, the anisotropy  $g$  (Welch A, 2011) (p159). The Henyey-Greenstein phase function,  $\rho$ , is given by:

$$\rho(\theta) = \frac{1}{4\pi} \frac{1 - g^2}{[1 + g^2 - 2g \cos(\theta)]^{3/2}} \quad (3.3)$$

with  $g$  = scattering anisotropy parameter or the mean cosine of the scattering angle  $\theta$ , for an isotropic medium  $g = 0$ .

After each scattering event, this function is used to determine the new direction of the photon.

### 3.2.5 Evaluations

The model is subdivided into multiple voxels or three dimensional pixels. The software keeps track of all the photons or rays entering and leaving each voxel as well as the photons that are absorbed in the voxel. The number of absorbed photons in the voxels in each predefined layer or slice, is used to determine the absorption in each slice (in the Z-direction or depth into the skin).

In the model two evaluating surfaces or detectors are used. One, a semi-dome is placed behind the light source to detect all the back reflected light and a second circular detector is

placed 0.2 mm after the last surface to detect all the light transmitted through the sample as indicated in Figure 3.2.

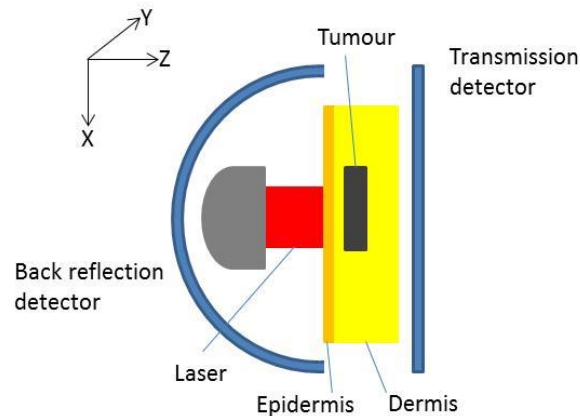


Figure 3.2: Schematic of the computer model with the detectors and the different layers.

The model was optimised in terms of the following parameters that are discussed in more detail in section 3.5.

- Slice thickness
  - Changes in the slice thickness do not significantly affect the output parameters. The model was standardised on a slice thickness of 0.1 mm (corresponding with the voxel dimensions).
- Voxel sizes
  - Voxel sizes of  $0.1 \times 0.1 \times 0.1 \text{ mm}^3$  were used. The number of voxels depended on the dimensions of the model.
- Number of rays
  - Most of the simulations were done with 3.1 million rays because of the reduced computing time required. Imaging simulations were done with a higher number of rays.
- Sensitivity to input power
  - A light source of 1 mW was used. Increasing the input power to 10 mW resulted in the same fractions of light reflected, absorbed and transmitted, the only difference was a tenfold increase in the absolute values.

The model worked effectively for its intended purpose.

### 3.3 NON-PLANAR EPIDERMAL/DERMAL INTERFACE

When evaluating the epidermal/dermal interface of skin under a microscope, it is apparent that the interface is not planar. This may influence the results of the computer model. Figure 3.3 is a typical skin image from an Optical Coherence Tomography (OCT) system from Thorlabs Inc. in the USA (model OCT1300SS). The ‘wavy’ nature of the interface is clearly visible. Measurements were done on a few images taken from the arms of various individuals to determine the length and the amplitude of the ‘wave’. The average length was 0.6 mm and the height varied between 0.025 and 0.05 mm.

This wavy interface was modelled in the software by using a sawtooth function that was rounded as illustrated in Figure 3.4. In testing the non-planar interface the skin model consisted of two layers, an epidermal layer (thickness of 0.09 mm) and a dermal layer (thickness of 3 mm). In order to evaluate the wavy interface, the bottom part of the sawtooth was kept at a depth of 0.09 mm and also moved to a depth of 0.12 mm into the skin (similar to an epidermal thickness of 0.12 mm).

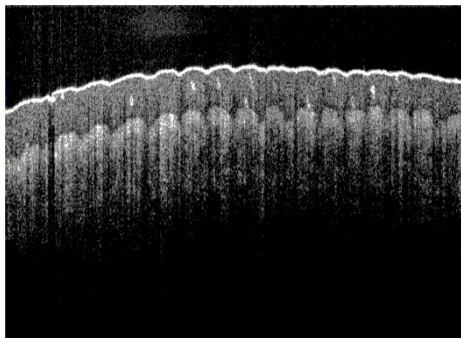


Figure 3.3: Typical OCT image of skin recorded at the NLC with a Thorlabs OCT system.

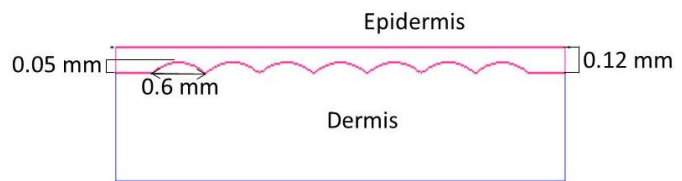


Figure 3.4: Wavy epidermis/dermis interface 0.12 mm into the skin with a wave amplitude of 0.05 mm and length of 0.6 mm.

The combinations used in the sawtooth model are described in Table 3.1.

Table 3.1: Optical parameters used in the sawtooth model.

Layer	Width (mm)	Start position (mm)	Thickness (mm)	$\mu_a(\text{mm}^{-1})$	$\mu_s(\text{mm}^{-1})$	$\mu'_s(\text{mm}^{-1})$	$n$	$g$
Epidermis	40	0	0.09, 0.12	0.1,1,2,3	22.4	4.48	1.5	0.8
Dermis	40	0.09, 0.12	3	0.15	13.9	2.78	1.4	0.9

In the models the portion of the light reflected and detected by the back reflection detector was determined and is reported in Table 3.2.

Table 3.2: Percentage of reflected light collected on the back reflection detector for the different sawtooth parameters described in Table 3.1 and the planar skin model with an epidermal thickness (ET) of 0.09 mm.

$\mu_a$ ( $\text{mm}^{-1}$ )	Epidermal thickness 0.09 mm		Epidermal thickness 0.12 mm		Planar model (ET 0.09 mm)
	Sawtooth height 0.05 mm	Sawtooth height 0.025 mm	Sawtooth height 0.05 mm	Sawtooth height 0.025 mm	
0.1	37	38	38	38	38
1	30	29	28	27	27
2	25	23	21	20	21
3	21	19	17	16	17

Good correlation was found between the planar model and the model where the epidermal sawtooth started at a depth of 0.12 mm with a wave amplitude of 0.05 mm. This good correlation is to be expected due to the following reasons.

- The change in refractive index between the epidermis and the dermis is less than 8% (1.5 to 1.4) and therefore it is not expected that the sawtooth interface would drastically increase the scattering at the interface.
- In this model (sawtooth depth = 0.12 mm and height = 0.05 mm) the integrated epidermal volume is the closest to the epidermal volume of the standard planar model (epidermal depth = 0.09 mm). The fraction of the light that is absorbed in the model does not depend so much on the inter-surface profile (when the refractive indices are close as in this case) as on the total ‘thickness’ or the integrated epidermal volume.

These results indicated that the simple planar skin model is sufficiently accurate to use. In the remainder of the work the planar skin model was used.

### 3.4 EXPERIMENTAL VERIFICATION AND VALIDATION OF THE COMPUTER MODEL

The next phase in the development of the computer model (described in section 3.2) was to verify and validate the model. It is not possible or practical to validate the models against data from *in vivo* skin and therefore skin simulating phantoms (both solid and liquid) were used in the validation. The skin models used consisted of one, two or three layers depending on the phantom that was simulated. The phantoms were prepared and the optical properties measured on the IS system. These values were then used as input values into the computer model. Transmission measurements through the phantoms were compared with the predicted values from the model as discussed in the paper in section 3.5.

As has been discussed in section 2.5, the phantoms consisted of both absorbing and scattering particles. For the solid phantoms the transmission of resin used in this work was

measured with an Ocean Optics USB-4000 spectrometer from Ocean Optics Inc. (Florida, USA). The transmission through a 2 mm thick slice of cured resin (without scatterers and absorbers added) is shown in Figure 3.5. The variance is less than 10% over the wavelength range of interest and therefore it is acceptable for this work. The black ink used in the phantom preparation is not a standardised ink and the absorption spectrum was measured on the spectrometer. The absorption is nearly constant over the wavelength range used (Figure 3.6).

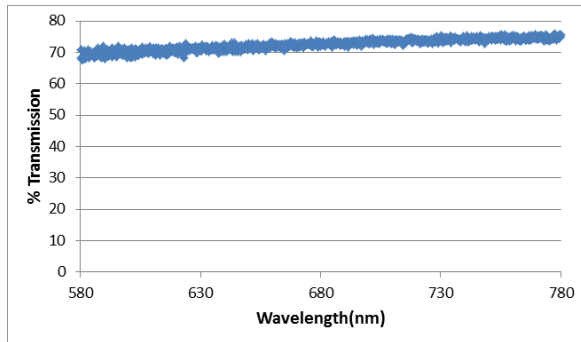


Figure 3.5: Transmission through the resin without the addition of absorbers and scatterers.

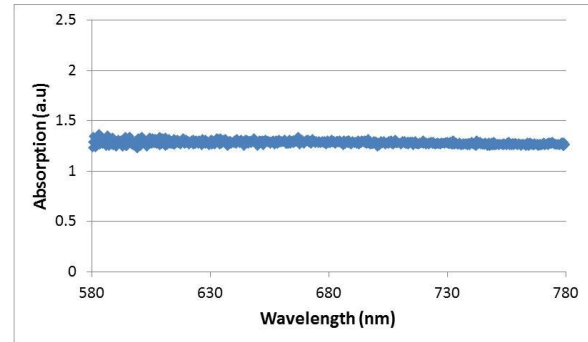


Figure 3.6: Absorption spectrum of the black ink used in the experiments.

In the comparison between the physical skin simulating models (various phantoms) and the computer models evaluations were done with a HeNe laser at a wavelength of 632.8 nm. In the comparison tests both the backscattered light and the light transmitted through the phantoms were evaluated. The backscattered light in the model, as detected on the back reflectance detector (see Figure 3.2), was compared to backscatter measurements on the physical phantom in the Integrating Sphere (IS) system. The IS transmission measurements were compared to the measurements on the transmission detector in the model (see Figure 3.2).

Intensity profiles at the back of the computer model were compared with intensity profiles of CCD images taken of the back of the phantom.

The computer model was optimised on one of the solid phantoms. As discussed in section 3.5, the optimisation was done in terms of:

- Slice thickness
- Number of voxels
- Number of rays
- Sensitivity to  $g$

### 3.5 PAPER ON THE EXPERIMENTAL VALIDATION OF THE COMPUTER MODEL

The paper *Experimental verification of a computer model for light–tissue interaction* was published in *Lasers in Medical Science* (2012) Volume 27, p79-86:

<http://www.springerlink.com/content/5154qr4103161214/fulltext.html>.

In presenting the paper here minor changes have been made. In order to allow for indexing, the Figure, Equation and Table numbers have been changed to be consistent with the rest of the chapter. For consistency, the referencing style of the thesis has also been applied to the paper instead of the numerical format prescribed by the journal. These changes have been applied to all the published papers presented in this thesis.

The data presented in Table 3.8 seems strange at a first glance. The sum of the absorbed, reflected and transmitted light does not add up to 100%. This is most likely due to the high scattering in the IL sample ( $\mu_s = 29.897 \text{ mm}^{-1}$ ) as compared to the solid phantom ( $\mu_s = 10.38 \text{ mm}^{-1}$ ). Light scattered and leaving the sample on the circular edges of the IL was not recorded in the model and may account for the “losses”.

# Experimental verification and validation of a computer model for light–tissue interaction

A E Karsten<sup>1,2</sup>, A Singh<sup>1</sup>, M W H Braun<sup>2</sup>

<sup>1</sup> Biophotonics Group, National Laser Centre, CSIR, P. O. Box 395, Pretoria, 0001, South Africa

<sup>2</sup> Department of Physics, University of Pretoria, Pretoria, 0002, South Africa

## ABSTRACT

Laser light is used frequently in both diagnostics and treatment of patients. For any laser treatment to be effective it is important to deliver the correct dose at the treatment site. Human skin scatters and absorbs laser light in the visible wavelength region which results in a decrease in fluence rate some distance into the skin. Computer simulations can be used to predict the fluence rate at the treatment site. Liquid and solid phantoms were prepared and the optical properties were measured. These values were then used as input values to a commercial software package simulating the different layers of skin representing phantoms. The transmission and reflected fractions of the different phantoms were measured with an integrating sphere and compared with the computer simulations. The results showed very good agreement with the measured values and the model can therefore be used with confidence to predict fluence rate at any treatment site inside the skin.

**Keywords:** laser, light propagation, tissue, phantom

## INTRODUCTION

Laser and light treatment modalities in the health and beauty fields are increasing rapidly world-wide. A large number of these treatments need to penetrate through some skin layers before reaching the target treatment area.

It is well reported in literature that the optical properties of human skin tissue influence the absorption and scattering of light through the tissue (Star WM, 1988), (Grossweiner LI, 1997), (Tuchin V, 2000), (Drakaki E, 2005), (Jacques SL, 2010). Absorption is wavelength dependent and is influenced by skin type. Melanin in the skin (present in the epidermis) is responsible for skin colour and absorbs light in the visible and near infrared (near IR) part of the light spectrum. The different skin types (Type I –VI on the Fitzpatrick scale (Agache P, 2004)) have different concentrations of melanin. In the South African population all the skin types are represented which poses a challenge in determining the correct dose for laser or light based treatment modalities.

Photodynamic therapy (PDT), a light based treatment for skin cancer, is currently under investigation in various research laboratories. The initial screening of the drug for a specific cancer is normally done on mono cell layers without the inclusion of the outer skin layers that are present during treatment in a clinical setting.

Computer modelling can be an invaluable tool to determine the laser dose that reaches the treatment site. The accuracy of any mathematical model depends on both the accuracy of the input parameters and the assumptions made in the model.

The aim of this work is to determine if the commercial software package, ASAP from Breault Research, for raytracing through turbid media, can be used to determine the fluence rate ( $W/cm^2$ ) at a pre-determined depth into the sample. If this can be achieved, the software can then be used to implement different geometries, including tumours in the skin, for the different skin types and accurately predict the fluence rate at the treatment depth.

A computer model of the interaction of light with skin was developed in the ASAP environment and tested on skin simulating phantoms. The total light transmitted through and reflected off several skin simulating phantoms were measured and compared with the values predicted by the computer model.

### Optical properties

In this paper the following optical properties will be used:

- Absorption coefficient ( $\mu_a$ ): the attenuation of light through a sample due to the absorption of the light.

- Scattering coefficient ( $\mu_s$ ): the attenuation of light through a sample due to the scattering of the light in the medium.
- Total attenuation coefficient ( $\mu_t$ ):  $\mu_t = \mu_s + \mu_a$
- Anisotropy ( $g$ ): the angular distribution of scatter in the medium ( $g = \langle \cos\theta \rangle$ ). The value of  $g$  varies between -1 and 1 (backscatter to forward scatter). For  $g = 0$ , the model describes a material with a uniform probability of scattering at all angles, but as  $g$  approaches 1 the distribution becomes highly peaked in the forward direction.
- Angular distribution of light scattered by small particles is described by the Henyey-Greenstein model. This model has been applied to numerous situations, ranging from the scattering of light by biological tissue to scattering by interstellar dust clouds (Henyey L, 1941). In this work, the angular distribution of scattered light is given by:

$$\rho(\theta) = \frac{1}{4\pi} \frac{1 - g^2}{[1 + g^2 - 2g\cos(\theta)]^{3/2}} \quad (3.4)$$

- Reduced scattering coefficient ( $\mu'_s$ ): a parameter combining the scattering coefficient ( $\mu_s$ ) and the scatter directionality ( $g$ ). This is a parameter normally measured in turbid media.

$$\mu'_s = (1 - g)\mu_s$$

According to Star (Star WM, 1997), measuring  $g$  accurately is very difficult. For most tissue types, including skin, the condition for validity of the diffusion approximation ( $\mu_a \ll \mu'_s$ ) is satisfied in the visible wavelengths (Star WM, 1997). This means that the precise value of  $g$  is not needed for the regions far from the boundaries and the light source. For the calculation of the light distribution in skin it is then sufficient to measure only  $\mu_a$  and  $\mu'_s$  accurately while knowing the value of  $g$  approximately. The sensitivity of the total transmission through the sample, to changes in  $g$  while keeping  $\mu'_s$  ( $\mu'_s = (1 - g)\mu_s$ ) constant, was tested for a specific solid phantom. Results showed very small changes and are described in more detail in the Optimisation section.

## MATERIALS AND METHODS

### Phantoms

Two types of phantoms were prepared, namely solid phantoms and liquid phantoms. Liquid phantoms are easy to prepare, but they have limitations in terms of durability/lifetime and only simple geometries are possible. Solid phantoms, which are much more cumbersome to prepare, have a longer lifetime and can be used to model multi layered structures, simulating the different layers of skin. Liquid phantoms are prepared from Intralipid, which is used widely to simulate skin and the optical properties are well documented in literature (Star WM, 1988), (van Staveren HJ, 1991), (Flock S, 1992), (Michielsen K, 1998), (Choukeife JE, 1999). For the solid phantoms the optical properties need to be measured.

### *Solid phantoms*

Solid phantoms were prepared according to the recipe of Firbank (Firbank M, 1993). Scattering particles (TiO particles, <25 nm particle size, density = 3.9 g/mL at 25 °C) and absorbing particles (Carbon Black) were added to an optically clear resin base (Akasel) and mixed for 5 minutes. Thereafter the hardener (Aka-cure slow, Akasel) was added to the mixture and stirred at 5 minute intervals, at least 3 times to prevent settling of particles and to eliminate air bubbles. The mixture was poured into plastic containers with a diameter of 30 mm. The mixture was allowed to cure at room temperature under a fume hood for 24 hours.

The cured solid phantoms were cut into discs with a thickness of approximately 2 mm and a diameter of 30 mm. The amount of TiO was varied while the carbon black concentration was kept constant. The ratios (per weight) were 133:2:31000 (TiO:carbon-black:resin) for sample A and 56.8:2:31000 for sample B. A two layered phantom was prepared by pouring one phantom mixture into the mould allowing it to cure and then pouring the new phantom mix onto the existing solid phantom. Both  $\mu_a$  and  $\mu'_s$  were measured with the integrating sphere (IS) system described below (Singh A, 2009).

### Liquid phantoms

The scattering properties of the skin can be simulated by Intralipid, a white, fat based emulsion with spherical particles (mean diameter of 0.4  $\mu\text{m}$ ) (Das BB, 1997). Intralipid phantoms were prepared by mixing 20% Intralipid (IL) (Sigma Aldrich, lot # 028K0740) and black ink. The black ink is used to simulate the absorption in skin. In the wavelength region 600–800 nm, the light scattering in tissue far exceeds the absorption in the tissue and therefore the diffusion approximation can be used and the reduced scattering coefficient ( $\mu'_s$ ) is sufficient to describe all the tissue scattering properties (Star WM, 1997), (Dimofte A, 2005).

The black ink was diluted in distilled water and the absorption coefficient ( $\mu_a$ ) of the black ink was measured with a HeNe laser at a wavelength of 632.8 nm, using Beer-Lambert law:

$$I = I_0 \exp^{-\mu_t d} \quad (3.5)$$

with

- $I$ : measured laser intensity after the sample
- $I_0$ : initial laser intensity
- $d$ : optical path length
- $\mu_t$ : total attenuation ( $\mu_t = \mu_s + \mu_a$ )

For the ink diluted in water it is assumed that there is no scattering, only absorption and therefore the Beer-Lambert law can be written as:

$$I = I_0 \exp^{-\mu_a d} \quad (3.6)$$

The ink solution and the IL solution were then mixed in a ratio of 1:1 before putting the liquid in the cuvette (Figure 3.7) for measurements.

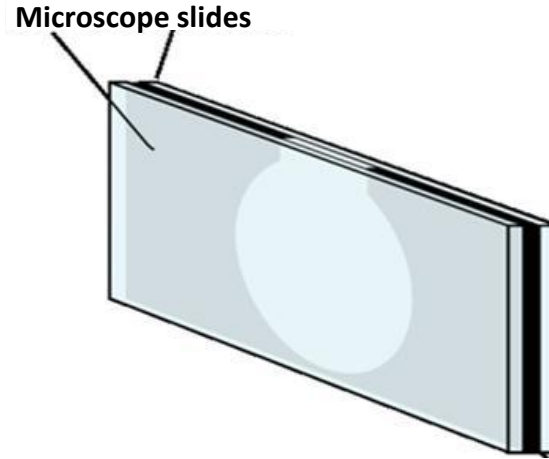


Figure 3.7: Schematic of the cuvettes for the Intralipid phantoms.

The optical properties of Intralipid-10% are well documented for a HeNe laser (wavelength of 632.8 nm (van Staveren HJ, 1991), (Flock S, 1992), (Michielsen K, 1998), (Choukeife JE, 1999). In the model,  $g$  was calculated using the relationship between  $g$  and  $\lambda$  in the work by Straveren (van Staveren HJ, 1991). The reduced scattering coefficient was calculated using the expression from the work of Michielsen (Michielsen K, 1998). His work expresses the reduced scattering coefficient as a function of the concentration of Intralipid. Most other papers only report the values for Intralipid-10%. The reduced scattering coefficient of the IL was calculated by (Michielsen K, 1998):

$$\begin{aligned} \mu'_s(\lambda = 633 \text{ nm}) &= 1.104 \text{ mm}^{-1} \times (\text{IL conc}) \\ \mu_a &= 0.15 \times 10^{-2} \text{ mm}^{-1} \times (\text{IL conc}) \end{aligned}$$

the value of  $\mu_a$  can be disregarded for the Intralipid-10%.

The anisotropy was calculated by (van Staveren HJ, 1991):

$$g = 1.1 - \alpha \lambda$$

where  $\alpha = 0.58 \mu\text{m}^{-1}$

### Cuvettes

The cuvette, used for the IL phantoms, was prepared by gluing two transparent glass microscope slides together with a black plastic spacer in-between (Figure 3.7). The optical path length,  $d$  (distance between the two microscope slides) is 1.47 mm and the diameter in the black plastic is 30 mm.

### Integrating sphere measurements

The measurements on the integrating sphere (IS) system (Figure 3.8) were used to extract the absorption and reduced scattering coefficients for each solid phantom using the multiple regression method on a well calibrated model (Dam JS, 2000(a)) (Singh A, 2008). These values were used as input parameters for the computer model.

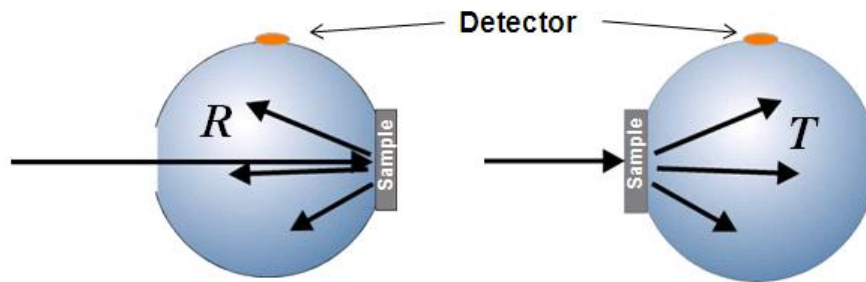


Figure 3.8: Integrating sphere system for reflection and transmission measurements.

The IS system comprised of a 7.4 mW HeNe laser ( $\lambda=632.8$  nm, JDS Uniphase laser) collimated to a beam diameter of 2-3 mm at the entrance and exit ports of the sphere (Labsphere, diameter 203.2 mm). Diffuse transmittance and reflectance and total transmittance for each sample was taken in triplicate on a spectrometer (Ocean Optics USB4000).

### Computer simulations

Raytracing software is commonly available and is mainly based on the Monte Carlo Multi-Layered (MCML) programs developed by Jacques (Jacques SL, 2008(a)). The software is downloadable online (Prah S, 2007(b)). These programs use the Monte Carlo raytracing techniques where ‘photons’ or ‘rays’ are traced through a medium with pre-defined absorption and scattering properties, until the photons are completely absorbed or leave the medium through the boundaries of the model (Breault Research, 2006), (Breault Research, 2007).

The Advanced Systems Analysis Program (ASAP®) from Breault Research, a commercial software package, with the advantage of allowing the user to *easily make geometry changes to a tissue model*, was used for this work. Different tissue geometries and tumours (e.g. layered structures, spheres and uneven surfaces) can be simulated in the software. Due to a lack of scientific publications making use of this software for modelling the interaction of light with skin tissue, this paper tries to verify the model with the use of custom made tissue simulating phantoms that can be measured in an optical laboratory. Before any laser treatment can progress to clinical trials, the safety of the treatment needs to be established. This model will be able to calculate the fluence rate at any given distance into the skin to ensure that safety standards and treatment parameters are met. The final aim of this work will be to model the absorption of laser light as it passes through skin tissue in the presence of a small tumour and the drug used in photodynamic therapy, a form of cancer therapy.

In the model the geometry of the phantom was described. A light source was created and traced through the sample. ASAP is in essence a non-sequential raytracing software package, which means that a ray interacts with the optical surfaces as they are encountered. Rays are allowed to split due to Fresnel reflections. ASAP ceases to trace a ray if its fluence rate has become too low. In ASAP a ray is a purely geometrical concept, it is basically a vector that simulates radiative transfer. Each ray has an individual power or fluence rate that contributes to the total fluence rate of the source (Breault Research, 2007).

In order to describe the optical system in ASAP, the geometry must be known as well as the absorption coefficient ( $\mu_a$ ), scattering coefficient ( $\mu_s$ ), anisotropy ( $g$ ) and refractive index ( $n$ ) of all the materials in the system.

A three layer slab model was created, but the number of layers can be changed as required. Two different geometries were created, the one presenting the liquid phantom or cuvette, and the other presenting a one or two layer solid phantom disc. A collimated light source with a diameter of 1 mm at a wavelength of 633 nm was used. A semi-spherical detector was placed behind the light source to collect all the back-scattered light and a round detector plate was placed 0.2 mm behind the last phantom surface in order to measure the transmitted light. These two detectors only serve as evaluation surfaces and are not part of the calculations in the models. 3.1 million rays were traced through the system. For evaluations the phantom was divided into three dimensional pixels (or voxels) of about  $0.1 \times 0.1 \times 0.1 \text{ mm}^3$ . The phantom was divided into thin slices (0.1 mm thick) in the Z-direction and the number of slices depended on the thickness of the sample. The absorption in each of the voxels is recorded. The total absorption in each layer is calculated as well as the absorption in the sides of the phantom (ring part of the disc). The transmitted light is measured with the circular detector just after the last surface of the phantom and the back-scattered light is measured with the semi-spherical detector behind the light source (Figure 3.9). In this model, the angular distribution of scatter is given by the Henyey-Greenstein phase function (Henyey L, 1941), discussed under Optical Properties.

The geometric parameters and optical properties of the IL phantoms are given in Tables 3.3 and 3.4. Six different IL phantoms were prepared. All the optical properties were kept the same except for the absorption coefficient.

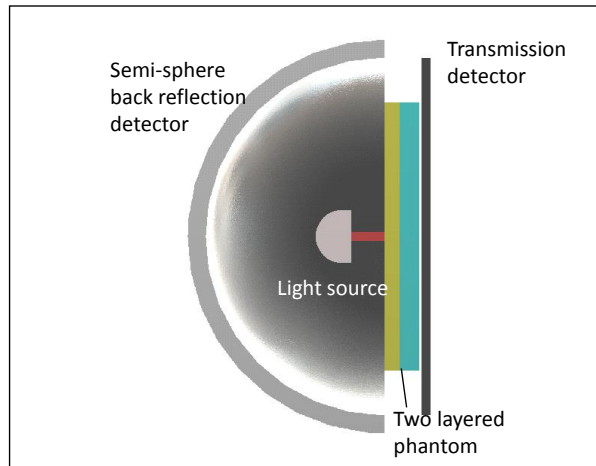


Figure 3.9: Side view of the computer model of a two-layered solid phantom. The semi-sphere back reflector detector as well as the circular detector plate is visible.

Table 3.3: Geometric parameters for the IL phantoms.

Layer	Width (mm)	Length (mm)	Diameter (mm)	Thickness (mm)
Glass	39	77	-	1.09
IL	-	-	30	1.47

Table 3.4: Optical parameters for the IL phantoms used in the model.

Sample	$\mu_a (\text{mm}^{-1})$	$\mu_s (\text{mm}^{-1})$	$g$	$n$
Glass	-	-	-	1.5
ILA	0.0000	39.897	0.72329	1.33
ILB	0.0515			
ILC	0.0816			
ILD	0.1665			
ILE	0.2350			
ILF	0.4565			

Table 3.5: Optical parameters for the solid phantoms. Parameters for the A and B samples are given. Sample C used the  $\mu_a$  and  $\mu_s$  values from A and B respectively for the 2 layers in the phantom.

Sample	$\mu_a$ (mm <sup>-1</sup> )	$\mu_s$ (mm <sup>-1</sup> )	$d$ (mm)	$n$	$g$
A	0.268	10.38	1.66	1.4	0.79
B	0.138	4.85	2.3	1.4	0.79
C	A and B values	A and B values	3.9 (1.7+2.2)	1.4	0.79

In all the calculations the step size was kept at 0.001 mm, which is small compared to  $\mu_t^{-1}$ , the average mean free path length of a photon (Prahl SA, 1989).

For each sample the absorption in each layer or slice is calculated. The fluence rate through the last layer in the sample is also calculated. The total transmitted power of the light through the sample (as a percentage of the input power) is measured with the IS system and with the detector plate in the model. The back-scattered light as a percentage of the input power, was also measured for all the phantoms using the IS system. In the model the backscattered light is 'measured' on the semi-sphere detector.

### Optimisation

Sensitivity of the model was tested on the solid phantom B. The following parameters were evaluated: effect of slice thickness, number of voxels, number of rays and sensitivity to  $g$ . The results are summarised in Table 3.6.

Table 3.6: Optimisation results showing the total absorption (mW) through the phantom, absorption (mW) in the last layer, the transmitted power (mW) and the standard deviation (Stdev) of the data.

Parameter	Total Absorption		Absorption in last layer		Transmitted	
	Mean	Stdev	Mean	Stdev	Mean	Stdev
Slice thickness (0.209-0.035 mm)	5.83E-1	1.58E-3	-	-	1.73E-1	0
# voxels (100-400)	5.85E-1	1.66E-4	1.10E-2	3.99E-4	1.73E-1	0
# rays (3.1M, 19.6M, 78.5M)	5.85E-1	0	1.12E-2	0	1.73E-1	0
$\mu_s$ and $g$	4.16E-1	1.13E-3	1.05E-2	5.66E-4	1.74E-1	1.18E-3

- Slice thickness:
  - The effect of the slice thickness (normally around 0.1 mm) was evaluated to establish if that has an effect on the total transmission through the sample. For the sample thickness of 2.3 mm the number of slices varied between 11 and 66 resulting in slice thicknesses between 0.209 mm and 0.035 mm.
  - Conclusion: Changes in the slice thickness does not significantly affect the output parameters. The model was standardised on a slice thickness of 0.1 mm.
- Number of voxels:
  - Changing the number of voxels in the X and Y directions from 100 to 400 resulted in small changes in the total absorption through the model and the absorption in the last layer.
  - Conclusion: 300 voxels were used in the X and Y direction to correspond to the 0.1 mm intervals of the Z-direction.
- Number of rays:
  - The number of rays traced through the sample was tested for 3.1, 19.5 and 78.5 million. The changes in the number of rays did not influence the total transmission or absorption results.
  - Conclusion: Simulations were all done with 3.1 million rays because of the reduced computing time required. Imaging simulations were done with the higher number of rays.
- Sensitivity for the model to  $\mu_s$  and  $g$ :
  - The product ( $\mu'_s = (1 - g)\mu_s = 1.019$  mm<sup>-1</sup>) was kept constant and the value of  $g$  varied from 0.6 – 0.8 with corresponding changes in  $\mu_s$ . The total absorption, transmitted light and the absorption in the last layer were relatively constant when 3.1 million rays were traced.
  - Conclusion: The model is insensitive to changes in  $g$ , while keeping the product ( $\mu'_s = (1 - g)\mu_s$ ) constant (Star WM, 1997).

### Experimental verifications

The IS system described earlier was used to measure the transmitted power as well as the back scattered power of each sample. The back plane (last surface) of each sample was also imaged with a CCD camera. The imaging experimental setup is shown in Figure 3.10. A Spiricon camera with detector dimensions 7.1 mm x 5.4 mm was used. An external lens was placed between the phantom and the camera and a magnification ( $M=v/u$ ) of 0.5 was used. Absorbing neutral density filters from Thorlabs were put in front of the detector to protect the camera from damage.

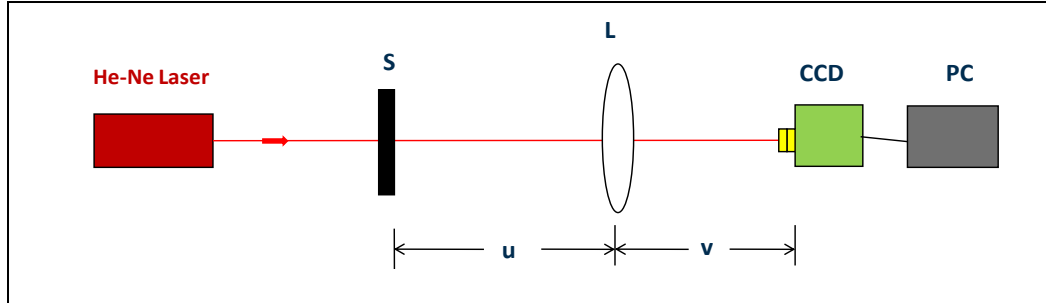


Figure 3.10: Experimental setup: S (Sample), L (Lens  $f=150\text{mm}$ ,  $D=50.8\text{mm}$ ), CCD (Camera), PC (Computer),  $u$  (Object distance = 450 mm),  $v$  (Image distance = 225 mm),  $F$ = filters,  $M$  ( $v/u$ )= 0.5, HeNe Laser power = 9 mW.

## RESULTS

The results for the absorption and transmission measurement comparisons are evaluated first and then the results for the imaging experiments on the IL samples.

### Transmitted and reflected power

Results comparing the reflective (%Refl) and transmission (%Trans) measurements on the IS with the calculations through the model as well as the total absorption (%Abs) through the model are presented in Tables 3.7 and 3.8.

#### *Solid phantoms*

Table 3.7: Comparisons between the model and measured values for the solid phantoms.

Sample	%Abs	%Trans (IS)	%Trans (Sim)	%Refl (IS)	%Refl (Sim)
A	65	9.9	8.8	27.4	25
B	59	19.3	17	25.3	24
C	70	3.0	2.7	26.6	26

All three samples gave good agreement when comparing the light transmitted through the phantom and the backscattered light calculated by the computer model and measured on the IS system.

#### *Liquid phantoms*

Table 3.8: Comparisons between the model and measured values for the liquid phantoms.

Sample	%Abs	%Trans (IS)	%Trans (Sim)	%Refl (IS)	%Refl (Sim)
ILA	0	12	7.6	72	63.6
ILB	7.4	7	6.7	61	60.6
ILC	13.1	6.6	6.2	59	59.1
ILD	21.1	2	5.0	55	54.8
ILE	27.9	1.9	4.2	54	51.8
ILF	44.2	0.29	2.4	39	44.0

The agreement between the measured and calculated values for the transmission and reflectance for the pure IL sample (ILA) and the sample with a high absorption coefficient (ILF) are not as good for the solid samples. However the agreement between the IS measurements and the simulations on the phantoms containing

both IL and a lower concentration black ink (samples ILB-ILE) was good. This is also the area of interest for most of the modelling work when applying the work to skin transmissions.

### CCD images

The back surfaces of the IL phantoms were imaged on a CCD camera as shown in Figure 3.10. The laser power was 9 mW. For consistency the same filters (Optical density 1 and 2) were used for each phantom. The images were converted to contour images and the minimum and maximum values for all three images were used to derive at 4 equally spaced contour values (Figure 3.11(a)). The fluence rate plot (images) of the last layer in the model was also converted to contour plots (Figure 3.11(b)) to compare with the CCD image contour plots.

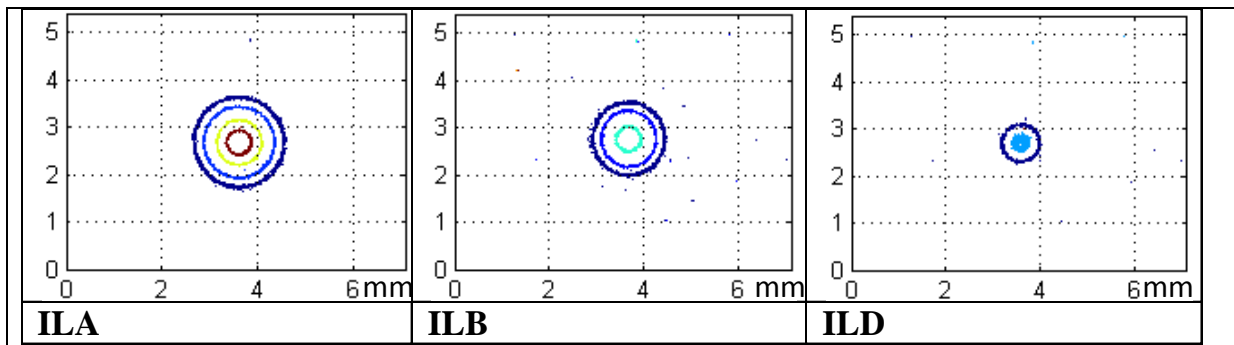


Figure 3.11(a): Fluence rate contour plots from the CCD images of the back surface of the liquid phantoms.

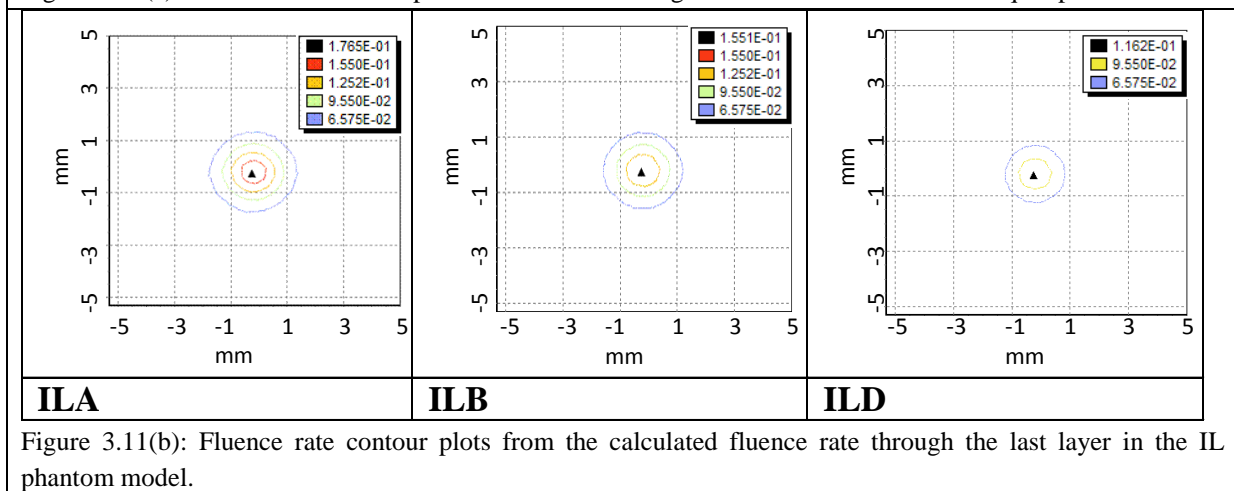


Figure 3.11(b): Fluence rate contour plots from the calculated fluence rate through the last layer in the IL phantom model.

There are very good similarities between the CCD image contour plots and those of the computer model in terms of the decreasing spot size of the beam with increased absorption in the sample.

## DISCUSSIONS AND CONCLUSION

The results in Table 3.7 showed good agreement between the calculated and measured values for the solid phantoms. There are small differences in the values for the solid phantom, that may be attributed to the error margins (<5%) that exists in the IS calibration model (Dam JS, 2000(a)) (Singh A, 2008).

Phantoms consisting of IL and ink are known to simulate the optical properties of skin. The  $\mu_a$  values used are comparable to the values that are expected to be present in the South African population. The parameters used for the IL simulations were based on the published data. The error margins for these values are not known. This, combined with errors introduced in the IS system when measuring low transmissions (typical error margin measures are  $\pm 5\%$ ) may explain the differences between the higher absorption samples in Table 3.8. These results imply that the model is not valid for the extremes in terms of no absorption and high absorption. This will impact on the validity of the model. At the present the model seems to be valid for  $\mu_a$  values between 0.05 and 0.26  $\text{mm}^{-1}$  for the HeNe wavelength of 632.8 nm. The validity of the model outside these boundaries still needs further investigations. The model was only tested for wavelength of 632.8 nm.

Qualitatively, the contour results also showed good agreement in terms of trends. Filters used in the experiments influence the ‘size’ of the beam in the image. The main value of the images is to show that the trend in terms of the beam size is the same in the phantoms as in the model.

The advantage of modelling software is the ability of the software to calculate the light fluence rate at any position inside the model/skin. If the front surface values (back-scattered) and the end values (transmission) of the model agree, it is a fair assumption to make that the values in the middle part are also correct. In the model an input power of 1 mW is used. In practice the laser power will be much more, but the important part is to use the absorbing, scattering and transmission fractions to predict the values for higher input powers. The model was also tested for an input power of 10 mW which resulted in higher absolute values (10X), but the same fractions.

The data presented here indicates that the computer model can be used to accurately calculate the light fluence rate at layers inside the sample. In the next phase more complicated geometries and drugs can be added to the model to simulate cancerous lesions.

### Acknowledgements

The authors would like to acknowledge Mr Bafana Moya for the work in the preparation and optical laboratories.

### References

- Breault Research. “The ASAP Primer.” <http://www.breault.com>. Breault Research. 2006. <http://www.breault.com/k-base.php> (accessed October 24, 2006).
- Agache P, Humbert P. *Measuring the skin*. ISBN 3-540-01771-2. Springer-Verlag, 2004.
- Breault Research. “ASAP Technical guide: Radiometric analysis.” <http://www.breault.com>. Breault Research. 2007. [http://www.breault.com/resources/kbasePDF/brotg0909\\_radiometry.pdf](http://www.breault.com/resources/kbasePDF/brotg0909_radiometry.pdf) (accessed 06 17, 2008).
- Choukeife JE, L’Huillier JP. “Measurements of Scattering Effects Within Tissue-like Media at Two Wavelengths of 632.8 nm and 680 nm.” *Lasers Med Sci* 14 (1999): 286–296.
- Dam JS, Dalgaard P, Fabricius PE, Andersson-Engels S. “Multiple polynomial regression method for determination of biomedical optical properties from integrating sphere measurements.” *Applied Optics* 39 (2000(a)): 1202-1209.
- Das BB, Liu F, Alfano RR. “Time-resolved fluorescence and photon migration studies in biomedical and model random media.” *Rep. Prog Phys* 60 (1997): 227-292.
- Dimofte A, Finlay JC, Zhu TC. “A method for determination of the absorption and scattering properties interstitially in turbid media.” *Phys. Med. Biol.* 50 (2005): 2291–2311.
- Drakaki E, Psycharakis S, Makropoulou M, Serafetinides AA. “Optical properties and chromophore concentration measurements in tissue-like phantoms.” *Optics Communications* 254 (2005): 40–51.
- Firbank M, Delpy DT. “A design for a stable and reproducible phantom for use in near infra-red imaging and spectroscopy.” *Phys. Med. Biol.* 38 (1993): 847-853.
- Flock S, Jacques S, Wilson B, Star W, van Gemert M. “Optical Properties of Intralipid: A phantom medium for light propagation studies.” *Lasers in Surgery and Medicine* 2 (1992): 510-519.
- Grossweiner LI. “PDT light dosimetry revisited.” *Journal of Photochemistry and Photobiology B: Biology* 38 (1997): 258-268.
- Heney L, Greenstein J. “Diffuse radiation in the galaxy.” *Astrophys. Journal* 93 (1941): 70-83.
- Jacques SL. “How tissue optics affect dosimetry of photodynamic therapy.. doi: 10.1117/1.3494561.” *Journal of Biomedical Optics*, 2010.
- Michielsen K, De Raedt H, Przeslawski J, Garcia N. “Computer simulation of time-resolved optical imaging of objects hidden in turbid media.” *Physics Reports* 304 (1998): 89-144.
- Prahl SA, Keijzer M, Jacques SL, Welch AJ. “A Monte Carlo Model of Light Propagation in Tissue.” In *SPIE Institute Series Vol. IS 5*, 102-111. SPIE, 1989.
- Singh A, Karsten AE, Dam, JS. “Robustness and accuracy of the calibration model for the determination of the optical properties of chicken skin.” *International Conference of the World Association of Laser Therapy*. Sun City: Medimond, 2008. 165-169.

- Singh A, Karsten AE, Mputle I, Chetty A and Naidoo K. "Determination of the optical properties of PNIPAAm gels used in biological applications." *European Conference on Biomedical Optics, Munich, 14-18 June 2009*. SPIE 7373, doi:10.1117/12.831882 , 2009. 107.
- SL, Jacques. "Modeling tissue optics using Monte Carlo modeling: a tutorial ." Edited by Roach WP, Thomas RJ Jacques SL. *Optical Interactions with Tissue and Cells XIX, SPIE Vol. 6854*. SPIE, 2008(a). 1605-7422.
- Star WM. "Light dosimetry in vivo." *Phys. Med. Biol.* 42 (1997): 763-787.
- Star WM, Marijnissen JPA, van Gemert MJC. "Light dosimetry in optical phantoms and in tissues: I. Multiple flux and transport theory." *Phys. Med. Biol.* 3, no. 4 (1988): 437-454.
- Tuchin V. *Tissue Optics: Light Scattering Methods and Instruments for Medical Diagnostics*. First. SPIE Press, 2000.
- van Staveren HJ, Moes CJM, van Marie J, Prahl SA, van Gemert MJC. "Light scattering in Intralipid-10% in the wavelength range of 400-1 100 nm." *Applied Optics* 31 (1991): 4507-4514.

### 3.6 CONTRIBUTION OF THE COMPUTER MODEL TO THE WORK

In this chapter the essential aspects of a layered skin model have been discussed. The computer model results compared favourably with laser measurements performed on skin simulating phantoms and may be implemented to predict laser fluence rate in skin.

The results of a computer model depend on both the accuracy of the model and the accuracy of the input data (optical properties). As discussed in section 2.3.2, data on the epidermal absorption coefficient for different skin phototypes are not readily available. This necessitated the development of a diffuse reflectance probe system that can be used to measure the absorption coefficient of skin *in vivo*.

In the next chapter the development of a system to extract the absorption coefficient from *in vivo* diffuse reflectance measurement is discussed as well as the measurements done on a small sample of the South African population.

## CHAPTER 4: THE ROLE OF EPIDERMAL ABSORPTION COEFFICIENTS APPLICABLE TO THE SOUTH AFRICAN POPULATION

As mentioned previously, the quality of any computer model is determined by the applicability of the assumptions and the accuracy of the input data. In the epidermal layer, the absorption coefficient of the epidermis is an important parameter as it contributes to the reduction in fluence rate as the light propagates through the tissue. As discussed in section 2.3.2 the values of  $\mu_a$  for the epidermis are not readily available in the literature for the different skin phototypes (see Table 2.3). The South African population presents a wide variety of skin phototypes. The difference in epidermal absorption of the different skin phototypes is an important parameter in laser treatment planning.

A non-invasive diffuse reflectance optical system was developed to calculate  $\mu_a$  from actual reflectance measurements. After the system was calibrated on liquid skin simulating phantoms, 30 volunteers were recruited at the National Laser Centre (NLC, CSIR) and measurements were done according to approved ethics protocols. Ethics approval was obtained from both the CSIR (Ref 17/2011, Appendix I) and the University of Pretoria (EC110830-060, Appendix II).

### 4.1 DIFFUSE REFLECTANCE THEORY AND MODEL DEVELOPMENT

The reflectance probe calibration and data reduction methods are mainly based on the work of Zonios (Zonios G, 2006), (Zonios G, 2008(a)). In order to use the diffuse reflectance theory, a few assumptions need to be made. These are that the tissue is a homogenous, semi-infinite and turbid medium (Zonios G, 2006). Part of the light incident on the tissue surface (skin) will be absorbed (dependent on  $\mu_a$ ) while part of the non-absorbed light will be scattered multiple times and eventually exit the skin surface as diffused reflected light as illustrated in Figure 4.1 (same as Figure 2.10 in section 2.3.1.6).

The total diffuse reflection ( $R_t$ ) is given by (Zonios G, 2006):

$$R_t = \frac{\mu'_s}{\mu'_s + \mu_a} \quad (4.1)$$

$R_t \rightarrow 0$  for high absorbance skin and  $R_t \rightarrow 1$  for low absorbance skin. This derivation is acceptable on a qualitative basis, but for a more quantitative expression an empirical factor,

$k$ , is introduced to rescale  $\mu'_s$  with  $\mu'_s/k$ . Introducing this in Eq 4.1 results in the following equation:

$$R_t = \frac{1}{1 + k \frac{\mu_a}{\mu'_s}} \quad (4.2)$$

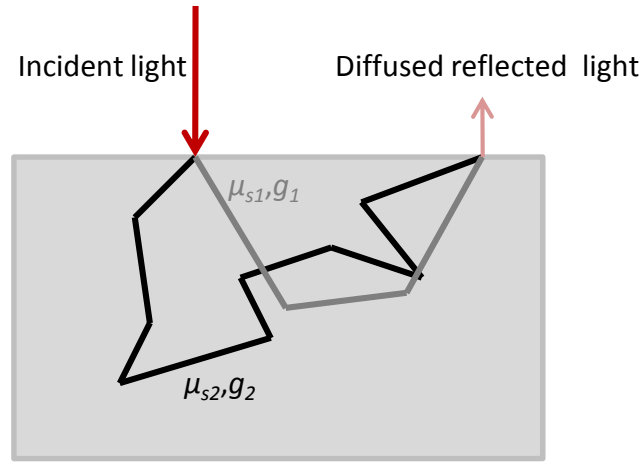


Figure 4.1: Diffuse reflected light.

Eq 4.2 is not suitable to describe diffuse reflectance measured with small diameter fibre optics. Due to the small fibre diameter (typically 200-400  $\mu\text{m}$ ), the fibre only measures part of the diffuse reflected light that emerges from the skin and breaks the inherent scale invariance in Eq 4.2. The scale invariance can be removed from Eq 4.2 by introducing an explicit dependence on  $\mu'_s$  and rewriting Eq 4.2 for the diffuse reflectance measured by the probe ( $R_p$ ) as (Zonios G, 2006):

$$R_p = \frac{1}{k_1 \frac{1}{\mu'_s} + k_2 \frac{\mu_a}{\mu'_s}} \quad (4.3)$$

where  $k_1$  and  $k_2$  are now parameters that depend on the probe geometry as well as the indices of reflection for the skin and the surrounding medium (usually air).

The major absorbing components in skin contributing to the absorption coefficient are the oxyhaemoglobin and deoxyhaemoglobin concentrations ( $c_{HbO_2}$  and  $c_{Hb}$ ), oxygen saturation ( $\alpha$ ) and melanin concentration ( $c_{mel}$ ). Water is also an absorber in skin, but in the wavelength band considered in this work (450-800 nm), the contribution of water is at least an order of magnitude smaller than that of the blood and melanin (see Figure 2.7) and is not included. The absorption of haemoglobin and melanin are wavelength dependent and contribute to the absorption coefficient through (Zonios G, 2006):

$$\mu_a(\lambda) = c_{HbO_2}[\alpha\varepsilon_{HbO_2}(\lambda) + (1 - \alpha)\varepsilon_{Hb}(\lambda)] + c_{mel}\varepsilon_{mel}(\lambda) \quad (4.4)$$

with:

$c_{HbO_2}$  = oxyhaemoglobin concentration

$c_{mel}$  = melanin concentration

$\varepsilon_{HbO_2}(\lambda)$  = extinction coefficient for oxyhaemoglobin (Prahl S, 1999)

$\varepsilon_{Hb}(\lambda)$  = extinction coefficient for deoxyhaemoglobin (Prahl S, 1999)

$\varepsilon_{mel}(\lambda)$  = extinction coefficient for melanin (Jacques SL, 1998(a))

$\alpha$  = oxygen saturation level of blood, defined as the ratio of the oxygenated

blood to the total blood concentration  $\alpha = \frac{c_{HbO_2}}{c_{HbO_2} + c_{Hb}}$

In order to model the scattering coefficient an effective scattering size ( $d_s$ ) is introduced as follows (Zonios G, 2008(a)):

$$\mu'_s(\lambda) = \left[ 1 - \left( \frac{d_0}{d_s} \right)^{1/2} \left( \frac{\lambda - \lambda_1}{\lambda_2 - \lambda_1} \right) \right] \mu'_s(\lambda_1) \quad (4.5)$$

with:

$d_0$  = constant = 0.0625  $\mu\text{m}$  (Zonios G, 2006)

$d_s$  = effective scatter size

$\lambda_1$  = min ( $\lambda$ ) = 450 nm

$\lambda_2$  = max ( $\lambda$ ) = 800 nm

The linear dependence of  $\mu'_s$  on wavelength is a reasonable approximation and is supported by the Mie theory for spherical scatterers (Zonios G, 2001). In the diffuse reflection model used for this work the particle size parameters were combined in a single parameter,  $c_d$ , that is related to the particle size. Eq 4.5 was then simplified to (Zonios G, 2008(b)):

$$\mu'_s(\lambda) = \left[ 1 - c_d \left( \frac{\lambda - \lambda_1}{\lambda_2 - \lambda_1} \right) \right] \mu'_s(\lambda_{min}) \quad (4.6)$$

with:

$c_d$  = scatter size parameter

$\lambda_1$  = min ( $\lambda$ ) = 450 nm

$\lambda_2$  = max ( $\lambda$ ) = 800 nm

The MATLAB function LSQCURVEFIT was used to solve Eq. 4.3 in a least-squares sense using nonlinear curve-fitting. The measured probe reflectance is described mathematically in terms of five coefficients ( $c_{HbO_2}$ ,  $\alpha$ ,  $c_{mel}$ ,  $c_d$ ,  $\mu'_s(\lambda_{min})$ ) that are adjusted to

best match the equation to the experimental data. The function requires an initial estimate of the parameters to be optimized and has the option to include constraints. According to the MATLAB online documentation the algorithm is a “subspace trust-region method and is based on the interior-reflective Newton method” described by Coleman (Coleman T, 1994), (Coleman T, 1996), where each iteration involves the approximate solution of a large linear system using the method of preconditioned conjugate gradients (PCG).

In Eq 4.4 provision is made for only one melanin extinction coefficient ( $\varepsilon_{mel}$ ) and the dominant eumelanin was used. For some of the volunteers, specifically those from southern Asian descent, significant poorer fit results were obtained for the measured  $R_p$  data. Further investigations led to the postulation that the melanin parameter in Eq. 4.4 should account for both the eumelanin and pheomelanin contributions. Eq. 4.4 was then rewritten to explicitly be dependent on both types of melanin:

$$\mu_a(\lambda) = c_{HbO_2}[\alpha\varepsilon_{HbO_2}(\lambda) + (1 - \alpha)\varepsilon_{Hb}(\lambda)] + c_{Eu}\varepsilon_{Eu}(\lambda) + c_{Pheo}\varepsilon_{Pheo}(\lambda) \quad (4.7)$$

with:

$c_{Eu}$  = eumelanin concentration

$c_{Pheo}$  = pheomelanin concentration

$\varepsilon_{Pheo}(\lambda)$  = extinction coefficient for pheomelanin (Jacques SL, 1998(a))

$\varepsilon_{Eu}(\lambda)$  = extinction coefficient for eumelanin (Jacques SL, 1998(a))

and others as used in Eq. 4.4

The measured probe reflectance can now be described mathematically in terms of six coefficients ( $c_{HbO_2}$ ,  $\alpha$ ,  $c_{Eu}$ ,  $c_{Pheo}$ ,  $c_d$ ,  $\mu'_s(\lambda_{min})$ ) that are adjusted to best match the equation to the experimental data. The data and fit results of three different volunteers are shown in Figure 4.2 for the two models. Model A2 (Eq 4.4 for  $\mu_a$ ) only uses a single melanin parameter and model D2 (Eq. 4.7 for  $\mu_a$ ) uses both the eumelanin and pheomelanin parameters. There is a definite improvement when model D2 is used on the medium skin phototype (Asian descent) without negative impact on the other skin phototypes.

The ability of the algorithm to separate the coefficients was tested by generating a curve with 6 coefficients with some random noise, representative of typical measured  $R_p$  values. The algorithm was then applied to the curve in the same manner that it was used on the measured data. In Table 4.1 the fitted parameters are compared with the input data to the curve and the typical fitted curves are shown in Figure 4.3.

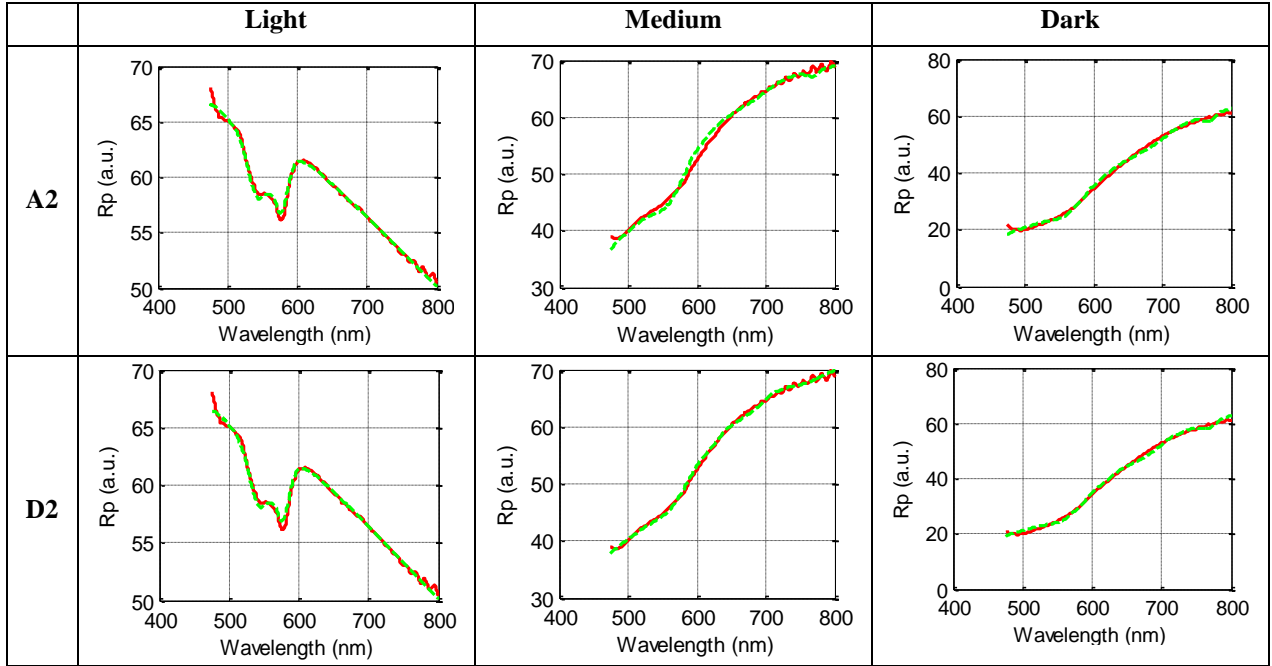


Figure 4.2: Comparing the two different melanin models for three volunteers each representing a different skin phototype. Model A2 only uses a single melanin parameter and model D2 uses both eumelanin and pheomelanin. Solid lines (—) represent the experimental data and the dashed lines (---) the fitted curve.

Table 4.1: Fitted parameters as compared to the input parameters into the algorithm.

Parameter	Set 1		Set 2	
	Input	Fitted	Input	Fitted
1	$3.20000 \times 10^{-5}$	$3.19565 \times 10^{-5}$	$8.00000 \times 10^{-5}$	$7.87171 \times 10^{-5}$
2	$1.00000 \times 10^{-2}$	$1.66647 \times 10^{-2}$	$7.00000 \times 10^{-1}$	$7.18282 \times 10^{-1}$
3	$7.75600 \times 10^{-3}$	$7.55275 \times 10^{-3}$	$8.00000 \times 10^{-3}$	$7.80733 \times 10^{-3}$
4	$2.60000 \times 10^{-4}$	$2.79790 \times 10^{-4}$	$2.00000 \times 10^{-3}$	$2.04942 \times 10^{-3}$
5	$1.00000 \times 10^0$	$9.99749 \times 10^{-1}$	$4.00000 \times 10^{-1}$	$3.96303 \times 10^{-1}$
6	$1.58000 \times 10^0$	$1.57090 \times 10^0$	$2.00000 \times 10^0$	$1.97998 \times 10^0$

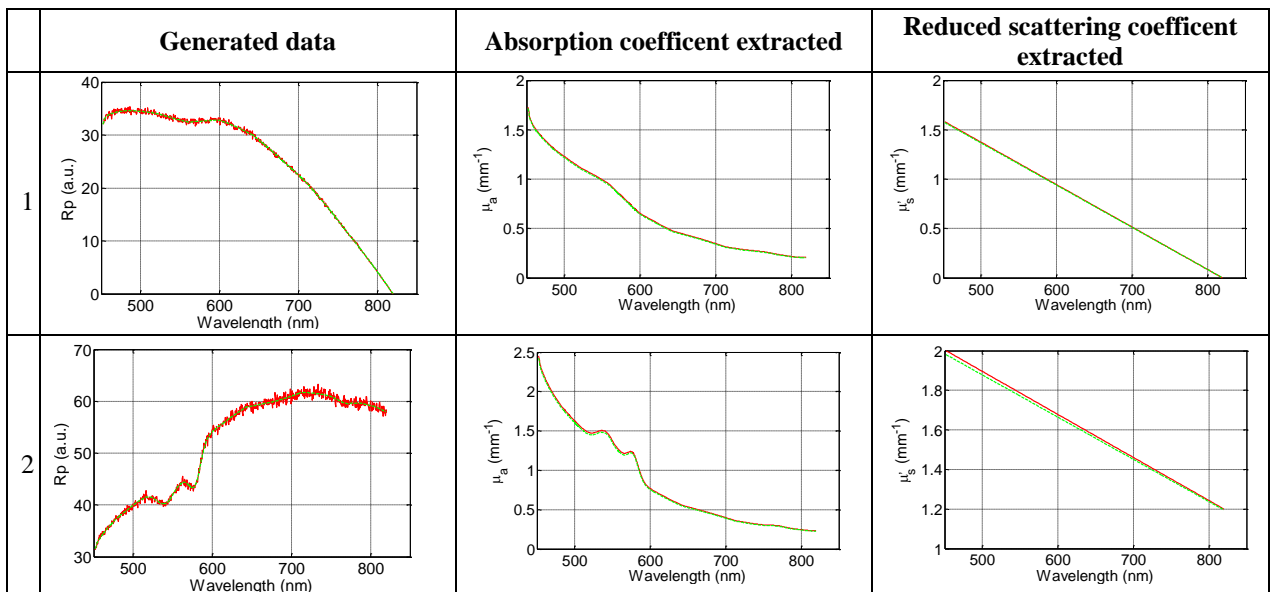


Figure 4.3: Comparison of input values to the fitted values for two different test cases. Solid lines (—) represent the input data and the dashed lines (---) the fitted curve.

## 4.2 PROBE CALIBRATION

An integrated diffuse reflectance probe (DRP) (R200-7-UV-VIS from Ocean Optics Inc. Florida, USA) was used in the experiments. The optimal transmission of the probe is between 250 and 800 nm. The probe contains seven fibres each with a diameter of 200  $\mu\text{m}$ . Six fibres arranged in a ring are used for light delivery and the 7<sup>th</sup> fibre in the centre of the probe is used to collect the diffuse reflected light (Figure 2.13 in section 2.4.2). A halogen white light source (HL-2000, Ocean Optics Inc. Florida, USA) emitting between 450 and 900 nm was used as illumination source. The reflected light is collected in the central fibre and used as input to an USB-4000 spectrometer (also from Ocean Optics). A reflectance standard, WS-1 Spectralon (Ocean Optics Inc. Florida, USA), was used to calibrate the reflectance probe for each set of experiments.

A set of 60 liquid calibration phantoms, consisting of IL and black ink, were prepared. This is different to the calibration phantoms used by other DRP users, but is a well-recognised procedure for preparing skin simulating phantoms (Star WM, 1988), (van Staveren HJ, 1991), (Farrel TJ, 1992), (Flock S, 1992), (Michielsen K, 1998). In the original paper (Zonios G, 2006) the calibration tissue phantoms were prepared by using 1.0  $\mu\text{m}$  diameter polystyrene beads (suspended in deionised water) and haemoglobin from bovine blood prepared in distilled water. For the calibration of the DRP in this work the IL+ink phantom solutions were poured into transparent 6-well cell culture plates (Lasec SA) with a diameter of  $\sim 35$  mm. The same phantom preparation procedures were followed here as for the liquid phantoms used in the computer model calibration as discussed in section 3.5 which contains the paper on the experimental verification of the computer model.

The thickness of the phantoms in the culture plates was about 10 mm. The culture plates were placed on a black paper during the experiments to ensure that no light is reflected from the table surface. Visual inspection in a dark room also indicated that no light was leaving the phantoms through the sides. Calibrations were performed in a laboratory where the temperature was kept between 22 and 23  $^{\circ}\text{C}$ . The experimental setup as used for both the calibration and the volunteers are shown in Figure 4.4.

A Z-translation stage was used to hold the probe in a vertical position, facing downwards. The probe was lowered until it just entered into the liquid phantom.

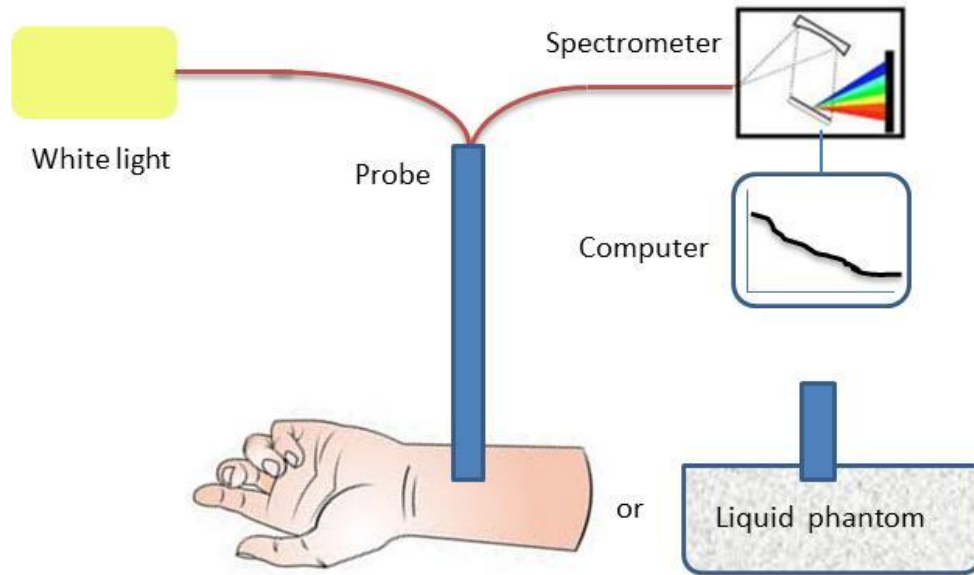


Figure 4.4: Experimental setup for calibration and *in vivo* tests.

All the evaluations were done at two wavelengths, 633 and 676 nm. These wavelengths were chosen for the applicability to PDT (676 nm) and the data available in literature for HeNe lasers ( $\lambda=632.8$  nm). For the phantoms the values of  $\mu_a$  were limited to between 0.068 and  $2.479 \text{ mm}^{-1}$  due to practical considerations in transmission through the phantoms. For high  $\mu_a$  the transmitted power became too low for accurate measurements. The optical path length for the cuvette used in the absorption measurements was 1.22 mm. In the calibration work  $\mu'_s$  was restricted between 0.539 and  $3.558 \text{ mm}^{-1}$ .

Before each set of experiments, the system was calibrated with the WS-1 reflectance standard. The standard was placed 5 mm from the end of the probe tip. This method was described by Zonios (Zonios G, 2008(a)). The DRP could not be placed in contact with the standard as this resulted in saturation of the detector during the reflectance standard measurements. Great care was taken during the experiments to ensure that the standard was always placed the same distance from the probe's end, by using the Z-translation stage to position the probe vertically.

The basic calibration procedure as described by Zonios (Zonios G, 2006) was followed to extract the probe's geometrical calibration constants  $k_1$  and  $k_2$ . The calibration constants were then used in the optimising algorithm to extract the  $\mu_a$  and  $\mu'_s$  values from measured data on the 30 volunteers.

The calibration process and control experiments are further described in the paper in section 4.2.1. In the calibration work two laser wavelengths (633 and 676 nm) were used in all the comparisons.

#### **4.2.1 Paper on Reflectance probe calibration**

The paper on the calibration of the reflectance probe was published online on 13 March 2012 in Lasers in Medical Science:

[<http://www.springerlink.com/content/e037471262313654/fulltext.html>].

As discussed in section 3.5, minor formatting changes have been made to the paper to follow the style of the thesis.

## Diffuse reflectance spectroscopy as a tool to measure the absorption coefficient in skin: system calibration

A E Karsten<sup>1,2</sup>, A Singh<sup>1</sup>, P A Karsten<sup>3</sup>, M W H Braun<sup>2</sup>

<sup>1</sup> Biophotonics Group, National Laser Centre, CSIR, P. O. Box 395, Pretoria, 0001, South Africa

<sup>2</sup> Department of Physics, University of Pretoria, Pretoria, 0002, South Africa

<sup>3</sup> Ballistics Research Group, Denel Land Systems, P O Box 7710, Pretoria, 0001, South Africa

### ABSTRACT

An individualised laser skin treatment may enhance the treatment and reduces risks and side-effects. The optical properties (absorption and scattering coefficients) are important parameters in the propagation of laser light in skin tissue. The differences in the melanin content of different skin phototypes influence the absorption of the light. The absorption coefficient at the treatment wavelength for an individual can be determined by diffuse reflectance spectroscopy, using a probe containing 7 fibres. Six of the fibres deliver the light to the measurement site and the central fibre collects the diffused reflected light. This is an *in vivo* technique, offering benefits for near real time results. Such a probe, with an effective wavelength band from 450 nm-800 nm, was used to calibrate skin-simulating phantoms consisting of intralipid and ink. The calibration constants were used to calculate the absorption coefficients from the diffuse reflectance measurements of three volunteers (skin phototypes, II, IV and V) for sun exposed and non exposed areas on the arm.

**Keywords:** diffuse reflectance, absorption coefficient, skin-simulating phantom

### INTRODUCTION

Lasers and other light sources offer non-invasive benefits both in terms of diagnostic and treatment modalities. For most non-invasive laser procedures, light must penetrate through some skin layers before reaching the diagnostic or treatment site. The absorption and scattering of laser light are the two major interactions that reduce the laser light intensity as it passes through human skin. The major contributors to the absorption of light in human skin are haemoglobin (both oxyhaemoglobin and deoxyhaemoglobin) and melanin, present in the epidermal layer. Scattering is mainly the result of the sub-cellular structures. The three most important properties for describing the propagation of light through tissue are the absorption ( $\mu_a$ ) and scattering ( $\mu_s$ ) coefficients as well as the anisotropy ( $g$ ). In order to reduce the complexity, the last two parameters are usually combined as the reduced scattering coefficient ( $\mu'_s = (1 - g)\mu_s$ ) (Pfefer TJ, 2003), (Martelli F, 2010).

In individualising laser treatment, the absorption and scattering properties at the treatment locale of the patient must be known. Due to the variance in the available data and the limited data available in open literature, it became important to measure the absorbance of different skin phototypes in the research laboratory. One of the non-invasive methods that can be used to determine  $\mu_a$  and  $\mu'_s$  is diffuse reflectance spectroscopy, a method that detects light that has been scattered multiple times within the sample (skin) under investigation. (Johns M, 2005), (Zonios G, 2006), (González FJ, 2010). The method was successful in identifying the change in a melanin index for specific skin conditions.

Epidermal melanin is responsible for skin phototype or skin tone (Costin GE, 2007). Melanin in the skin is located in the melanosomes and consists of solid absorbing particles with a diameter between 20-40 nm. It is an optically dense material which absorbs radiation in the visible wavelength range. Melanin is not a single pigment, but is composed of a number of different chromophores with varying optical and physical properties (Alaluf S, 2001). Melanin can broadly be divided into two families according to chemical structure and colour (Agache P, 2004). Eumelanins are black-brown in colour and are sulphur poor, while pheomelanins are yellow-reddish in colour and sulphur rich (Agache P, 2004), (Costin GE, 2007).

The composition of melanin in an individual depends on both genetic and environmental factors. Eumelanin provides better photo protection than pheomelanin. In healthy, photo-exposed skin, the distribution of melanin is different depending on whether it was exposed to UVA, UVB or PUVA (Psoralen + UVA, a treatment for psoriasis, eczema and vitiligo). Exposure to UVB radiation increases the production of melanin and the transfer into keratinocytes. This leads to an increase in the concentration of melanin in the epidermis. After UVA exposure, a large amount of melanin is found in melanocytes and keratinocytes of the basal layer, but the melanin concentration in the rest of the epidermis remains unchanged (Agache P, 2004).

This paper describes the calibration process for a diffuse reflectance probe system on a set of liquid calibration phantoms prepared from intralipid (IL) and black ink. The calibrated system is then used to deduce the absorption coefficient from measurements on three individuals with different skin phototypes (skin phototypes II, IV and V on the Fitzpatrick scale (Fitzpatrick TB, 1988)). Ethics approvals for these measurements were obtained from both the University of Pretoria (EC110830-060) and the CSIR (Ref 17/2011).

## MATERIALS AND METHODS

### Diffuse reflectance measurements

Light that enters the skin is scattered due to various processes. The most important processes are the changes in optical density between different layers (refractive index changes), Mie scattering (scattering where the scattering particles are of the order of the photon wavelength) and Rayleigh scattering (scattering of light by structures much smaller than the photon wavelength). Some of the light is scattered back in the direction from where it entered and leaves the skin (see Figure 4.5). This diffusely reflected light can be collected and measured with a fibre optic based diffuse reflectance probe (see Figure 4.6).

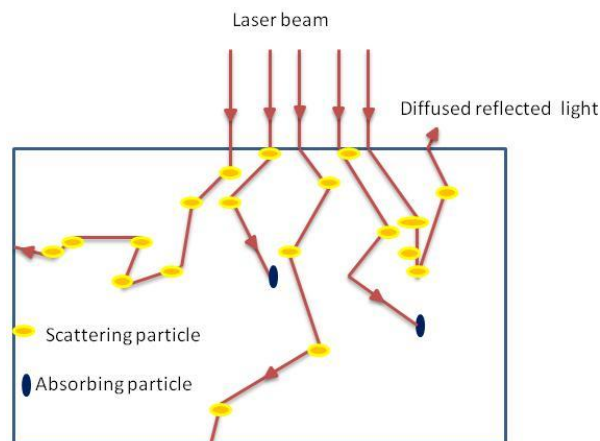


Figure 4.5: Absorption and scattering in skin.

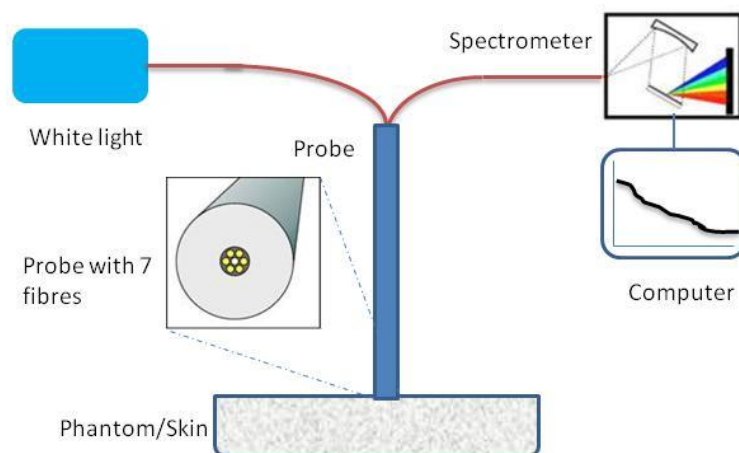


Figure 4.6: Experimental setup.

A diffuse reflectance probe usually consists of a few optical fibres grouped together. A typical configuration consists of 7 optical fibres, with 6 light transmitting fibres arranged around the central collecting fibre. The signal collected by the central fibre is used as the input to a spectrometer. The diffused back reflected signal as a function of wavelength is recorded on a computer.

The diffuse reflectance spectra measured with the optical probe contain entangled information regarding the scattering and absorption of light in tissue (Zonios G, 2006). A spectral analysis model describing the diffuse reflectance in terms of these optical properties was proposed by Zonios (Zonios G, 2006). This is an inverse model, starting with the measured diffuse reflectance spectrum to calculate the reduced scattering coefficient ( $\mu'_s$ ) and the absorption coefficient ( $\mu_a$ ) of the skin sample measured. To minimize mathematical complexity, the skin is modelled as a semi-infinite turbid medium. Zonios tested the validity of the model on tissue-simulating phantoms and with the analysis of diffuse reflectance spectra from human skin *in vivo* (Zonios G, 2006).

Due to the limitation imposed by measurements with a diffuse reflectance probe, the diffuse reflectance can be expressed by an explicit dependence on  $\mu'_s$  (Zonios G, 2006). The reflectance probe backscattered signal ( $R_p$ ) can be described by (Zonios G, 2006):

$$R_p(\lambda) = \frac{\mu'_s(\lambda)}{k_1 + k_2\mu_a(\lambda)} \quad (4.8)$$

where  $k_1$  and  $k_2$  are parameters that depend on the probe geometry and need to be calculated from the probe calibration data.

The absorption coefficient ( $\mu_a$ ) as a function of wavelength is given by:

$$\mu_a(\lambda) = c_{HbO_2}[\alpha\varepsilon_{HbO_2}(\lambda) + (1 - \alpha)\varepsilon_{Hb}(\lambda)] + c_{Eu}\varepsilon_{Eu}(\lambda) + c_{Pheo}\varepsilon_{Pheo}(\lambda) \quad (4.9)$$

and the reduced scattering coefficient ( $\mu'_s$ ) by:

$$\mu'_s(\lambda) = \left[1 - c_d \left(\frac{\lambda - \lambda_1}{\lambda_2 - \lambda_1}\right)\right] \mu'_s(\lambda_{min}) \quad (4.10)$$

with:

$\varepsilon_{HbO_2}(\lambda)$  = extinction coefficient for oxyhaemoglobin (Prahl S, 1999)

$\varepsilon_{Hb}(\lambda)$  = extinction coefficient for deoxyhaemoglobin (Prahl S, 1999)

$\varepsilon_{Eu}(\lambda)$  = extinction coefficient for eumelanin (Jacques S, 2001)

$\varepsilon_{Pheo}(\lambda)$  = extinction coefficient for pheomelanin (Prahl S, 1999)

$c_d$  = parameter related to melanin particle size

$c_{HbO_2}$  = oxyhaemoglobin concentration

$c_{Hb}$  = deoxyhaemoglobin concentration

$\alpha$  = oxygen saturation level of blood, defined as the percentage of the oxygenated blood of the total blood concentration  $\alpha = \frac{c_{HbO_2}}{c_{HbO_2} + c_{Hb}}$

$\lambda_1$  = min ( $\lambda$ )

$\lambda_2$  = max ( $\lambda$ )

Eq. 4.10 describes a linear dependence of the reduced scattering coefficient on the wavelength. This is a reasonable approximation which is supported by Mie theory calculations for spherical scatterers with a Gaussian distribution in size (Zonios G, 2001).

### Experimental methods

The liquid phantoms were prepared from a mixture of 20% Intralipid (IL) (Sigma Aldrich, lot # 028K0740) and black ink (Trodar colour 7011). IL and ink are often used as optical simulants for human skin (van Staveren HJ, 1991), (Flock S, 1992). More detail on the phantom preparations can be found in (Karsten AE, 2012(a)).

A diffuse reflectance probe from Ocean Optics is used in the experiments. The illumination is done with a white-light source through the outer fibre ring and the diffused reflected data is collected through the centre fibre as illustrated in Figure 4.6. The diffuse reflectance probe system consists of the following components (see Figure 4.6):

- Diffuse reflectance probe, 5 mm outer diameter, (R200-7-UV-VIS, optimal transmission between 250-800 nm) with fibre diameter 200  $\mu\text{m}$  (Ocean Optics). The probe contains 7 fibres, 6 fibres in a ring for light delivery and the 7th fibre in the centre of the probe to collect the diffuse reflectance spectrum.
- Halogen white light source (HL-2000) emitting between 450 and 900 nm (Ocean Optics).
- USB-4000 spectrometer (Ocean Optics) sensitive between 350 nm and 1000 nm.
- Computer.
- WS-1 Spectralon reflectance standard (Ocean Optics), used to calibrate the reflectance data for each set of experiments.

Matching the wavelength transmission through the different components of the system results in an effective wavelength band from 450 nm-800 nm.

Before each set of experiments, the system was calibrated with the WS-1 reflectance standard and a calibrated solid phantom (reference phantom with known optical properties) to ensure proper operation of all the components of the system.

During phantom experiments, the probe was inserted, from the top, into the solution eliminating intralipid-air interfaces for the probe. The probe tip was facing vertically down towards the bottom of the container just touching the liquid.

Raw data collected by the probe was corrected for the detector dark current and normalised with respect to the white reflecting standard (WS-1) according to eq. 4.11. The Reflectance wizard in the Spectra Suite software from Ocean Optics was used to measure the back reflected light.

$$R_p(\lambda) = -\log_{10} \left[ \frac{I_{meas}(\lambda) - I_D(\lambda)}{I_{ref}(\lambda) - I_D(\lambda)} \right] \quad (4.11)$$

where:

- $I_{meas}(\lambda)$  = raw reflection data
- $I_D(\lambda)$  = detector dark current
- $I_{ref}(\lambda)$  = spectrum obtained from WS-1

All the measurements were done with the main lights in the laboratory switched off and only a reading lamp for lighting. During the experiments the light was turned away, to ensure that there is no interference from the light. This was tested by comparing spectra with the reading light turned away and spectra with the reading light switched off. The spectra were identical. The temperature in the laboratory was maintained between 22 and 23 °C.

### Calibration phantoms

Skin-simulating liquid phantoms consist of a mixture of IL and ink. The assumption is made that the IL does not absorb light and that the ink does not scatter light in the wavelength range used in this study. The IL and ink samples were prepared separately and characterised before mixing the IL and ink to form the skin-simulating phantoms used for calibration of the system. Each phantom consisted of 5 ml IL solution and 5 ml ink solution mixed together to form a 10 ml phantom. Eleven IL solutions and twenty ink solutions were prepared. Three of the IL solutions were mixed with the twenty ink solutions to form a 3x20 calibration matrix. The solutions were poured into transparent 6-well cell culture plates (Lasec SA) with a diameter of ~35 mm. The depth of the solution was ~10 mm. The 6 well plates were used to ensure that there are no interference from light reflected from the sides and bottom of the plate (semi infinite layer assumption). The plates were placed on a black absorbing surface and the probe was lowered with a translation stage to just touch the surface of the liquid phantom. An 8 mW HeNe laser ( $\lambda=632.8$  nm from Spectraphysics) and a locally constructed diode laser ( $\lambda=676$  nm) with output power 25 mW were used in the absorption measurement of the ink solutions.

The different IL concentrations used for the phantoms and the corresponding  $\mu'_s$  values (calculated from (Michielsen K, 1998)) are listed in Table 4.2. Absorption through the ink samples were measured with both lasers on three separate days. The Beer-Lambert law was used to calculate the  $\mu_a$  values for the different ink solutions listed in Table 4.3. The ink absorption values were averaged for the three measurements and the standard deviations calculated (Microsoft Excel 2007 calculations), are reported in Table 4.3. The range of  $\mu_a$  and  $\mu'_s$  values used were selected to cover the typical published  $\mu_a$  and  $\mu'_s$  values for skin (Tuchin V, 2007).

Table 4.2: IL concentrations and corresponding  $\mu'_s$  values at  $\lambda = 632$  and  $676$  nm.

IL sample	IL concentration (%/vol)	$\mu'_s$ at $\lambda = 632$ nm ( $\text{mm}^{-1}$ )	$\mu'_s$ at $\lambda = 676$ nm ( $\text{mm}^{-1}$ )
1	0.500	0.624	0.593
2	0.750	0.936	0.890
3	1.000	1.248	1.186
4	1.250	1.560	1.483
5	1.500	1.872	1.779
6	1.750	2.184	2.076
7	2.000	2.496	2.372
8	2.250	2.808	2.669
9	2.500	3.120	2.965
10	2.750	3.432	3.262
11	3.000	3.744	3.558

Table 4.3: Ink sample and the  $\mu_a$  values calculated with the Beer-Lambert law using the transmission measurements.

Ink sample	$\lambda = 632$ nm		$\lambda = 676$ nm	
	Average $\mu_a$ ( $\text{mm}^{-1}$ )	Standard deviation	Average $\mu_a$ ( $\text{mm}^{-1}$ )	Standard deviation
1	0.126	0.011	0.068	0.001
2	0.199	0.010	0.099	0.028
3	0.289	0.014	0.153	0.066
4	0.359	0.019	0.196	0.120
5	0.496	0.010	0.277	0.060
6	0.613	0.009	0.326	0.057
7	0.620	0.015	0.341	0.068
8	0.753	0.020	0.412	0.238
9	0.849	0.022	0.465	0.078
10	0.968	0.017	0.533	0.062
11	1.305	0.018	0.758	0.094
12	1.576	0.015	0.844	0.062
13	1.695	0.016	0.805	0.026
14	2.372	0.261	1.635	0.003
15	2.114	0.015	1.224	0.071
16	2.372	0.017	1.219	0.062
17	2.524	0.027	1.405	0.117
18	2.842	0.046	1.688	0.100
19	3.222	0.022	1.928	0.533
20	3.737	0.024	2.479	0.325

To evaluate the dependence of the diffuse reflectance ( $R_p$ ) as a function of  $\mu'_s$ , the eleven IL concentrations listed in Table 4.2 were used. Three IL samples (2, 6 and 11) were used in combination with the 20 ink samples to prepare 60 phantoms.

In order to extract the  $\mu_a$  values from the liquid phantoms, the extinction coefficient of the ink must be known. This can be derived via absorbance measurements. In order to verify the experimental procedure to extract the extinction coefficient, neutral density absorbing filters (OD = 0.2, 0.4 and 0.6) from Thor Labs were

used as ‘absorbers’. The neutral density filters do not have scattering materials and only act as absorbers. The filters were placed in-between the 676 nm laser and an Ophir power meter. The absorption coefficient was calculated by using the Beer-Lambert law.

$$I_a = I_0 e^{-\mu_a d} \quad (4.12)$$

with:

$I_a$  = light intensity after the ink/filter

$I_0$  = intensity from light/laser source

$d$  = optical path length (mm)

The absorbance was also measured with the Absorbance wizard in the SpectraSuite software from Ocean Optics. The extinction coefficient for each filter was then calculated from the absorbance data and used to calculate  $\mu_a$  by rewriting eq. 4.9 as

$$\mu_a(\lambda) = c_{filter} \varepsilon_{filter}(\lambda) \quad (4.13)$$

reflecting the absence of haemoglobin and the filter absorbance as substitute for melanin. The absorbance ( $A(\lambda)$ ), as measured by the Absorbance wizard is given by:

$$A(\lambda) = -\log_{10} \left( \frac{I_a(\lambda) - I_D(\lambda)}{I_0(\lambda) - I_D(\lambda)} \right) = OD \quad (4.14)$$

with:

$I_a(\lambda)$  = signal with the ink/filter

$I_0(\lambda)$  = signal from light source without ink/filter

$I_D(\lambda)$  = detector dark current as a function of wavelength

$OD$  = optical density

The absorption coefficient from the Absorbance wizard can then be calculated by:

$$\mu_a(\lambda) = -\left(\frac{1}{d}\right) \ln(10^{-A(\lambda)}) \quad (4.15)$$

Good agreement was found between the  $\mu_a$  values calculated using the Beer-Lambert law and the Absorbance wizard measurements. The results are listed in Table 4.4.

Table 4.4: Comparison between the different methods to calculate  $\mu_a$  for the neutral density absorbing filters at a wavelength of 676 nm.

Optical Density (from supplier @ 633 nm)	0.2	0.4	0.6
Optical Density (calculated @ 633 nm)	0.1859	0.3967	0.6019
Filter thickness (mm)	1.35	0.74	1.30
$I_0$ (mW)	25.6	25.8	26.4
$I_a$ (mW) after filter	16.5	10.6	7.0
$\mu_a$ (mm <sup>-1</sup> ) (Beer-Lambert)	0.3254	1.2021	1.0211
$\mu_a$ (mm <sup>-1</sup> ) (Absorbance wizard)	0.3035	1.1307	0.9799

The absorbance measured for the different filters as a function of wavelength is shown in Figure 4.7(a). The optical density (OD) for each filter is given in the graph and compares well with the suppliers specified OD at a wavelength of 633 nm. It shows very good correlation with the OD calculated from the Absorbance wizard measurements.

The same procedure was repeated to calculate the extinction coefficient of the ink. This derived ink extinction coefficient was then used to calculate  $\mu_a$  from the reflectance probe data in the phantoms (IL+ink). The result of the data points that adhere to the condition ( $\mu_a < \mu'_s$ ) are plotted in Figure 4.7(b) where the  $\mu_a$  values calculated from the reflectance probe measurements are compared to the true  $\mu_a$  values as per Table 4.3.

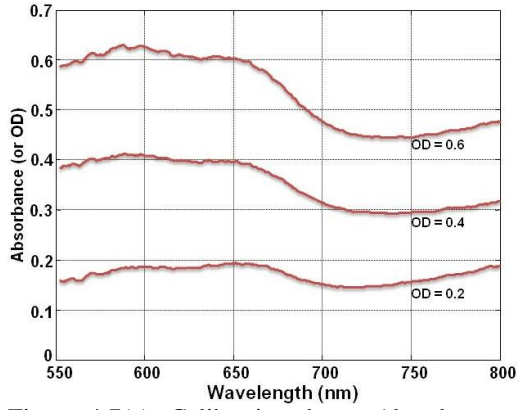


Figure 4.7(a): Calibration data - Absorbance as function of the wavelength for the different OD filters.

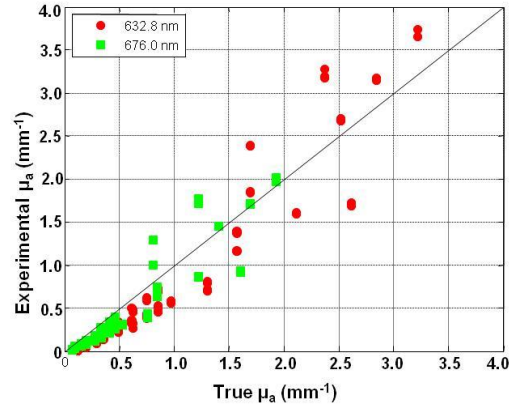


Figure 4.7(b): Calibration data -  $\mu_a$  values extracted from the DRP measurements compared to the true  $\mu_a$  values (measured using the beer Lambert law) of the ink phantoms.

### Diffuse Reflectance probe measurements on skin

Reflectance measurements were done on three South African volunteers with skin phototypes II, IV and V. The probe was placed on the measurement site, just touching the skin. Two different skin sites were measured on each volunteer:

- Inside upper arm (no/little sun exposure)
- Outside lower arm (sun exposed)

At each position three measurements were taken within a two minute period. All measurements were done on the same day. For both the skin data and the calibration data, the integration time for the probe measurements were 20 ms and the signal was averaged 4 times.

### Data analysis

The MATLAB function LSQCURVEFIT was used to solve eq. 4.8 in a least-squares sense using nonlinear curve-fitting. The measured probe reflectance is described mathematically in terms of 6 coefficients ( $c_{HbO_2}$ ,  $\alpha$ ,  $c_{Eu}$ ,  $c_{Pheo}$ ,  $c_d$ ,  $\mu'_s(\lambda_{min})$ ) that are adjusted to best match the equation to the experimental data. The function requires an initial estimate of the parameters to be optimized and has the option to include bound constraints. According to the MATLAB documentation the algorithm is a subspace trust-region method and is based on the interior-reflective Newton method described in (Coleman T, 1994), (Coleman T, 1996), where each iteration involves the approximate solution of a large linear system using the method of preconditioned conjugate gradients (PCG).

## RESULTS AND DISCUSSIONS

The skin-simulating liquid phantoms were used to determine the probe geometry calibrations constants  $k_1$  and  $k_2$  in eq. 4.8. Figure 4.8(a) shows the linear dependence of the reflectance probe values  $R_p$  on  $\mu'_s$ . This is consistent with data published by other authors using fibre optic probes to measure the diffused back reflectance (Amelink A, 2004), (Johns M, 2005), (Zonios G, 2006). The results are also consistent with previous findings that the linear dependence of  $R_p$  on  $\mu'_s$  is only valid for  $\mu'_s$  up to  $3.2 \text{ mm}^{-1}$  (Zonios G, 2008(a)).

The dependence of  $R_p$  on  $\mu_a$  exhibits the expected monotonic behaviour (Figure 4.8(b)). Diffused reflectance measurements for three different  $\mu'_s$  values, namely  $0.89$ ,  $2.076$  and  $3.558 \text{ mm}^{-1}$ , were fitted to eq. 4.8. Table 4.5 shows the fit results.

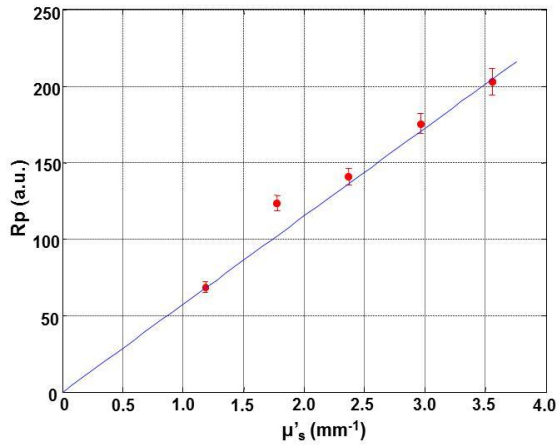


Figure 4.8(a): Reflectance probe measurement as a function of  $\mu'_s$  at  $\lambda=676$  nm when only IL was used ( $\mu_a = 0$ ).

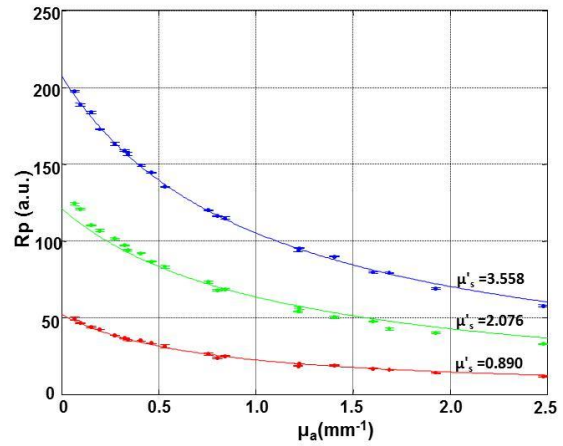


Figure 4.8(b): Reflectance probe measurement as a function of  $\mu_a$  at a  $\lambda=676$  nm for three different  $\mu'_s$  solutions.

Table 4.5: Geometrical parameters ( $k_1$  and  $k_2$ ), calculated from the reflectance measurements of the IL+ ink phantoms in Figures 4.8(a) and 4.8(b).

	$k_1$	$k_2$
Min	0.015247	0.015407
Max	0.017333	0.025437
Mean	0.016312	0.019144

### Skin measurements

Diffused reflectance as a function of wavelength is shown in Figure 4.9(a) for all three individuals. In some cases the three separate measurement lines are distinguishable (e.g. Type II Not exposed), but in other cases not (e.g. Type II sun exposed). The three measurements for each individual were averaged for the data analysis. Using eq. 5.8, the  $\mu_a$  values at wavelengths 633 nm and 676 nm were extracted and are shown in Figure 4.9(b). The data was analysed for the minimum, maximum and mean  $k_1$  and  $k_2$  values. The average values were plotted in Figure 4.9(b) and the error bars indicate the standard deviation of the data. For clarity, the values are also listed in Table 4.6.

Table 4.6: Absorption coefficients calculated using the mean  $k_1$  and  $k_2$  values for the different skin types at wavelengths of 633 nm and 676 nm.

Skin phototype	$\mu_a$ (mm <sup>-1</sup> ) Sun exposed		$\mu_a$ (mm <sup>-1</sup> ) Non exposed	
	633 nm	676 nm	633 nm	676 nm
II	0.0157	0.0112	0.0041	0.0021
IV	0.509	0.400	0.205	0.161
V	1.39	1.04	0.896	0.703

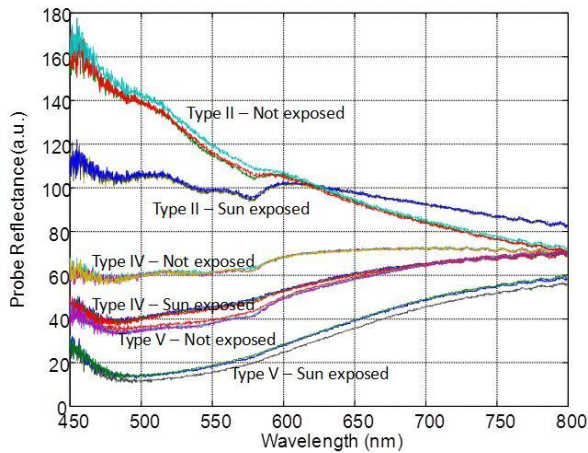


Figure 4.9(a): Reflectance probe measurements on three individuals with skin phototype II, IV and V. Three measurements were taken on both the lower outer arm (sun exposed) and the inner upper arm (not sun exposed).

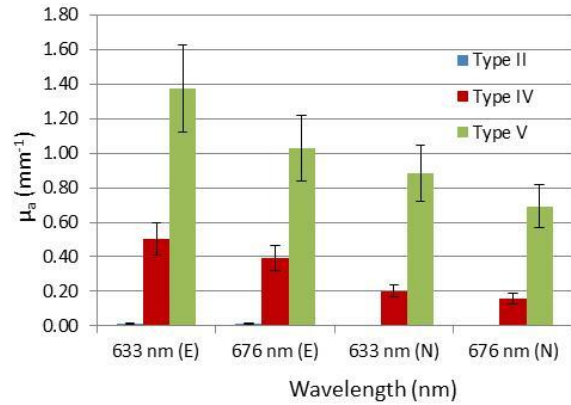


Figure 4.9(b): Absorption coefficient values calculated from the reflection probe measurements for three different skin phototypes at wavelengths 633 nm and 676 nm on sun exposed (E) and non- exposed (N) parts of the arm.

## CONCLUSIONS

Most papers reporting on the diffuse reflectance probe technique do not provide values for the absorption coefficient. Great care was taken in ensuring that the calibration models were set up correctly due to the influence of the calibration constants ( $k_1$  and  $k_2$ ) on the results. Originally all 60 IL+ink phantoms were used to compare the calculated absorption coefficient obtained using the reflectance probe to the absorption coefficient of the ink calculated using the Beer-Lambert law. The deviations were greatly reduced when only data points compliant with the diffusion condition  $\mu_a < \mu'_s$ , were used (Star WM, 1997), (Zonios G, 2001). The variance in the data was larger than anticipated, but when compared to other publications, the error bars are comparable (Tseng S, 2009).

*In vivo* skin measurements remain a challenge. The detection fibre in the reflectance probe has a diameter of only 200  $\mu\text{m}$ . During the skin measurements the probe was held in position on the same spot, but due to blood flow, breathing, unsteadiness of the volunteers, it is not easy to ensure that all three measurements were done under exactly the same conditions. Despite the limitations, relatively good agreement was found with Simpson (Simpson R, 1998(a)) where *ex vivo* skin samples were measured on an Integrating Sphere. Simpson used sample from areas of the skin that are not normally exposed to the sun. They measured  $\mu_a$  values, at a wavelength of 633 nm, of around  $0.035 \text{ mm}^{-1}$  for ‘caucasian’ skin and  $0.25 \text{ mm}^{-1}$  for ‘negroid’ skin. Tseng (Tseng S, 2009) measured  $\mu_a$  values of  $0.060 \text{ mm}^{-1}$  (for skin type I-II),  $0.062 \text{ mm}^{-1}$  (for skin type III-IV) and  $0.071 \text{ mm}^{-1}$  (for skin type V-VI) for the upper inner arm (not sun exposed) and  $0.063 \text{ mm}^{-1}$  (for skin type I-II),  $0.065 \text{ mm}^{-1}$  (for skin type III-IV) and  $0.074 \text{ mm}^{-1}$  (for skin type V-VI) for the dorsal arm (sun exposed).

In order to quantify the absorption coefficient for the range of the South African skin types a clinical test with more volunteers needs to be conducted. The results of such a study will enable laser users in the medical profession to individualise laser skin treatments.

## Acknowledgements

The authors would like to acknowledge Mr Bafana Moya for the work in the laboratories.

## References

- Agache P, Humbert P. *Measuring the skin*. ISBN 3-540-01771-2. Springer-Verlag, 2004.
- Alaluf S, Heath A, Carter N, Atkins D, Mahalingam H, Barrett K, Kolb R, Smit N. "Variation in Melanin Content and Composition in Type V and VI Photoexposed and Photoprotected Human Skin: The Dominant Role of DHI." *Pigment Cell Res* 14 (2001): 337–347.
- Amelink A, Sterenborg H, Bard M, Burgers S. "In vivo measurement of the local optical properties of tissue by use of differential path-length spectroscopy." *Opt. Lett.* 29 (2004): 1087-1089.
- Coleman T, Li Y. "An Interior Trust Region Approach for Nonlinear Minimization Subject to Bounds." *SIAM Journal on Optimization* 6 (1996): 418-445.
- Coleman T, Li Y. "On the Convergence of Reflective Newton Methods for Large-Scale Nonlinear Minimization Subject to Bounds." *Mathematical Programming* 67 (1994): 189-224.
- Costin GE, Hearing VJ. "Human skin pigmentation: Melanocytes modulate skin color in response to stress." *FASEB J* 21 (2007): 976-994.
- Fitzpatrick TB. "The validity and practicality of sunreactive skin type-I through type-VI." *Arch Dermatol* 124 (1988): 869–871.
- Flock S, Jacques S, Wilson B, Star W, van Gemert M. "Optical Properties of Intralipid: A phantom medium for light propagation studies." *Lasers in Surgery and Medicine* 2 (1992): 510-519.
- González FJ, Martínez-Escanamé M, Muñoz RI, Torres-Álvarez B, Moncada B. "Diffuse reflectance spectrophotometry for skin phototype determination." *Skin Research and Technology* 16 (2010): 397-400 .
- Jacques S. *Oregon Medical Laser Centre website*. 2001. <http://omlc.ogi.edu/spectra/melanin/index.html> (accessed November 24, 2011).
- Johns M, Giller CA, German DC, Liu H. "Determination of reduced scattering coefficient of biological tissue from a needle-like probe." *Optics Express* 13 (2005): 4828-4842.
- Karsten AE, Singh A, Braun MW. "Experimental verification and validation of a computer model for light–tissue interaction." *Lasers Med Sci* 27 (2012a): 79–86.
- Martelli F, Del Bianco S, Ismaelli A, Zaccanti G. *Light Propagation through Biological Tissue and Other Diffusive Media*. ISBN 978-0-8194-7658-6. SPI Press , 2010.
- Michielsen K, De Raedt H, Przeslawski J, Garcia N. "Computer simulation of time-resolved optical imaging of objects hidden in turbid media." *Physics Reports* 304 (1998): 89-144.
- Pfefer TJ, Matchette L S, Bennett CL, Gall JA, Wilke JN, Durkin AJ, Ediger M. "Reflectance-based determination of optical properties in highly attenuating tissue." *Journal of Biomedical Optics* 8 (2003): 206–215.
- Prahl S. *Oregon Medical Laser Centre website - Optical Absorption of Hemoglobin*. 1999. <http://omlc.ogi.edu/spectra/hemoglobin/index.html> (accessed November 24, 2011).
- Simpson R, Kohl M, Essenpreis M, Cope M. "Near-infrared optical properties of ex vivo human skin and subcutaneous tissues measured using the Monte Carlo inversion technique." *Phys. Med. Biol* 43 (1998(a)): 2465–2478.
- Star WM. "Light dosimetry in vivo." *Phys. Med. Biol.* 42 (1997): 763-787.
- Tseng S, Bargo P, Durkin A, Kollias N. "Chromophore concentrations, absorption and scattering properties of human skin in-vivo." *Optics Express* 17 (2009): 14599-14617.
- Tuchin V. *Tissue Optics: Light Scattering Methods and Instruments for Medical Diagnostics*. 2nd edition, p 165-175. SPIE Press, 2007.
- van Staveren HJ, Moes CJM, van Marie J, Prahl SA, van Gemert MJC. "Light scattering in Intralipid-10% in the wavelength range of 400-1 1 00 nm." *Applied Optics* 31 (1991): 4507-4514.
- Zonios G, Bassukas I, Dimou A. "Comparative evaluation of two simple diffuse reflectance models for biological tissue applications." *Applied Optics* 47 (2008a): 4965-4973.
- Zonios G, Bykowski J, Kollias N. "Skin melanin, haemoglobin, and light scattering properties can be quantitatively assessed in vivo using diffuse reflectance spectroscopy." *J. Invest. Dermatol* 117 (2001): 1452-1457.
- Zonios G, Dimou A. "Modeling diffuse reflectance from semi-infinite turbid media: application to the study of skin optical properties." *Optics Express* 14 (2006): 8661-8674.

### 4.3 CONTRIBUTION OF THE DIFFUSE REFLECTANCE PROBE CALIBRATION TO THE WORK

The principle of using the diffuse reflectance probe measurements to calculate the absorption coefficient of skin has been established in the work described so far in this chapter. The initial measurements led to the notion that the contribution of eumelanin and pheomelanin should be separated in the data extraction algorithm. This was a new insight that was not explicitly found in the literature.

The next step was to implement the diffuse reflectance probe measurement system to determine the absorption coefficients for various South African skin phototypes. This work is described in the next section.

### 4.4 *IN VIVO* TESTS

In order to determine the extent of the absorption coefficient variation to be encountered in the South African population, a diverse group of 30 volunteers were recruited from the NLC staff for *in vivo* measurements with the diffuse reflectance probe. Due to the voluntary nature of the recruitment, the clinical study did not include individuals with skin phototype VI on the Fitzpatrick scale. In order to protect anonymity, only numbers were used to identify volunteers. For record purposes the outer part of the hand of each volunteer was placed next to a Fitzpatrick colour card to identify the skin phototype (see Figure 4.10, the same as Figure 2.5). This process has limited accuracy as there are only six colours/shades available to classify an individual's skin phototype, but at least provides some indication of the skin phototype. This was all that was required to do the initial data analysis.

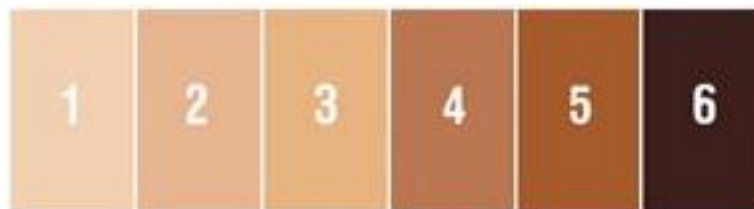


Figure 4.10: Fitzpatrick skin tone colour card.

As discussed in section 4.1, the results indicated the need to separate the contribution of melanin into the eumelanin and the pheomelanin. In literature there are a few hints to this effect, but to the knowledge of the author, it has not explicitly been used in the modelling work to extract the melanin concentrations. Two authors (Alaluf S, 2002(a)),

(Zonios G, 2006) indicated that there is a difference between the ratios of eumelanin and pheomelanin for individuals of different descent. In the later work of Zonios (Zonios G, 2008(c)) they favour a formulation that expresses the melanin extinction coefficient in terms of an exponential function with the decay governed by a parameter  $k_m$ . The value of  $k_m$  dictates the rate of the melanin extinction as function of wavelength. The shape of the extinction curves for different values of  $k_m$  do not provide an exact match for the published extinction curve data of eumelanin and pheomelanin. Being a parameter derived from the curve fit to the reflectance probe data, its purpose is to strike an amiable match between the distinct eumelanin and pheomelanin behaviour. Zonios (Zonios G, 2008(c)) has reported  $k_m$  values between 2 and 3 for skin phototype VI, which favours the more gradual extinction associated with predominantly eumelanin. For skin phototype III, they reported  $k_m$  values between 5 and 6.5, which accounts for the more rapid extinction associated with a greater presence of pheomelanin (Figure 4.11, the same as Figure 2.4 section 2.2.1.2).

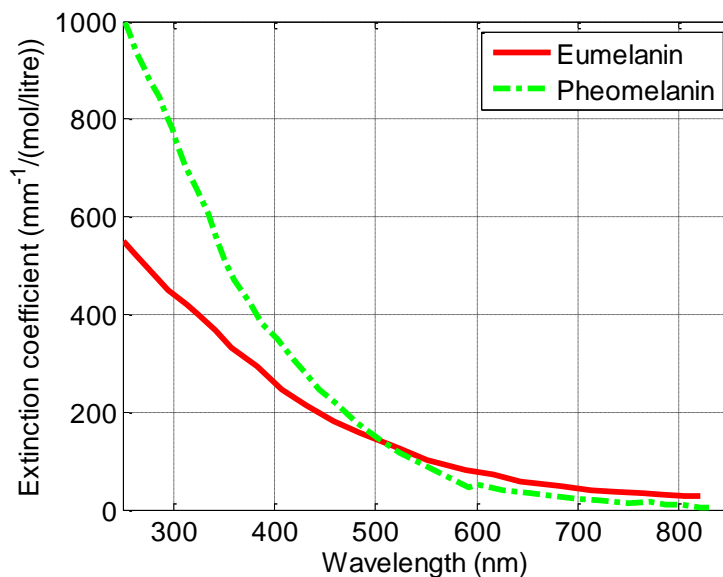


Figure 4.11: Absorption spectra of eumelanin and pheomelanin (data from (Jacques S, 2001)).

In a paper by Alulaf (Alulaf S, 2002(a)) it is stated:

“We observed a statistically significant trend (t-test;  $P < 0.05$ ), indicating that melanin composition becomes progressively more enriched with alkali soluble melanins as you move from the darkest (African) to the lightest (European) skin types. Similarly, a direct comparison of photoexposed and photoprotected skin within each ethnic group revealed (in most cases) a trend towards enrichment of alkali soluble melanins at photoprotected sites that was also consistent with previous observations, but was considerably smaller in magnitude than the variation in composition observed between different ethnic skin types.”

“As the relative contribution from different coloured melanin components varies in the skin, the colour of the final melanin pigment is likely to vary. Hence, skin may appear lighter, not only because it contains less melanin, but also because the melanin it contains is more lightly pigmented. Moreover, the manner in which this melanin is dispersed: either as single particles or as aggregated clusters may also affect how that final colour is perceived.”

Our results show that the ratio of eumelanin/pheomelanin concentrations for dark skin (phototype V) is 2.24 with a standard deviation of 1.82 and for the light skin phototypes I-III the ratio is 0.81 with a standard deviation of 0.30. Due to the limitations imposed by the ethical approval, the study could not include more volunteers in order to be able to statistically validate the data and compare the ratios. This is an area of research for the future.

Extracting the  $\mu_a$  values from the measured  $R_p$  spectra for the darker skin phototypes resulted in higher values than published in literature. Alaluf (Alaluf S, 2002(a)) reported eumelanin/pheomelanin concentration ratios for the sun-exposed ‘African skin’ (comparable to our phototype V skin) of 8.13 and 1.64 for the ‘European skin’ (comparable to our phototype I-II). Both ratios for Alaluf are about 3 times higher than our ratios. It should be noted that it is difficult to compare the results established by chemical extractions (used by Alaluf) with those of the integrated path optical method (used in this DRP work) in terms of the total absolute melanin ratios. At this point it may be important to note that the optical based values may be of more value for optical based treatments (laser based treatments) while chemical extraction may be more applicable to treatments based on pharmaceutical-chemical treatments.

Data presented in the paper below compares well with published data for the lower absorbance skin types (typically skin phototypes I-III). Our data indicated a difference in the  $\mu_a$  values for the skin areas exposed to sun and those that are not. This expected behaviour is also reported by Tseng (Tseng S, 2009) and Alaluf (Alaluf S, 2002(a)).

The depth of penetration for light in the diffuse reflectance measurements also has an effect on the calculated  $\mu_a$ . Meglinsky (Meglinsky IV, 2001) investigated the depth of measurement or measurement volume for different distances between the light source and the detector in diffuse reflectance systems. They concluded that a light source-detector spacing of 250  $\mu\text{m}$  primarily samples the epidermal layer and the papillary dermis. The light source-detector spacing in the probe used in this work was 200  $\mu\text{m}$ , indicating that the epidermal layer and the papillary dermis were sampled.

For the very light skin phototypes, the effect of the haemoglobin is visible in the  $R_p$  values (see Figure 4.12) through the local absorption peaks at 541 nm and 576 nm for

oxyhaemoglobin and 556 nm for deoxyhaemoglobin. This resulted in less accurate  $\mu_a$  values for the epidermis because the light also sampled the dermis (where the blood is present). The effect of such an error is not really significant in the application of this work. As reported later in Chapter 5, the effect of  $\mu_a$  between 0.001 and 0.05  $\text{mm}^{-1}$ , did not affect the light transmission values much. In the very dark skin phototypes (typically type V) in Figure 4.12, the effect of the haemoglobin is not visible in the  $R_p$  measurements. As such, the DRP is an applicable instrument to measure the absorption coefficient of the epidermis.

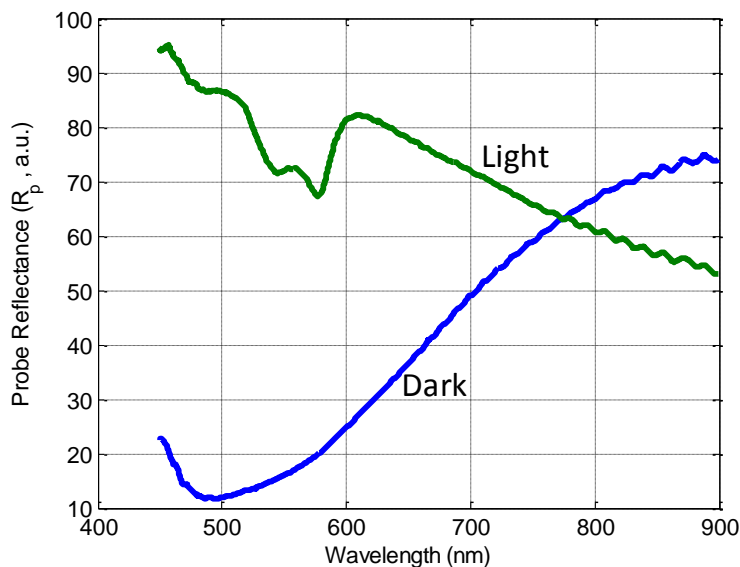


Figure 4.12: Reflectance measurements for two different skin phototypes.

More accurate methods may be available, but the diffuse reflectance probe offers a non-invasive, portable system with a quick turn-around time. It may be applicable in a clinical setting to quickly supply data that a health practitioner may use to establish optimal treatment parameters for an individual of any skin phototype.

#### 4.4.1 Paper on *in vivo* tests

The paper on the results of the *in vivo* study on the 30 volunteers was published online on 14 August 2012 in *Photochemistry and Photobiology* [doi: 10.1111/j.1751-1097.2012.01220.x].

Once again some minor alterations have been done to the published format of the paper to follow the style of the thesis.

## Diffuse reflectance spectroscopy as a tool to measure the absorption coefficient in skin: South African skin phototypes

A E Karsten<sup>1,2,\*</sup>, A Singh<sup>1</sup>, P A Karsten<sup>3</sup>, M W H Braun<sup>2</sup>

<sup>1</sup> Biophotonics Group, National Laser Centre, CSIR, P. O. Box 395, Pretoria, 0001, South Africa

<sup>2</sup> Department of Physics, University of Pretoria, Pretoria, 0002, South Africa

<sup>3</sup> Ballistics Research Group, Denel Land Systems, P O Box 7710, Pretoria, 0001, South Africa

\*Corresponding author's name and email: Aletta E Karsten (akarsten@csir.co.za)

### ABSTRACT

In any laser skin treatment, the optical properties (absorption and scattering coefficients) are important parameters. The melanin content of skin influences the absorption of light in the skin. The spread in the values of the absorption coefficients for the South African skin phototypes are not known. A diffuse reflectance probe consisting of a ring of six light delivery fibres and a central collecting fibre was used to measure the diffused reflected light from the arms of 30 volunteers with skin phototypes I-V (on the Fitzpatrick scale). The absorption coefficient was calculated from these measurements. This real time *in vivo* technique was used to determine the absorption coefficient of sun-exposed and sun-protected areas on the arm. The range of typical absorption coefficients for the South African skin phototypes is reported. The values for the darker South African skin types were much higher than was previously reported for darker skin phototypes. In the analysis the contributions of the eumelanin and pheomelanin were separated, which resulted in improved curve fitting for volunteers of southern Asian ethnicity without compromising the other groups.

### INTRODUCTION

Laser applications in both the medical and cosmetic industries have increased in recent years (Overton G, 2011). In many of these applications the laser light has to penetrate through some skin layers to reach the intended target site. Some laser treatments e.g. laser hair removal, rely on the penetration of the light through the outer skin layers to the root of the hair follicle. In the darker skin phototypes, light is absorbed in the outer skin layers and may cause burn wounds in the patient (Lanigan S, 2003). It is important that the treatment parameters are established accurately for each patient. The phototype of a patient's skin has been widely used to assist in the setting of these parameters.

At present, classifications of skin phototype or skin tone are mostly done according to the Fitzpatrick scale (Fitzpatrick TB, 1988). This subjective classification is based on the reaction of skin to sunlight (how easily an individual's skin will burn or change colour when exposed to sunlight or UV light) and is influenced by ethnicity and chronic sun exposure and cannot be used to determine the melanin content in skin (González FJ, 2010). This may not be sufficient for accurate and safe treatments (González FJ, 2010).

The epidermis contains basically three cell types: melanocytes, keratinocytes and Langerhans cells. Melanin is produced by the melanocytes. The diversity of the human skin phototypes is directly related to the melanin concentration in the epidermis. Melanin, located in the epidermal layer of the skin, consists of two major groups, eumelanin (black-brown colour) and pheomelanin (yellow-red colour). Darker skins do not necessarily have more melanocytes than lighter skins, but the melanocytes are more active (Störriing M, 2004).

For laser related treatment both the laser wavelength and the melanin concentration in the epidermis have a major influence on the penetration depth of light and its absorption. In most applications direct, *in vivo*, measurements of the penetrated fluence rate are impractical. Computer simulations can be used to predict the fluence rate of laser light some distance into skin (Störriing M, 2004), (Prahl S, 2007(a)), (Karsten AE, 2012(a)).

In order to use computer simulations, both the absorption coefficient ( $\mu_a$ ) and reduced scattering coefficient ( $\mu'_s$ ) of the skin must be known. Published data on the optical properties of skin are available but are

quite varied (Simpson R, 1998(a)), (Tuchin V, 2007) and are therefore difficult to apply to a specific individual. All the skin phototypes are present in the South African population, which poses an even greater challenge when laser treatment parameters from other parts of the world are applied locally.

Diffuse reflectance spectroscopy is a non-invasive *in vivo* measurement technique that has been used to estimate the optical properties ( $\mu_a$  and  $\mu'_s$ ) of skin (Johns M, 2005), (Zonios G, 2006). The technique takes very little time and can consequently be used to assess an individual just before treatment.

The work presented in this paper was done to establish whether (and to what extent) a diffuse reflectance probe can be used to determine the absorption coefficient of different skin phototypes, *in vivo*, in the South African population. A secondary objective was to establish the range of values of  $\mu_a$  and  $\mu'_s$  that reasonably represent the South African skin types.

In this work, the only source of difference between the respective volunteers was the melanin concentrations in the epidermal layer. Differences in the epidermal thickness were not explicitly taken into account, but formed part of the measurement. The effect of both the oxygenated and deoxygenated blood was also accounted for.

## MATERIALS AND METHODS

**Diffuse reflectance probe:** A diffuse reflectance probe (Ocean Optics R200-7-UV-VIS), a Halogen white light source (Ocean Optics HL-2000) and an Ocean Optics USB-4000 spectrometer, all from Ocean Optics Inc. (Florida, USA) were used in the experiments (Figure 4.13). The diffuse reflectance probe consists of seven 200  $\mu\text{m}$  optical fibres. The white light, emitting between 450 and 900 nm, was used for illumination and the spectrometer was used as a detector. The effective wavelength band for the system was from 450-800 nm.

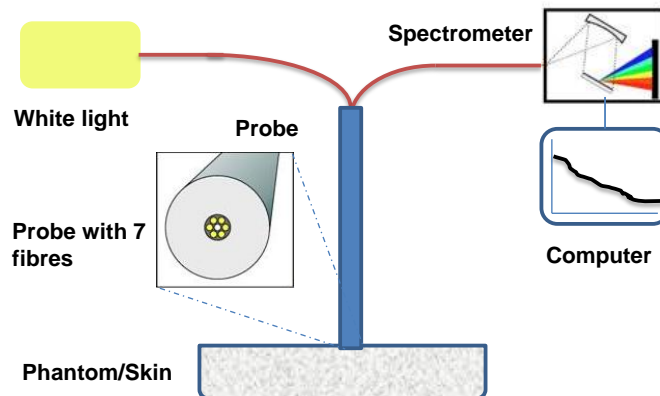


Figure 4.13: Experimental setup with the main system components (Karsten A, 2012(b)).

The Reflectance Wizard from the Ocean Optics Spectra Suite software was used in the measurements of the back reflected light. A calibration standard, WS-1 from Ocean Optics was used to calibrate the reflectance measurements. The back reflected light ( $R_p$ ) as a function of wavelength is given by:

$$R_p(\lambda) = -\log_{10} \left[ \frac{I_{meas}(\lambda) - I_D(\lambda)}{I_{ref}(\lambda) - I_D(\lambda)} \right] \quad (4.16)$$

where:

$I_{meas}(\lambda)$  = reflection spectrum

$I_D(\lambda)$  = detector dark current measurement

$I_{ref}(\lambda)$  = reflection spectrum obtained from the WS-1 calibration standard

The probe calibration procedure is described in an earlier paper (Karsten A, 2012(b)). The probe was calibrated on a set of liquid phantoms. The liquid phantoms were prepared from a mixture of 20% Intralipid (IL) (Sigma Aldrich, lot # 028K0740) and black ink (Trodat colour 7011). Calibration is required to map the geometrical parameters of the probe to the measured reflection data.

Diffuse reflectance can be expressed by an explicit dependence on  $\mu'_s$  and  $\mu_a$  (Zonios G, 2006). The diffused reflectance signal collected by the probe ( $R_p$ ) can be described by Eq. 4.17 (Zonios G, 2006):

$$R_p(\lambda) = \frac{\mu'_s(\lambda)}{k_1 + k_2\mu_a(\lambda)} \quad (4.17)$$

where  $k_1$  and  $k_2$  are calibration parameters that depend on the probe geometry and the experimental setup. These parameters were calculated from the phantoms as  $k_1 = 0.016312$  and  $k_2 = 0.019144$  (Karsten A, 2012(b)). Eq. 4.17 is based on the model described by Zonios (Zonios G, 2006) that assumes a single semi-infinite, homogeneous medium or layer. This simplified approach of the layered structure of the skin has been successfully used previously (Wu J, 1993), (Zonios G, 2006).

The major absorbing chromophores in human skin are haemoglobin, melanin water, carotene and bilirubin (Kollias N, 1995), (Dam JS, 2000(b)), (Meglinski IV, 2002), (Bashkatov AN, 2005). In the wavelength band 450-800 nm, used in this work, the effect of water absorption is at least an order of magnitude smaller than that of the haemoglobin and melanin (Dam JS, 2000(b)). The effect of the carotene and bilirubin was also excluded as parameters (Meglinski IV, 2002) in Eq 4.18 and Eq 4.19. The absorption coefficient ( $\mu_a$ ) can then be expressed in terms of the major absorbers, i.e. the blood (both oxyhaemoglobin and deoxyhaemoglobin) and melanin (Zonios G, 2006):

$$\mu_a(\lambda) = c_{Hb}[\alpha\varepsilon_{HbO_2}(\lambda) + (1 - \alpha)\varepsilon_{Hb}(\lambda)] + c_{mel}\varepsilon_{mel}(\lambda) \quad (4.18)$$

Due to unsatisfactory regression results to Eq. 4.17 with a single melanin parameter  $c_{mel}\varepsilon_{mel}(\lambda)$  for volunteers from southern Asian descent (with a yellow-red undertone), and the possibility that the ratio's between eumelanin and pheomelanin for individuals may vary (Alaluf S, 2002(a)), (Zonios G, 2006), the two different melanin types (eumelanin and pheomelanin) are accommodated explicitly (for all skin types) by rewriting Eq. 4.18 as:

$$\mu_a(\lambda) = c_{HbO_2}[\alpha\varepsilon_{HbO_2}(\lambda) + (1 - \alpha)\varepsilon_{Hb}(\lambda)] + c_{Eu}\varepsilon_{Eu}(\lambda) + c_{Pheo}\varepsilon_{Pheo}(\lambda) \quad (4.19)$$

The fibre optic probe introduces a linear dependence of the reflectance on the reduced scattering coefficient (Zonios G, 2006). The linear dependence of  $\mu'_s$  on wavelength (in the wavelength band 450 – 800 nm) has been justified by Zonios as a reasonable approximation which is supported by the Mie theory for spherical scatterers (Zonios G, 2001), (Zonios G, 2006), (Zonios G, 2008(b)). The reduced scattering coefficient ( $\mu'_s$ ) can be described by ((Zonios G, 2006)):

$$\mu'_s(\lambda) = \left[1 - c_d \left(\frac{\lambda - \lambda_1}{\lambda_2 - \lambda_1}\right)\right] \mu'_s(\lambda_{min}) \quad (4.20)$$

with:

- $\varepsilon_{HbO_2}(\lambda)$  = extinction coefficient for oxyhaemoglobin (Prahl S, 1999)
- $\varepsilon_{Hb}(\lambda)$  = extinction coefficient for deoxyhaemoglobin (Prahl S, 1999)
- $\varepsilon_{mel}(\lambda)$  = extinction coefficient for melanin (Jacques S, 2001)
- $\varepsilon_{Eu}(\lambda)$  = extinction coefficient for eumelanin (Jacques S, 2001)
- $\varepsilon_{Pheo}(\lambda)$  = extinction coefficient for pheomelanin (Jacques S, 2001)
- $c_d$  = parameter related to the effective light scatterer size in skin (Zonios G, 2001), (Zonios G, 2008(b))
- $c_{HbO_2}$  = oxyhaemoglobin concentration
- $c_{Hb}$  = deoxyhaemoglobin concentration
- $c_{mel}$  = melanin concentration
- $c_{Eu}$  = eumelanin concentration
- $c_{Pheo}$  = pheomelanin concentration
- $\alpha$  = oxygen saturation level of blood, defined as the percentage of the oxygenated blood of the total blood concentration  $\alpha = \frac{c_{HbO_2}}{c_{HbO_2} + c_{Hb}}$
- $\lambda_1$  = min ( $\lambda$ ) = 450 nm
- $\lambda_2$  = max ( $\lambda$ ) = 800 nm
- $\mu'_s(\lambda_{min})$  = ordinate of reduced scattering coefficient at  $\lambda_{min}$

The extinction coefficients are tabulated functions of wavelength (Prahl S, 2007(a)) and the associated concentrations are established through fitting procedures. The model assumes that all the chromophores contributing to the measurement are known in advance and that  $\mu'_s$  has a linear dependence on wavelength. This

is required to allow the separation of  $\mu_a$  and  $\mu'_s$  from the measured reflectance (Zonios G, 2006), (Tseng S, 2009). This technique can therefore not be used in a situation where unknown parameters need to be identified. At this stage the application of the technique is a non-invasive, real time, *in vivo* measurement to establish  $\mu_a$  for the skin of a specific individual. Fortunately the extinction coefficients for all the included chromophores are known (Tseng S, 2009).

The LSQCURVEFIT function from MATLAB was used to solve Eq. 4.17 through multiple linear regression. The measured probe reflectance is described mathematically in terms of 6 coefficients ( $c_{HbO_2}$ ,  $\alpha$ ,  $c_{Eu}$ ,  $c_{Pheo}$ ,  $c_d$ ,  $\mu'_s(\lambda_{min})$ ) that are adjusted to best match the equations to the experimental data. This simplistic technique was utilised with satisfactory effect by Zonios (Zonios G, 2006) and Marchesini (Marchesini R, 2009). The more complex alternative is a Monte Carlo simulation process as used by Meglinsky (Meglinsky IV, 2001), Johns (Johns M, 2005) and Reif (Reif R, 2007).

**Clinical data:** Volunteers were recruited at the National Laser Centre (NLC) and measurements were performed according to approved ethics proposals (CSIR: Ref 17/2011 and University of Pretoria: EC110830-060).

Measurements were done on the right arm of volunteers at two positions, one location was on the lower outer arm (sun exposed) and the other on the upper inner arm (not usually exposed to sun). These two positions were used in order to evaluate the inter-person difference due to the sun exposure on the melanin production and therefore skin tones. Ages of the volunteers ranged from 21 to 69 years and the group of 30 volunteers consisted of 11 females and 19 males. Skin phototypes of the volunteers were evaluated with a colour chart according to the Fitzpatrick scale and ranged from skin phototype I-V.

All the diffused reflectance measurements were done on the same day with the same reflectance standard calibration. The output of the halogen light source was monitored for 6 hours and over that period the fluctuations were less than 2.2 %, resulting in a very stable output.

Three measurements were done at each measurement position while the probe was kept in light contact with the skin surface. For each measurement the integration time for the probe was 20 ms and the signal was averaged 4 times, resulting in a total measurement time of 80 ms per measurement. Between volunteers, the probe was wiped clean with ethanol (99.9% from Promark Chemicals) for hygienic reasons and to remove any dirt/oiliness that may have been present on the probe.

## RESULTS

The results of reflectance probe ( $R_p$ ) measurements performed on the 30 volunteers are shown in Figure 4.14. In order to simplify the graph, the average spectrum of the three measurements per position for each individual was used except in a few cases where two of the spectra were close together and one was substantially distinct, most probably due to movement of the volunteer, which resulted in a sub-optimal measurement. From Figure 4.14 it is clear that the reflectance profiles for the different skin phototypes can be roughly categorised into three groups with respect to the overall trends in the graphs.

The trend for group A (typically of Caucasian descent) starts with a high  $R_p$  value and then decreases steadily, but with the effect of oxyhaemoglobin (local absorption peaks at 541 nm and 576 nm) and deoxyhaemoglobin (local absorption peak at 556 nm) manifesting between 540 nm and 580 nm. For group B (typically people from Indian, Asian and some African descent with a yellowish skin undertone) the absorption in the epidermis is higher and therefore the measurements start with a lower  $R_p$  value. The increased melanin concentrations mask the features associated with the haemoglobin. All group B measurements exhibit a generally horizontal trend as a function of wavelength.  $R_p$  values for group C (typical of African descent), begin much lower with an initial decrease up to around 500 nm and then show a steady increase in the reflectance value. In the third group the effect of the blood absorbance peaks is not visible in the reflectance graphs at this scale. This agrees with the expected general trend that higher absorbance skin types (higher melanin concentrations) will exhibit reduced diffuse reflectance due the increased melanin absorbance.

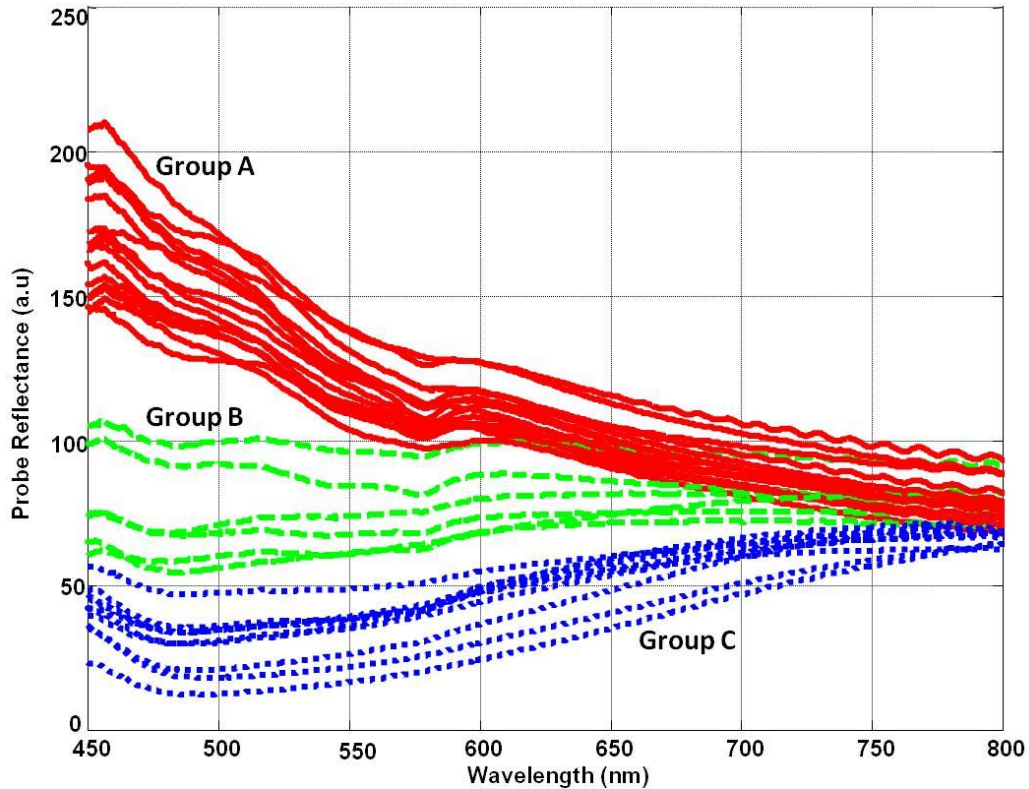


Figure 4.14: Reflectance probe measurements on the inner arm as a function of wavelength for all volunteers. Line styles were used to group graphs with similar trends.

Data analysis was then performed on all the measurements. For clarity in the graphical presentations the data was classified into two groups according to skin phototypes I-III and IV-V respectively. For one of the datasets, 29, the measurements were too scattered to be considered reliable and is not presented. Datasets 3 and 11 are also not presented because they gave unexpectedly high absorption values and the trend was quite different from the rest of the measurements. This ‘abnormality’ will require extensive further investigation before it may be considered as representative.

In Figure 4.15, the absorption coefficients (as calculated at a wavelength of 633 nm) are presented as bar graphs with the sun-exposed (outer arm) and non-exposed (inner arm) data for each volunteer. The lower absorbance skin types were grouped together in Figure 4.15(a) and the higher absorbance skin types were grouped together in Figure 4.15(b). One dataset, a skin phototype II, had a high value for the sun-exposed part of the arm ( $\mu_a = 0.084 \text{ mm}^{-1}$  for the outer arm). This result may be attributed to chronic sun exposure (permission to mention this fact was obtained from the volunteer concerned). This value is not shown in Figure 4.15(a), due to the influence on the  $\mu_a$  scale in the graph. Due to the spread in the  $\mu_a$  values some of the smaller values are not visible in Figure 4.15(b).

This first set of measurements is sufficiently accurate to set the ranges for absorption values for modelling purposes. In order to use the method on a routine basis before treatment, one must await standardised protocols over a range of many individuals of the skin types populations present in diverse.

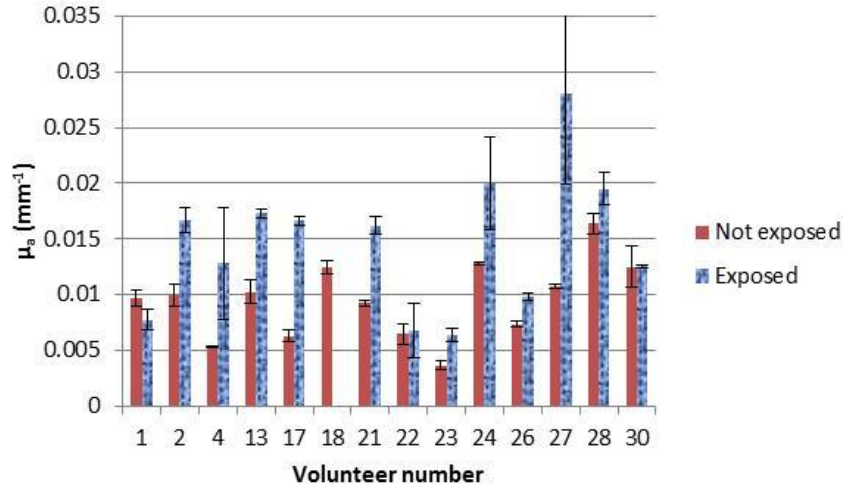


Figure 4.15(a): Absorption coefficients ( $\text{mm}^{-1}$ ) as calculated at a wavelength of 633 nm, for volunteers of skin phototypes I-III. The volunteer numbers are displayed on the X-axis. Sun-exposed value ( $0.084 \text{ mm}^{-1}$ ) for volunteer 18 is excluded from the graph for scaling purposes.

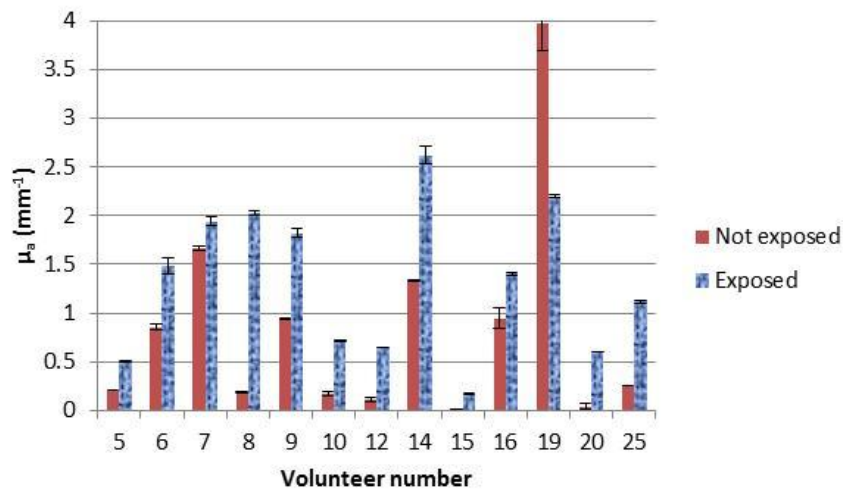


Figure 4.15(b): Absorption coefficients ( $\text{mm}^{-1}$ ) as calculated at a wavelength of 633 nm, for volunteers of skin phototypes IV-V. The volunteer numbers are displayed on the X-axis. The not exposed value ( $0.0075 \text{ mm}^{-1}$ ) for volunteer 15 is barely visible.

As a rule, the data shows the expected trend that the absorption coefficient is larger on the sun-exposed site than on the non-exposed site. For the lower absorbance skin types this assumption fails for only one person (volunteer 1). For the higher absorbance skin types (Figure 4.15(b)) there is only one exception to the generally expected behaviour that falls outside the experimental errors (volunteer 19). The reason for this is not clear at present, but there are two likely explanations. Shininess of the skin due to the use of moisturising creams (normally only applied to hands and lower arms – the measurement sites were not prepared or specifically cleaned before the measurements) is a possible reason. The use of moisturising creams was overlooked as a question in the questionnaire and was therefore not an exclusion criterion. Moisturising creams are normally applied to the hands and lower arm, resulting in a higher reflection from the skin and therefore a reduced ‘perceived’ absorbance. This was subsequently confirmed with measurements before and after applying petroleum based cream to the outer arm of a volunteer. The second possibility is sub-optimal probe contact with the skin of the upper arm which would typically result in lower  $R_p$  measurements.

In Figure 4.16 the absorption coefficient as a function of wavelength is given for the outer arm measurements on (Figure 4.16(a)) the lower absorbance skin group and (Figure 4.16(b)) the higher absorbance skin group.

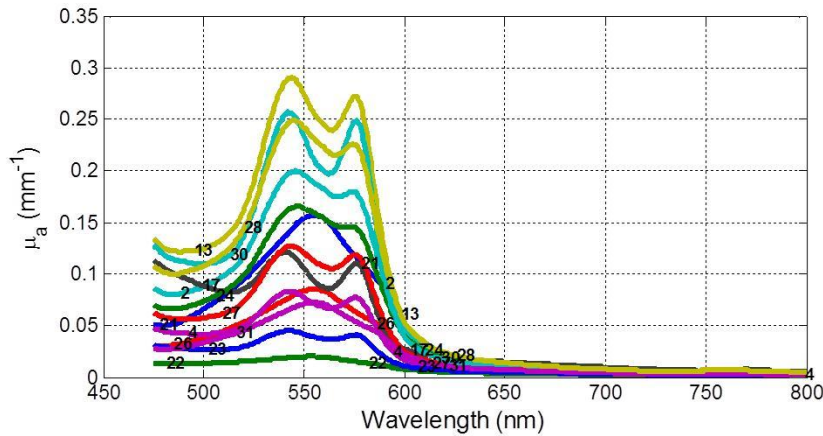


Figure 4.16 (a): Absorption coefficient as a function of wavelength for the lower absorbance volunteers. Measurements were done on the outer arm (sun-exposed).

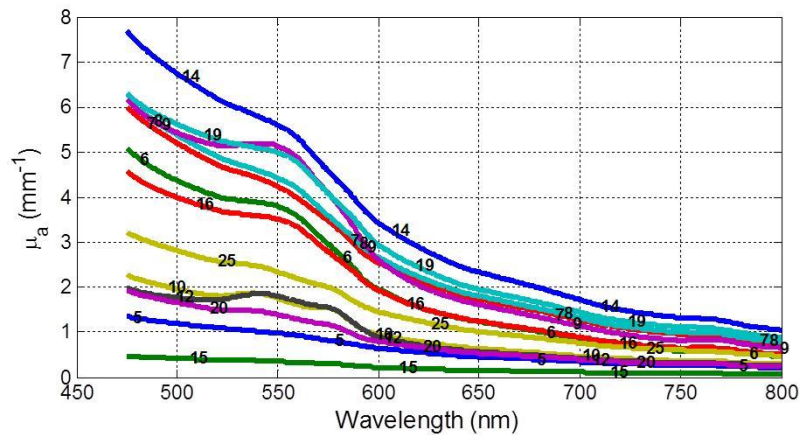


Figure 4.16(b): Absorption coefficient as a function of wavelength for the higher absorbance volunteers. Measurements were done on the outer arm (sun-exposed).

The results in Figure 4.16(a), clearly show the effect of the oxyhaemoglobin (double absorption peaks at wavelengths 511 nm and 576 nm) and deoxyhaemoglobin (single absorption peak at wavelength 556 nm) on  $\mu_a$ . This effect is not as clear in the higher absorbance skin types (Figure 4.16(b)). This is most likely attributable to the greater absorbing effect of increased melanin in the epidermis that obscures the haemoglobin absorption. The data in Figure 4.16(b) mimics the general trend of the melanin extinction coefficient, a decrease as a function of increasing wavelength. Most laser treatments that need to penetrate the skin use longer wavelengths (> 600 nm) in order to limit the effect of haemoglobin absorption.

This study was conducted to extract the typical range for  $\mu_a$  for a sample of the South African population. In Table 4.7, the minimum and maximum  $\mu_a$  and  $\mu'_s$  values for three wavelengths are listed. These wavelengths were selected due to the relevance for typical laser treatment wavelengths.

Table 4.7: Minimum and maximum  $\mu_a$  and  $\mu'_s$  values at wavelengths, 561, 633 and 676 nm.

$\lambda$ (nm)	Skin phototype I-III				Skin phototype IV-V			
	$\mu_a(\min)$ ( $\text{mm}^{-1}$ )	$\mu_a(\max)$ ( $\text{mm}^{-1}$ )	$\mu'_s(\min)$ ( $\text{mm}^{-1}$ )	$\mu'_s(\max)$ ( $\text{mm}^{-1}$ )	$\mu_a(\min)$ ( $\text{mm}^{-1}$ )	$\mu_a(\max)$ ( $\text{mm}^{-1}$ )	$\mu'_s(\min)$ ( $\text{mm}^{-1}$ )	$\mu'_s(\max)$ ( $\text{mm}^{-1}$ )
561	0.019	0.140	1.072	2.218	0.045	7.491	1.188	3.521
633	0.004	0.028	0.996	1.874	0.009	3.939	1.187	3.424
676	0.003	0.021	0.951	1.667	0.007	3.090	1.186	3.366

The eumelanin/pheomelanin ratio is also important to note. The results of this study showed that for the darkest skins (Phototype V) the sun-exposed eumelanin/pheomelanin ratio is 3.12 with a standard deviation of 1.85 and for the lighter skin phototypes I-III the ratio is 0.64 with a standard deviation of 0.58. At present this is just an indication of the variance in the ratio and to establish statistically reliable results, a study should be done on a much larger population.

## DISCUSSION

The results in this paper indicate that a diffuse reflectance probe can be used non-invasively on an individual basis to establish optical properties ( $\mu_a$  and  $\mu'_s$ ) of skin for the purpose of determining optimal and safe treatment parameters for Fitzpatrick skin types I-IV. For the skin type V the procedure results in higher than expected  $\mu_a$  values for some individuals. Treatment regimens can be optimised for all skin types by adjusting the laser intensity, the exposure time and the number of treatments.

In the sampling done for this work, there were no volunteers of skin phototype VI. Most indigenous South Africans are classified between I and V on the Fitzpatrick scale and as such the sample represented the range of South African skin phototypes.

Upper and lower limits of  $\mu_a$  for skin in the general South African population (see Table 4.7) were established. In Table 4.8 some of the comparable published data are presented. Very few results are available for higher absorbance skin types.

Table 4.8: Absorption coefficients from literature using similar diffuse reflectance techniques (Reflectance) as well as an integrating sphere (IS).

Method	$\mu_a$ (mm <sup>-1</sup> )	Position	Skin phototype	$\lambda$ (nm)	Ref
Reflectance <i>in vivo</i>	0.017±0.001	Outer Forearm	-	633	(Doornbos R, 1999)
Reflectance <i>in vivo</i>	0.0128±0.0005	Outer Forearm	-	660	(Doornbos R, 1999)
Reflectance <i>in vivo</i>	0.009±0.0002	Outer Forearm	-	700	(Doornbos R, 1999)
IS <i>ex vivo</i>	0.035	Abdominal and breast	Caucasian	633	(Simpson R, 1998(a))
IS <i>ex vivo</i>	0.022	Abdominal and breast	Caucasian	676	(Simpson R, 1998(a))
IS <i>ex vivo</i>	0.25	Abdominal and breast	Negroid	633	(Simpson R, 1998(a))
IS <i>ex vivo</i>	0.18	Abdominal and breast	Negroid	676	(Simpson R, 1998(a))
Reflectance <i>in vivo</i>	0.060	Inner upper arm	I-II	633	(Tseng S, 2009)
Reflectance <i>in vivo</i>	0.0616	Inner upper arm	III-IV	633	(Tseng S, 2009)
Reflectance <i>in vivo</i>	0.0705	Inner upper arm	V-VI	633	(Tseng S, 2009)
Reflectance <i>in vivo</i>	0.063	Outer Forearm	I-II	633	(Tseng S, 2009)
Reflectance <i>in vivo</i>	0.066	Outer Forearm	III-IV	633	(Tseng S, 2009)
Reflectance <i>in vivo</i>	0.073	Outer Forearm	V-VI	633	(Tseng S, 2009)
IS post mortem	0.069±0.013	-	Caucasian	600	(Tuchin V, 2007)

Data presented in this paper compares well with published data for the lower absorbance skin types. Our data indicated a difference in the  $\mu_a$  values for the skin areas exposed to sun and those that are not. This expected behaviour is also reported by Tseng (Tseng S, 2009) and Alaluf (Alaluf S, 2002(a)). When reporting on the measured data in this paper, the data was not grouped together according to the Fitzpatrick skin phototypes and averages reported, as is often done. When a patient is treated with a laser, the best treatment parameters would be those measured and calculated on the patient at the treatment site and not the skin type obtained by visual comparison with a colour chart that follows the Fitzpatrick scale. In this work an optical characterization method was used to identify the absorption coefficient that can be used in planning for optical treatments.

Our measurements for the higher absorbance skins differ from previously reported data (Table 4.8). The reason for this is not clear at present. Tseng (Tseng S, 2009) reported much smaller  $\mu_a$  values than one would expect (see Table 4.8). Alaluf (Alaluf S, 2002(a)) reported on melanin concentration for the different skin phototypes (typically South African). Their findings were that the 'African' skin had about double the melanin

concentration of the ‘European’ skin in the epidermis. This was true for both the sun exposed and not sun-exposed skin samples retrieved from 4 mm punch biopsies. Our results showed significantly higher differences in the absorption coefficient between lower and higher absorbance skin types.

The method used in this work measures the integrated optical effect of the different scatterers and absorbers (chromophores) present in skin. This is an optical measurement as opposed to a chemical analysis process where the melanin is extracted from the skin biopsy samples and the concentrations reported. When calibrations were done on skin simulating phantoms, the absorber was a single component, black ink. In this case there was a linear relation between the ink concentration and  $\mu_a$ . In skin it seems that the relation between the melanin concentration and  $\mu_a$  is not linear. It has been reported that the melanin particle sizes differ for skin types and are generally larger for the darker skin types (Tseng S, 2009). Tseng (Tseng S, 2009) has reported the possibility of crosstalk between  $\mu_a$  and  $\mu'_s$ , which may be due to melanin particles being partially scatterers as well as primarily absorbers. This potential crosstalk needs further investigation.

The skin was treated as an equivalent single layer bulk tissue and not as separate layers. As such the optical properties extracted for the measurements are average values over the different skin layers. The assumption of a mono layer is an oversimplification, but due to the small distance between the light delivery and light collection fibres, the probe only samples the epidermis and the dermis (Meglinski IV, 2002), (Zonios G, 2006). The fixed probe geometry used (six light delivery fibres surrounding a single collection fibre) does not allow for adjustment of measurements depths. The probe was calibrated on a single layer phantom and the calibration constants also took the geometry of the experimental setup into account. The main aim of this work was to measure the absorption coefficient of different skin phototypes non-invasively.

In most laser applications for skin treatment (both medical and cosmetic), the laser light penetrates some distance into the skin for the effective treatment. In such applications it is important that the absorption due to the melanin in the epidermis is understood in order to prevent damage, e.g. skin burning, as has been reported during laser hair removal for higher absorbance skin types (Lanigan S, 2003), (Battle E, 2004).

Regarding the depth of measurements of the probe, Meglinsky (Meglinski IV, 2002) investigated the depth of measurement or measurement volume for different distances between the light source and the detector in diffuse reflectance measurements. They concluded that a light source-detector spacing of 250  $\mu\text{m}$  primarily samples the epidermal layer and the papillary dermis. The light source-detector spacing in the probe used in this work was 200  $\mu\text{m}$ , indicating that the epidermal layer and the papillary dermis were sampled.

The data extraction in this paper separated the contribution of eumelanin and pheomelanin and this appeared necessary to allow the inclusion of people of southern Asian ethnicity. The average sun-exposed eumelanin/pheomelanin ratio for the darkest skins (Phototype V) calculated from our results is 3.12 and for the lighter skin (Phototypes I-III) the ratio is 0.64. Alaluf (Alaluf S, 2002(a)) reported eumelanin/pheomelanin ratios for the sun-exposed ‘African skin’ (comparable to our Phototype V skin) of 8.13 and 1.64 for the ‘European skin’ (comparable to our Phototype I-II). Both ratios for Alaluf are around 2.5 times higher than our ratios. Alaluf used 4 mm punch skin biopsies from 48 volunteers on both sun-exposed and non-exposed sites (three to four biopsies per site). Chemical analysis was used to extract the different melanin components through a process described in (Alaluf S, 2002(a)). It should be noted that it is difficult to compare the results established by chemical extractions with those of the integrated path optical method in terms of the total absolute melanin ratios.

The results of this pilot study showed that the diffuse reflectance probe has the potential to be used as a fast, non-invasive absorption measurement technique just before laser treatment. The absorption coefficient values obtained through this method can be implemented in software that models the light propagation through skin. In order to apply the technique with confidence in a clinical setting, the technique still needs to be verified with diffuse reflectance probe measurements on a much larger sample of the population. In future studies, experimental procedure should include the preparation of the measurement site by cleansing with an alcohol swab to ensure the best possible consistency of the skin surface.

## Acknowledgements

The authors would like to acknowledge Mr Bafana Moya for his work in the laboratories.

## REFERENCES

- Alaluf S, Atkins D, Barrett K, Blount M, Carter N, Heath A. "Ethnic Variation in Melanin Content and Composition in Photoexposed and Photoprotected Human Skin." *Pigment Cell Res* 15 (2002a): 112-118.
- Bashkatov AN, Genina EA, Kochubey VI, Tuchin VV. "Optical properties of human skin, subcutaneous and mucous tissues in the wavelength range from 400 to 2000 nm." *J. Phys. D: Appl. Phys.* 38 (2005): 2543-2555.
- Battle E, Hobbs L. "Laser-assisted hair removal for darker skin types." *Dermatologic Therapy* 17 (2004): 177-183.
- Dam JS. *Optical analysis of biological media - continuous wave techniques*. ISBN 91-628-4546-2. Lund Reports on Atomic Physics LRAP-265, 2000.
- Doornbos R, Lang R, Aalders M, Cross F, Sterenborg H. "The determination of in vivo human tissue optical properties and absolute chromophore concentrations using spatially resolved steady-state diffuse reflectance spectroscopy." *Phys. Med. Biol* 44 (1999): 967-981.
- Fitzpatrick TB. "The validity and practicality of sunreactive skin type-I through type-VI." *Arch Dermatol* 124 (1988): 869-871.
- González FJ, Martínez-Escanamé M, Muñoz RI, Torres-Álvarez B, Moncada B. "Diffuse reflectance spectrophotometry for skin phototype determination." *Skin Research and Technology* 16 (2010): 397-400 .
- Jacques S. *Oregon Medical Laser Centre website*. 2001. <http://omlc.ogi.edu/spectra/melanin/index.html> (accessed November 24, 2011).
- Johns M, Giller CA, German DC, Liu H. "Determination of reduced scattering coefficient of biological tissue from a needle-like probe." *Optics Express* 13 (2005): 4828-4842.
- Karsten A, Singh A, Karsten P, Braun M. "Diffuse reflectance spectroscopy as a tool to measure the absorption coefficient in skin: system calibration." *Lasers in Medical Science* DOI 10.1007/s10103-012-1079-2 (2012(b)).
- Karsten AE, Singh A, Braun MW. "Experimental verification and validation of a computer model for light-tissue interaction." *Lasers Med Sci* 27 (2012a): 79-86.
- Kollias N. "The Physical Basis of Skin Color and its Evaluation." *Clinics in Dermatology* 13 (1995): 361-367.
- Lanigan S. "Incidence of side effects after laser hair removal." *J Am Acad Dermatol* 49 (2003): 882-886.
- Marchesini R, Bono A, Carrara M. "In vivo characterization of melanin in melanocytic lesions: spectroscopic study on 1671 pigmented skin lesions." *Journal of Biomedical Optics* 14 (2009): 014027.
- Meglinski IV, Matcher SJ. "Quantitative assessment of skin layers absorption and skin reflectance spectra simulation in the visible and near-infrared spectral regions." *Physiol. Meas.* 23 (2002): 741-753.
- Overton G, Anderson S, Belforte D, Hausken T. "Annual review and forecast." *Laser Focus World* 47 (2011): 40-60.
- Prahl S, *Oregon Medical Laser Centre website - Optical Absorption of Hemoglobin*. 1999. <http://omlc.ogi.edu/spectra/hemoglobin/index.html> (accessed November 24, 2011).
- Prahl S, *Oregon Medical Laser Centre website*. 2007. <http://omlc.ogi.edu/software/> (accessed December 13, 2011).
- Reif R, A'Amar O, Bigio I. "Analytical model of light reflectance for extraction of the optical properties in small volumes of turbid media." *Applied Optics* 46 (2007): 7317-7328.
- Simpson R, Kohl M, Essenpreis M, Cope M. "Near-infrared optical properties of ex vivo human skin and subcutaneous tissues measured using the Monte Carlo inversion technique." *Phys. Med. Biol* 43 (1998(a)): 2465-2478.
- Störning M. *Computer vision and human skin colour*. Ph.D. dissertation, Aalborg University, Denmark, URL: <http://www.cvmt.dk/~mst>, 2004.
- Tseng S, Bargo P, Durkin A, Kollias N. "Chromophore concentrations, absorption and scattering properties of human skin in-vivo ." *Optics Express* 17 (2009): 14599-14617.
- Tuchin V. *Tissue Optics: Light Scattering Methods and Instruments for Medical Diagnostics*. 2nd edition, p 165-175. SPIE Press, 2007.

- Wu J, Partovi F, Field MS, Rava RP. "Diffuse reflectance from turbid media: an analytical model of photon migration." *Applied Optics* 32 (1993): 1115-1121.
- Zonios G, Bykowski J, Kollias N. "Skin melanin, haemoglobin, and light scattering properties can be quantitatively assessed in vivo using diffuse reflectance spectroscopy." *J. Invest. Dermatol* 117 (2001): 1452-1457.
- Zonios G, Dimou A. "Melanin optical properties provide evidence for chemical and structural disorder in vivo." *Optics Express* 16 (2008(b)): 8263-8268.
- Zonios G, Dimou A. "Modeling diffuse reflectance from semi-infinite turbid media: application to the study of skin optical properties." *Optics Express* 14 (2006): 8661-8674.

#### 4.5 VALUE OF THE DIFFUSE REFLECTANCE PROBE MEASUREMENTS

The usefulness of the optical properties extracted from the probe measurements lie in their use in the computer model as minimum and maximum values for the absorption coefficient. The model however has some limitations. One of the limitations is that the current probe system does not allow for measurements at different depths into the skin. The depth of measurement is dictated by the distance between the emitting and collecting fibres and to some extent the absorption coefficient.

Another limitation in the experimental procedure was that the measurement site was not specifically prepared before measurements. In future work the site must be cleaned before the measurements to ensure there is no 'unwanted' residue of skin treatment products that may influence the measurements.

The extracted absorption coefficients are average values over the depth of the measurements. In future work the design of a probe with more than one collecting fibre at different distances must be investigated to evaluate the absorption coefficient at different depths into the skin and resolve the contributions of various skin layers.

The effect of blood absorption is noticeable in most of the data and it does have an influence on the absorption coefficient at shorter wavelengths. At the wavelengths considered in this work (and for most laser therapeutic applications), the effect is not important. At the treatment wavelengths (typically  $> 650$  nm), the effect of the blood on the dermal absorption is negligible and therefore the absorption coefficient extracted can be attributed mainly to the epidermal absorption.

The measurements were done on a very small sample of the population. The technique still needs to be refined on a much larger sample of the South African population before the system may be used with confidence in a clinical setting. The aim of the measurements was to establish the upper and lower limits for the epidermal absorption coefficients to be used in the computer model and was adequate for this limited purpose.

In the next chapter the epidermal absorption coefficients calculated from the diffuse reflectance probe measurements are used in the computer model to predict the influence of epidermal absorption on the treatment times during laser treatment.

## CHAPTER 5: EFFECT OF THE OPTICAL PROPERTIES OF THE EPIDERMIS ON LASER TREATMENT PARAMETERS

For most laser treatments the target site is some distance into the skin. The thickness of the epidermal layer in skin varies with location across the body. The absorption coefficient is a measure of the absorption (attenuation) of light through the medium (skin). The penetration depth of light in skin is determined by the total attenuation, constituted by the scattering and absorption coefficients. It stands to reason that a thicker epidermis will absorb more light than thinner epidermal layers. In determining the fluence rate reaching a specific position (depth) in the skin, both the epidermal thickness and the absorption coefficient need to be taken into account. The computer model developed and described in Chapter 3 was adapted to account for the different skin layers. Photodynamic Therapy (PDT), a potential treatment for skin cancer, was the application chosen to demonstrate the influence of the epidermis on the fluence rate in skin.

The aim of the model was to be as uncomplicated as possible to evaluate the influence of specific parameters. In the development of the model only the essential skin layers were used, i.e. the epidermis and dermis and no hair or blood vessels were included. The main reason for the model development is to quantify the expected fluence rate losses in the tissue before reaching the treatment site, in this case the tumour. The major contributions to the loss of fluence rate through the tissue are the absorption in the epidermis and the scattering of the light. Scattering of light leads to an increase in the spot size and as such reduces the ‘power density’ or fluence rate deeper in the skin. Consequently the loss in laser light intensity due to absorption depends on both the absorption coefficient and the path length through the medium (in this case the epidermis). As such the epidermal thickness is an important parameter.

At present there is no easy way to measure the epidermal thickness *in vivo*, therefore the data published by Whitton (Whitton JT, 1973) was used. It is the most comprehensive work on epidermal thicknesses that could be found. Only areas of the skin that are usually exposed to sunlight were selected because that would be the areas most prone to skin cancer. In those areas the published values of the epidermal thickness varies from 39  $\mu\text{m}$  on the cheek to 85  $\mu\text{m}$  on the back of the hand. For easier comparisons, the epidermal thickness in the model was varied between 40 and 90  $\mu\text{m}$ .

Two skin cancers prevalent in South Africa, squamous cell carcinomas (SCC) and nodular basal cell carcinomas (NBCC), were evaluated. For comparison purposes the tumours were assumed to be embedded 0.2 mm into the skin. Optimisation of the model in terms of the voxel sizes and number of photons launched was done in the original model development in Chapter 3. A laser beam diameter of 1.2 cm was used to simulate a typical laser that may be used in a clinical setting. Such a laser was used in some of the *in vitro* cell work that led to the defining of the laser dose parameters (Karsten AE, 2011), (Maduray K, 2011).

Due to the thin epidermal layer, the evaluation slice thickness was reduced to 0.01 mm. The number of slices in depth (Z-direction) was varied to keep the slice thickness constant. The value of  $g$  was constant at 0.8 (using the data from Salomatina (Salomatina E, 2006)). The output power of a typical laser would be around 50 mW. In section 3.5 it was shown that if the input laser power was 1 mW the results can be scaled up to the required input laser power by simple multiplication. The results in section 3.5 clearly indicated that the output values for the model when 10 mW was used are 10 times the values when an input power of 1 mW was used. For simplicity an input power of 1 mW was used which allows for easy ‘upscaling’ when more powerful lasers are required.

Even though absorption coefficients as high as  $3.36 \text{ mm}^{-1}$  (at  $\lambda=676 \text{ nm}$ ) were measured with the reflectance probe, the values were constrained to  $3 \text{ mm}^{-1}$ , to be conservative. As reported in section 4.4.1, the values of the absorption coefficient measured with the reflectance probe were higher than previously reported values.

There are numerous reports on blistering occurring as a result of laser hair removal treatments (Adrian RM, 2000), (Lanigan S, 2003), (Battle E, 2004), (Lepselter J, 2004). Laser hair removal is a procedure that has been used for a number of years where the hair follicles are irradiated by a laser to prevent or slow hair growth. For the laser light to reach the follicle it needs to penetrate the epidermis. In this application of red lasers (wavelengths around 630 nm) the effect of epidermal absorption is important (see Figure 2.8 section 2.3.1.3). One of the conclusions of laser hair removal for skin phototypes V-VI is that longer pulses (i.e. longer treatment time) must be used (Lepselter J, 2004). This is in line with the findings of this work (see the paper in section 5.1) that for the treatment dose to stay the same, the irradiation time should be increased rather than increasing the laser power to limit possible side effects e.g. burning or blistering.

Results of the computer model are presented in the paper in the next section. In the model the typical spread in epidermal absorption coefficients of the South African skin phototypes

were used (as measured with the diffuse reflectance probe, section 4.4.1). The major advantage of the computer model was that the extent of the absorption effect could be quantified. Use of the model allows the clinician to compensate for the absorption and establish safe and effective treatment power and times before treatment commences. When comparing treatment time between skin of phototype I and V and keeping the fluence rate constant at  $44.2 \text{ mW/cm}^2$ , the treatment time is increased from 235 s (phototype I) to 374 s (phototype V), an increase of more than 50 %.

The paper based on epidermal influence on light penetration has been submitted to the journal: Lasers in Medical Science. The paper is included in section 5.1.

## **5.1 PAPER ON THE EFFECT OF THE EPIDERMIS ON LASER TREATMENT PARAMETERS**

The paper on the effect of the epidermis on the treatment parameters is currently under review for publication in Lasers in Medical Science.

As in the earlier papers in this thesis, the format has been altered by changing the Figure and Table numbers to follow numbering in the thesis. The referencing style has also been changed to follow the style of the thesis.

## Effect of epidermal absorption on PDT dose calculations

A E Karsten<sup>1,2</sup>, A Singh<sup>1</sup>, P A Karsten<sup>3</sup> M W H Braun<sup>2</sup>

<sup>1</sup> Biophotonics Group, National Laser Centre, CSIR, P.O. Box 395, Pretoria, 0001, South Africa

<sup>2</sup> Department of Physics, University of Pretoria, Pretoria, 0002, South Africa

<sup>3</sup> Ballistics Research Group, Denel Land Systems, P O Box 7710, Pretoria, 0001, South Africa

### ABSTRACT

Skin cancer treatments such as Photodynamic Therapy (PDT) rely on light, generally obtained from a laser source, to activate a drug. Penetration of laser light through human skin is highly dependent on the optical properties of skin. The absorption coefficient of the epidermis varies with the amount of melanin in the epidermis (or the skin phototype). The absorption and scattering of the light in the outer skin layers determine the fluence rate of the light reaching the intended treatment site. For effective treatment the losses due to the scattering and absorption must be taken into account. A two layer skin model with an embedded tumour was developed in the ASAP raytracing software environment. The spread in absorption coefficients for the typical South African skin phototypes (Caucasian, African and southern Asian descent) were used as input to the computer model to determine the fluence rate reaching the tumour at a depth of 200  $\mu\text{m}$ . When the epidermal thickness is taken into account for various sun exposed skin areas, the treatment time (for a fixed laser power density) may increase from 235 s to as much as 374 s to deliver the same dose to the tumour.

**Keywords:** epidermal absorption modelling, South African skin phototypes, light transmission modelling, photodynamic therapy

### INTRODUCTION

The effectiveness of lasers in photodynamic treatment (PDT) of cancerous tumours has been described widely (Sharman WM, 1999), (Brown SB, 2004), (Wilson BC, 2008), (Sekkat N, 2012). In the initial testing phase of a potential treatment, tests are done in biochemical laboratories with single cell layers in a Petri dish. Adapting the treatment parameters to be used in clinical settings on patients is not a trivial process. Not all tumours are situated on the surface of the skin. In most clinical applications the laser light needs to penetrate through some skin layers before reaching the treatment area or tumour. The optical properties of the skin layers influence the light propagation through the tissue and as such the distribution of the laser fluence rate at any given depth into the tissue.

“Skin cancer (consisting of basal cell carcinomas (BCC), squamous cell carcinomas (SCC) and malignant melanoma) is the most common type of cancer in the South Africa with about 20 000 reported cases each year” (Mqoqi N, 2004). Australia and South Africa have the highest incidence of skin cancer in the world (Cansa, 2001), (Mqoqi N, 2004). “Basal cell carcinoma accounts for more than 90 percent of all skin cancers. Basal cell cancer grows slowly and does not usually spread to other parts of the body. However, if left untreated, it can spread to nearby areas and invade bone and other tissues under the skin. Squamous cell cancer is much less common than BCC. SCC can be more aggressive than BCC and is also more likely to grow deep below the skin and spread to distant parts of the body. When squamous or basal cell skin cancers are found early, there is nearly a 100 percent chance for cure” (National Cancer Institute, 2011).

PDT is one of the newer cancer treatments (Robertson CA, 2009), (Sekkat N, 2012). PDT is a procedure in which a photosensitiser (PS) or drug is administered orally or topically to the patient and after the absorption of the PS in the cells, the tumour is irradiated with a light source (normally a laser) tuned to an absorption peak of the PS in the visible to near infrared region of the light spectrum. The formation of highly reactive singlet oxygen in the cells leads to cell death through apoptosis or necrosis (Kessel D, 1998), (Bouchier-Hayes L, 2005), (Robertson CA, 2009). Due to the short lifetime of the singlet oxygen in biological systems only molecules close to the PS are affected. The half-lifetime of singlet oxygen is less than 40 ns, and the radius of the action of singlet oxygen is in the order of 20 nm (Castano AP, 2004). PDT is a localised treatment, having

less of an adverse effect on the healthy cells not irradiated by the light source. PDT has been approved in a number of countries for selected cancers and drugs (Calzavara-Pinton PG, 2007), (Sekkat N, 2012).

Human skin is considered a turbid medium due to the highly scattering nature of skin for light in the visible and near infrared wavelength regions (the wavelength region of interest for most laser treatments). In skin the multiple scattering and absorption of light attenuates the laser fluence rate. Computer modelling is a technique that can be used to determine the laser fluence rate reaching a pre-determined depth in the skin. Three of the most important optical properties describing the propagation of light through tissue are the absorption ( $\mu_a$ ) and scattering ( $\mu_s$ ) coefficients as well as the anisotropy or direction of scatter ( $g$ ). In order to reduce the complexity, the last two parameters are usually combined as the reduced scattering coefficient  $\mu'_s$ , ( $\mu'_s = (1 - g)\mu_s$ ) (Pfefer TJ, 2003), (Fabrizio M, 2010). In most of the systems used to measure the optical properties of tissue, values of  $\mu'_s$  are measured and not  $\mu_s$  (Dam JS, 2000(a)), (Zonios G, 2006), (Johns M, 2005).

Skin can be modelled as a layered structure. With the optical properties of each layer known, laser light can be traced through the skin to determine the losses due to the absorption and scattering of the light as well as the spreading of the light.

The epidermis of the skin contains the melanocytes that are responsible for the melanin production which in turn is responsible for the skin phototype or skin colour. A higher absorption coefficient is associated with the darker skin phototypes. The thickness of the epidermal layer is a function of the position on the human body (Whitton JT, 1973).

A computer model was developed in ASAP, a ray tracing software package from Breault Research, to predict the laser fluence rate reaching a pre-determined depth into skin. Here the model is applied to the prediction of optimal treatment parameters in PDT applications for skin cancer. In general, the first screening tests for PDT applications are done in *in vitro* cell samples (cancerous and normal, healthy skin cell, e.g. fibroblast cells). In this application the cells are irradiated directly with the laser without any outer cell layers on top of the sample (Robertson CA, 2009), (Maduray K, 2011), (Nombona N, 2011) as would be the situation in the *in vivo* treatment applications. Computer modelling can be an effective tool to bridge the step between *in vitro* laboratory tests and clinical tests (both animal and human). It can also be used to illustrate the effect of the light absorption in the epidermis due to the different skin phototypes.

The work presented here was done with a computer model which is able to determine the effect of both the epidermal thickness and the absorption coefficient of the epidermis on the light transmitted 100  $\mu\text{m}$  and 200  $\mu\text{m}$  into a skin. The model consisted of an epidermal and a dermal layer with a tumour embedded in the dermis. The expected range of epidermal absorption coefficients present in the South African population was used.

## MATERIALS AND METHODS

Monte Carlo ray tracing programs are efficient in predicting the behaviour of laser light transmission through various media, including human tissue (Jacques S, 2008(b)), (Breault Research, 2006). ASAP is a Monte Carlo ray tracing software package that allows the user to follow multiple rays through a pre-defined geometry (Breault Research, 2006). Each ray is traced until it is absorbed in the model or leaves the boundaries of the model.

In ASAP the anisotropy is substituted into the Henyey-Greenstein equation (Henyey L, 1941) to determine the scattered light distribution as a function of the angle ( $\theta$ ) (Michel B, 2005), (Stevenson MA, 2009):

$$p(\theta) = \frac{1}{4\pi} \frac{1 - g^2}{[1 + g^2 - 2g \cos(\theta)]^{3/2}} \quad (5.1)$$

where the anisotropy,  $g$ , is the average directional cosine of the scattered light with a value between -1 and 1.

The ASAP volumetric scatter model is based on the angular distribution and the radiative transport equation (Ishimaru A, 1989) and can be written as (Michel B, 2005), (Stevenson MA, 2009):

$$\frac{dI(r, \omega)}{ds} = -(\mu_a + \mu_s)I(r, \omega) + \frac{\mu_s}{4\pi} \int_{4\pi} p(\omega, \omega')I(r, \omega')d\omega' \quad (5.2)$$

with

$I(r, \omega)$  = radiance at position  $r$  directed towards the solid angle  $\omega$

$\frac{dI}{ds}$  = directional derivative of  $I$

$p(\omega, \omega')$  = phase function describing the angular distribution of the scattered light

In the model the skin was described as a multilayered system. For each layer the following optical properties need to be specified.

- Geometrical description of the layer
- Absorption coefficient ( $\mu_a$ )
- Scattering coefficient ( $\mu_s$ )
- Refractive index ( $n$ )
- Anisotropy ( $g$ )

In skin the optical properties within layers may vary, but for purposes of this model the assumption was made that optical properties are homogenous within each layer. This model has been tested previously by comparing the transmission through the model with that measured on both liquid and solid skin representing phantoms on an integrating sphere (IS) system (Karsten AE, 2012(a)).

Data regarding the optical properties of human skin are widely published (Cheong WF, 1990), (Tuchin V, 2007), with the most comprehensive reference the book by Tuchin (Tuchin V, 2007). Obtaining optical properties from the literature is not an easy process due to the variance in the published data in terms of skin site, measurement technique used and sample handling for which information is reported. Most of the published measurements were performed on ex vivo skin samples (Tuchin V, 2007). The absorption coefficient,  $\mu_a$ , in the epidermis is an important parameter that depends on the melanin concentration in the epidermis. In the published literature the variance in  $\mu_a$ , due to changes in the epidermal melanin concentration, is not readily available. For this work, values measured with a diffuse reflectance probe on 30 individuals in South Africa (volunteers of European, African and Indian subcontinent descent) were used as the upper and lower limits for the  $\mu_a$  values (Karsten A, 2012(c)).

Salomatina (Salomatina E, 2006) used an IS system to measure the optical properties of the epidermis, dermis and non-melanoma cancers (nodular basal cell carcinomas (NBCC), infiltrative basal cell carcinomas (IBCC) and invasive SCC) separately. For consistency all the optical properties used in the model are from Salomatina (Salomatina E, 2006), except for the absorption coefficient of the epidermis. Both SCC and NBCC were used in the model.

A two-layer skin model (see Figure 5.1(a)) was described consisting of an epidermal and a dermal layer with a tumour embedded in the dermis. In the skin model the skin layers are described as planar surfaces however in actual skin the upper part of the dermis is not planar. To evaluate the influence of an un-even epidermal/dermal interface, a 'wavy' skin surface was constructed as a comparison to the planar interface. An Optical Coherence Tomography system (OCT 1300SS from Thorlabs) was used to do non-invasive measurements on the arms a few volunteers in order to establish a typical profile of the epidermal-dermal interface. In the model a wavy interface was derived from a sawtooth profile that is rounded on the top resulting in a profile as shown in Figure 5.1(b). A circular, Gaussian laser source (output power of 50 mW and beam diameter 1.2 cm) at a wavelength of 676 nm was defined and traced through the model. Two evaluation detectors were put in place. A semi-sphere back-reflection detector was placed behind the laser source to collect all the light reflected from the model (both direct reflections and diffused reflections). A flat, circular transmission detector was placed 0.2 mm behind the last surface of the dermis and used to collect all the light that was transmitted through the model. These detectors, combined with the absorption data in the model were used to ensure that all the rays (total input power) can be accounted for. The dimensions and optical properties of the different layers are listed in Table 5.1. The value of the anisotropy ( $g$ ) was kept constant at 0.8 for all the layers and the refractive index ( $n$ ) for the epidermis was 1.5 and for the dermis and tumour 1.4 (Salomatina E, 2006).

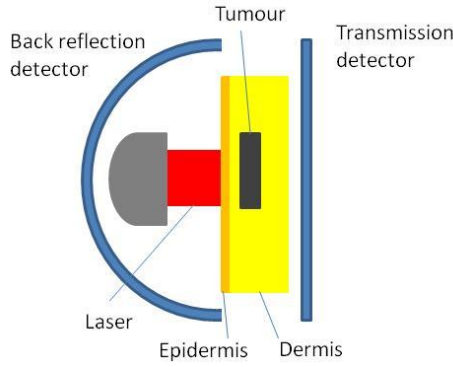


Figure 5.1(a): Schematic of the computer model with the detectors and the different layers.

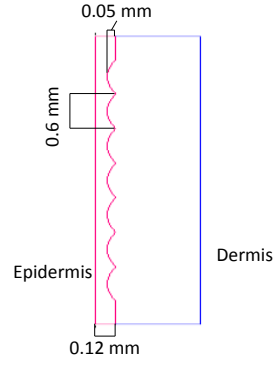


Figure 5.1(b): Structure of the un-even epidermis-dermis interface.

Table 5.1: Geometrical dimensions for the planar surfaces and optical properties of the different layers in the skin model.

Layer	Width (mm)	Start position (mm)	Thickness (mm)	$\mu_a$ ( $\text{mm}^{-1}$ )	$\mu_s$ ( $\text{mm}^{-1}$ )	$\mu_s'$ ( $\text{mm}^{-1}$ )
Epidermis	40	0	0.04-0.09	0.002-3	22.4	4.48
Dermis	40	0.04-0.09	3	0.15	13.9	2.78
Tumour (SCC)	10	0.2	2	0.11	8.55	1.71
Tumour (NBCC)	10	0.2	2	0.09	10.35	2.07

The thickness of the epidermis depends on the skin site. For this work skin sites that are commonly exposed to sunlight were chosen. The epidermal thickness ( $d_{\text{epi}}$ ) varies from 39  $\mu\text{m}$  on the cheek to 85  $\mu\text{m}$  on the back of the hand (Whitton JT, 1973). At other skin sites the epidermis may be much thicker (up to 369  $\mu\text{m}$  at the fingertip (Whitton JT, 1973)). Due to the influence of the absorption coefficient on the light that penetrates into the skin, different epidermal thicknesses were modelled. For the current model  $d_{\text{epi}}$  was varied between 40 and 90  $\mu\text{m}$ . The values of  $\mu_a$  were varied between 0.002 and 3.0  $\text{mm}^{-1}$ , according to the measurements reported in (Karsten A, 2012(c)).

The wavy interface was only evaluated on the thicker epidermis of 90  $\mu\text{m}$ . The effect of having the interface at a depth of 0.09 mm and 0.12 mm was evaluated as well as changing the height of the wave from 0.025 mm to 0.05 mm. Evaluations were only done for  $\mu_a$  values of 0.1, 1, 2 and 3  $\text{mm}^{-1}$ . The length of a wave was kept to 0.6 mm as indicated in Figure 5.1(b).

In the model the laser beam consists of 3.1 million rays which were traced separately through the model (Karsten AE, 2012(a)). The model is divided into evaluation voxels of 0.2 mm x 0.2 mm x 0.01 mm (X, Y, Z). The accumulated absorbance and fluence rate up to a depth of 100  $\mu\text{m}$  (the depth just after the thickest epidermal layer) were evaluated as well as the light reaching the two evaluation detectors. The optical properties of the two tumours do not differ dramatically, but the difference has a slight influence on the laser fluence rate in the skin.

## RESULTS AND DISCUSSIONS

In the models the percentage of the light reflected and detected by the back reflection detector was monitored and reported in Table 5.2. Very good correlation was found between the planar model and the model where the epidermal wave interface started at a depth of 0.12 mm (epidermal thickness of 0.12 mm) with a wave amplitude of 0.05 mm. The results vindicate the use of a planar epidermal/dermal interface as the integrated effect of a wavy interface can be correlated with an equivalent effect from a planar interface at a slightly different depth. The equivalent depth of the planar interface can be approximated by the average of the troughs and peaks of the wavy interface. The rest of the evaluations were done with a planar epidermal/dermal interface.

Table 5.2: % Light reflected from the model for the different wave interface parameters described above.

$\mu_a$ ( $\text{mm}^{-1}$ )	Epidermal thickness 0.09 mm		Epidermal thickness 0.12 mm		Planar model (epidermal thickness 0.09 mm)
	Wave height 0.05 mm	Wave height 0.025 mm	Wave height 0.05 mm	Wave height 0.025 mm	
0.1	37	38	38	38	38
1	30	29	28	27	27
2	25	23	21	20	21
3	21	19	17	16	17

For ease of comparison, all the evaluations are reported at a depth of 100  $\mu\text{m}$  into the model (the upper part of the dermis) even though the epidermal thickness ranged from 40 to 90  $\mu\text{m}$ .

In Figure 5.2 the fraction of the light that is absorbed in the first 100  $\mu\text{m}$  of the model is presented as a function of  $\mu_a$  for the different epidermal thicknesses for both the NBCC and SCC cells. The optical properties of the dermis and the scattering coefficient for the epidermis were kept the same for the different  $\mu_a$  values even though there is evidence that the dermal  $\mu_s$  values increase in higher absorbing skins, (Tseng S, 2009), (Karsten A, 2012(c)).

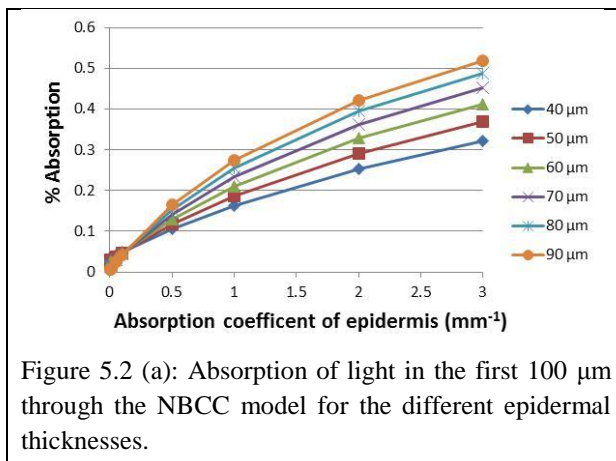


Figure 5.2 (a): Absorption of light in the first 100  $\mu\text{m}$  through the NBCC model for the different epidermal thicknesses.

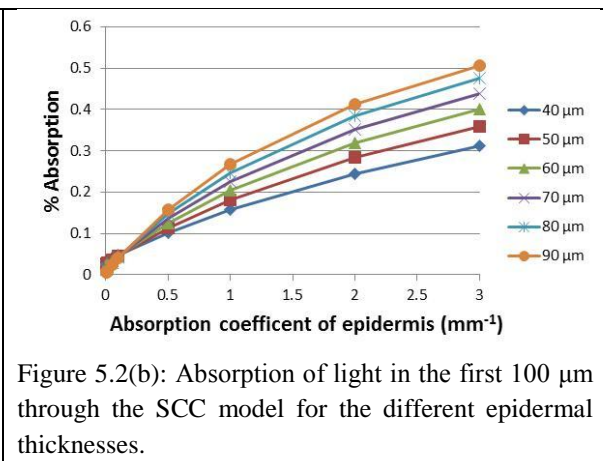


Figure 5.2(b): Absorption of light in the first 100  $\mu\text{m}$  through the SCC model for the different epidermal thicknesses.

The trends for the two different tumours are very similar. The differences are due to the difference in the optical properties of the tumour. For the highest  $\mu_a$ , up to 50% of the incident light is absorbed in the thick epidermis and just over 30% for the thinnest epidermis. For  $\mu_a = 3 \text{ mm}^{-1}$ , the absorption is one to two orders of magnitude higher than at the very low  $\mu_a$  values.

The fluence rate reaching 100  $\mu\text{m}$  into the skin for the two different tumours are presented in Figure 5.3.

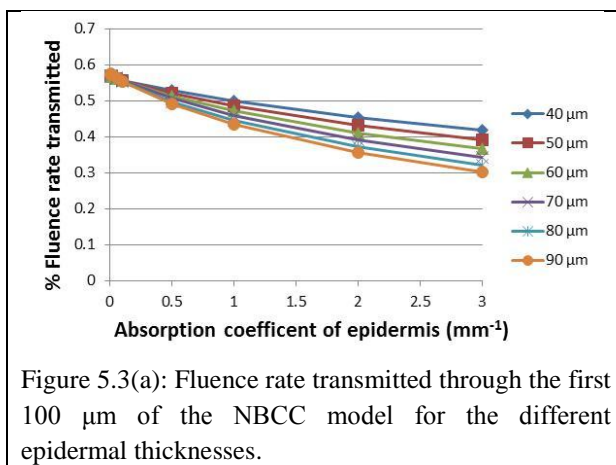


Figure 5.3(a): Fluence rate transmitted through the first 100  $\mu\text{m}$  of the NBCC model for the different epidermal thicknesses.

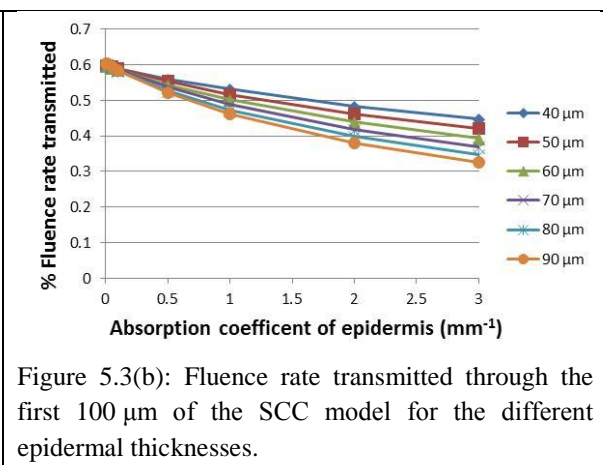
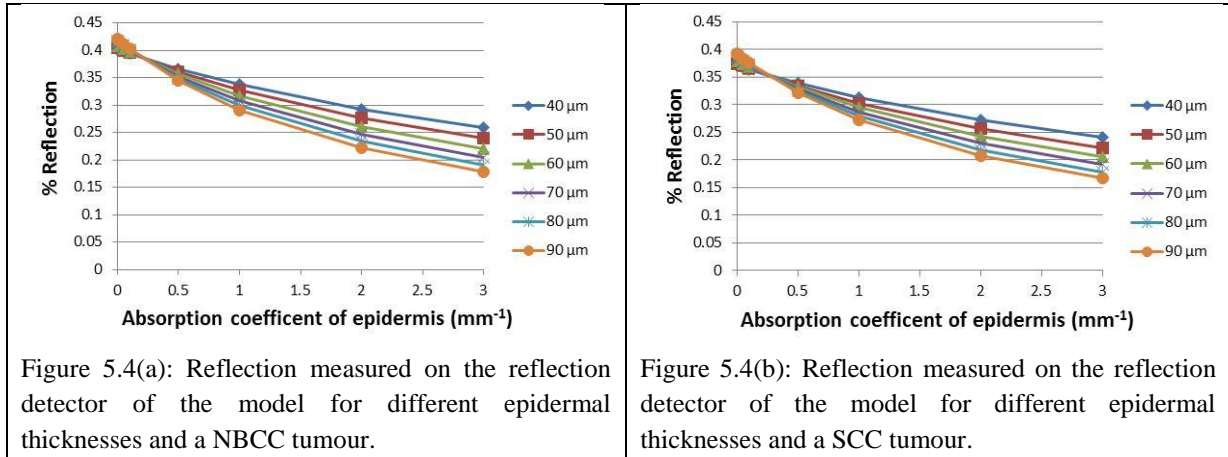


Figure 5.3(b): Fluence rate transmitted through the first 100  $\mu\text{m}$  of the SCC model for the different epidermal thicknesses.

As expected, the transmitted fluence rate values decrease with an increase in the absorption coefficient and with an increase in epidermal thickness. Once again the effect is similar for both tumours.

In the model all the reflected light (both direct reflection and diffuse reflection) is detected on the back reflection detector behind the light source (Figure 5.1(a)). The measured reflection decreases with an increase in the absorption coefficient (Figure 5.4 (a,b)). The decrease in reflection can be ascribed to the fact that an increase in absorption coefficient reduces the amount of light that can be reflected and is therefore the expected behaviour.



Even though the tumour properties have an influence on the fluence rate just before the tumour, the major contributions are attributable to the epidermal thickness and absorption coefficient.

#### Clinical applications of the model

For the application of the model in a clinical setting, the fluence rate reaching the tumour site is important. The treatment light dose is normally specified in J/cm<sup>2</sup> which allows optimising of the contribution of the laser power (normally a continuous wave laser or light source) as well as the treatment time. Apart from the absorption taking place in the skin, the light distribution also changes from the original beam profile due to the scattering in the skin, leading to a larger beam diameter.

In this model the initial laser beam diameter was 1.2 cm and the power 50 mW resulting in a fluence rate of 44.2 mW/cm<sup>2</sup>. A laser treatment dose of 4.5 J/cm<sup>2</sup> at a wavelength of 676 nm is a typical parameter established for effectively killing SCC with Photosense® (a commercial PS) in a research laboratory setting in a Petri dish. (Karsten AE, 2011), (Maduray K, 2011). This implies that the cells need to be illuminated for 102 s with the laser. The fraction of the light that is absorbed in the outer skin layers is an important parameter and must be taken into account when calculating the laser dose delivered onto the skin. In the model, the beam spread to about 1.3 cm at a depth of 200 μm with a reduced fluence rate of 38 mW/cm<sup>2</sup>. In Table 5.3 the fraction of the initial power (mW) at a depth of 100 μm is listed for the average over all the epidermal thicknesses used in this work to illustrate the effect of the absorption coefficient on the transmitted power.

Table 5.3: Fraction of power reaching 100 μm into the skin, just entering the dermis for the SCC tumour.

$\mu_a(\text{mm}^{-1})$	0.002	0.005	0.01	0.05	0.10	0.50	1.0	2.0	3.0
Power fraction transmitted	0.60	0.60	0.60	0.60	0.59	0.54	0.49	0.43	0.38

The fraction of the power reaching the tumour at a depth of 200 μm into the model is listed in Table 5.4 for the average over all the epidermal thicknesses. The tumour depth used is an assumption for illustrative purposes. The tumour position can be moved as required by the application.

Table 5.4: Fraction of power reaching the SCC tumour at a depth of 200  $\mu\text{m}$  into the skin and the resulting treatment time to deliver a light dose of 4.5  $\text{J}/\text{cm}^2$  onto the tumour. The laser beam diameter is 1.3 cm at the tumour depth.

$\mu_a$ ( $\text{mm}^{-1}$ )	0.002	0.005	0.01	0.05	0.10	0.50	1.0	2.0	3.0
Power fraction transmitted	0.51	0.51	0.51	0.51	0.50	0.46	0.42	0.36	0.32
Treatment time (s)	235	235	235	235	239	260	285	332	374

For the lighter skins (low  $\mu_a$  values) typically up to skin phototype III, the transmitted power is nearly constant (about 50% of the initial power). In the darker skin (higher  $\mu_a$  values) much less power reaches the tumour, only about 30% of the initial fluence rate. This significantly affects the optimal treatment parameters for the different skin phototypes and may require adjustment in treatment time for the darker skins (up to 50% longer).

Both the epidermal thickness and  $\mu_a$  determine the fluence rate reaching the tumour. In a clinical setting the absorption coefficient can be measured non-invasively before the treatment commences. A diffuse reflectance probe (Zonios G, 2006), (Karsten A, 2012(c)) can be used for these measurements. Specific procedures to maximise the accuracy of the probe are still under investigation. The  $\mu_a$  for most of the lighter skin phototypes (I-III on the Fitzpatrick scale) is below 0.05  $\text{mm}^{-1}$ .

The non-invasive measurement of the epidermal thickness is more problematic and does not fall within the scope of this paper. Data on the epidermal thickness for different skin sites are reported by Whitton (Whitton JT, 1973).

## CONCLUSIONS

Both the thickness of the epidermis and the absorption coefficient of the epidermis are important parameters in PDT treatment planning for embedded tumours. An increase in the epidermal thickness results in increased absorption of light in the epidermis. For the absorption coefficients evaluated, the ratio in the absorption between the thinner (40  $\mu\text{m}$ ) and thicker (90  $\mu\text{m}$ ) epidermal layers stays nearly constant. For the parameters used in this work, the effect of the absorption coefficient in the epidermis (due to the skin phototype) is more important than the effect of the epidermal thickness. The analysis for this work was aimed at typical sun exposed areas of the skin where the incidence of skin cancer is more likely. Other areas of the skin may have thicker epidermal layers which will affect the results. In future work the effect of a non-planar epidermal surface should be investigated as this may potentially have a larger influence on the backscattered light from the epidermis due to the higher differences between the index of refraction for the two media.

In most PDT applications there is a minimum fluence rate required to activate the PS and a maximum beyond which healthy cells will be adversely affected. Within this range, the power of the laser can be adjusted to compensate for light absorbed before reaching the tumour. According to the ANSI laser safety standard (Laser Institute of America, 2007), the safe power density for skin at 676 nm is 200  $\text{mW}/\text{cm}^2$ . When nearing this skin damage threshold, the safer option will be to adjust the irradiation time to result in the required dose instead of increasing the laser power. This irradiation time, for the data used in this work, needs to be increased from 235 s for the lightest skin to 374 s for the darkest skin.

The increase in absorption of laser light in the visible and near infrared wavelengths for darker skins as well as blistering has been reported before (Alaluf S, 2002(a)), (Lanigan S, 2003), (Battle E, 2004). This is in agreement with the result presented here where darker skins (higher  $\mu_a$  values) absorb more of the laser light. The major advantage of this computer model is that the extent of the absorption effect can be quantified and it is consequently possible to compensate for the absorption and establish safe and effective treatment times before treatment commences.

A number of other laser treatments (e.g. hair removal, skin rejuvenation) are typically developed in countries with a more homogenous ethnic base than in South Africa. The absorption coefficients used in the model are typical of that present in the South African population and as such are applicable for the range of South African skin phototypes (inclusive of individuals from Caucasian, African and southern Asian descent). The model can be applied to compensate for different skin types in therapeutic as well as other procedures.

## References

- Breault Research. "The ASAP Primer." <http://www.breault.com>. Breault Research. 2006. <http://www.breault.com/k-base.php> (accessed October 24, 2006).
- Alaluf S, Atkins D, Barrett K, Blount M, Carter N, Heath A. "Ethnic Variation in Melanin Content and Composition in Photoexposed and Photoprotected Human Skin." *Pigment Cell Res* 15 (2002(a)): 112-118.
- Battle E, Hobbs L. "Laser-assisted hair removal for darker skin types." *Dermatologic Therapy* 17 (2004): 177-183.
- Bouchier-Hayes L, Lartigue L, Newmeyer DD. "Mitochondria: pharmacological manipulation of cell death." *J Clin Invest* 115 (2005): 2640-2647.
- Brown SB, Brown EA, Walker I. "The present and future role of photodynamic therapy in cancer treatment." *Lancet Oncol* 5 (2004): 497-508.
- Calzavara-Pinton PG, Venturini M, Sala R. "Photodynamic therapy: update 2006 Part 1: Photochemistry and photobiology." *JEADV* 21 (2007): 293-302.
- Cansa. *Statistics - National cancer registry*. 2001. [http://www.cansa.org.za/cgi-bin/giga.cgi?cmd=cause\\_dir\\_news&cat=821&cause\\_id=1056&limit=all&page=0&sort=D](http://www.cansa.org.za/cgi-bin/giga.cgi?cmd=cause_dir_news&cat=821&cause_id=1056&limit=all&page=0&sort=D) (accessed March 14, 2012).
- Castano AP, Demidova TN, Hamblin MR. "Mechanism in photodynamic therapy: part one – photosensitizers, photochemistry and cellular location." *Photodiagnosis and Phototherapy* 1 (2004): 279-293.
- Cheong WF, Prahl SA, Welch AJ. "A Review of the Optical Properties of Biological Tissues." *IEEE J. Quantum Electronics* 26 (1990): 2166-2185.
- Dam JS, Dalgaard P, Fabricius PE, Andersson-Engels S. "Multiple polynomial regression method for determination of biomedical optical properties from integrating sphere measurements." *Applied Optics* 39 (2000(a)): 1202-1209.
- Fabrizio M, Del Bianco S, Ismaelli A, Zaccanti G. *Scattering and Absorption Properties of Diffusive Media*. SPIE Press, 2010.
- Heney L, Greenstein J. "Diffuse radiation in the galaxy." *Astrophys. Journal* 93 (1941): 70-83.
- Ishimaru A. "Diffusion of light in turbid material." *Applied Optics* 28, no. 12 (1989): 2210-2215.
- Jacques S, Pogue BW. "Tutorial on diffuse light transport." *Journal of Biomedical Optics* 13 (2008(b)): 1-19.
- Johns M, Giller CA, German DC, Liu H. "Determination of reduced scattering coefficient of biological tissue from a needle-like probe." *Optics Express* 13 (2005): 4828-4842.
- Karsten A, Singh A, Karsten P, Braun M. "Diffuse reflectance spectroscopy as a tool to measure the absorption coefficient in skin: South African skin phototypes." *Photochemistry & Photobiology*, 2012(c): DOI: 10.1111/j.1751-1097.2012.01220.
- Karsten AE, Singh A, Braun MW. "Experimental verification and validation of a computer model for light-tissue interaction." *Lasers Med Sci* 27 (2012(a)): 79-86.
- Karsten AE, Singh A, Ndhundhum IM. "Resin phantoms as skin simulating layers." *SA Institute of Physics Conference, St George Hotel, Pretoria, 12-15 July 2011*. SAIP <http://hdl.handle.net/10204/5665>, 2011. 1-6.
- Kessel D, Lou Y. "Mitochondrial photodamage and PDT-induced apoptosis." *J Photochem Photobiol B* 42 (1998): 89-95.
- Lanigan S. "Incidence of side effects after laser hair removal." *J Am Acad Dermatol* 49 (2003): 882-886.
- Laser Institute of America. *ANSI Z136.1 - 2007 for Safe Use of Lasers*. Laser Institute of America, 2007.
- MA, Stevenson. *Human Skin and Tissue Phantoms in Optical Software: Engineering Design and Future Medical Applications*. The University of Arizona, <http://hdl.handle.net/10150/146219>, 2009.
- Maduray K, Karsten A, Odhav B, Nyokong T. "In vitro toxicity testing of zinc tetrasulfophthalocyanines in fibroblast and keratinocyte cells for the treatment of melanoma cancer by photodynamic therapy." *Journal of Photochemistry and Photobiology B: Biology* 103 (2011): 98-104.
- Michel B, Beck TJ. "Raytracing in Medical Applications." *Laser+Photonik* 5 (2005): 38-40.
- Mqoqi N, Kellest P, Sitas F, Jula M. *Incidence Of Histologically Diagnosed Cancer In South Africa, 1998 – 1999*. 2004. <http://www.cansa.org.za/unique/cansa/files/stats98.pdf> (accessed May 14, 2012).

- National Cancer Institute. *Learning about skin cancer*. 2011. <http://www.genome.gov/10000184> (accessed January 15, 2012).
- Nombona N, Maduray K, Antunes E, Karsten A, Nyokong T. "Synthesis of phthalocyanine conjugates with gold nanoparticles and liposomes for photodynamic therapy." *Journal of Photochemistry and Photobiology B: Biology* 107 (2011): 35–44.
- Pfefer TJ, Matchette L S, Bennett CL, Gall JA, Wilke JN, Durkin AJ, Ediger M. "Reflectance-based determination of optical properties in highly attenuating tissue." *Journal of Biomedical Optics* 8 (2003): 206–215.
- Robertson C A, Hawkins Evans D, Abrahamse H. "Photodynamic therapy (PDT): A short review on cellular mechanisms and cancer research applications for PDT." *Journal of Photochemistry and Photobiology B: Biology* 96 (2009): 1–8.
- Salomatina E, Jiang B, Novak J, Yaroslavsky AN. "Optical properties of normal and cancerous human skin in the visible and near-infrared spectral range." *Journal of Biomedical Optics* 11, no. 6 (2006): 064026-1.
- Sekkat N, van den Bergh H, Nyokong T, Lange N. "Like a Bolt from the Blue: Phthalocyanines ." *Biomedical Optics Molecule* 17 (2012): 98-144.
- Sharman WM, Allen CM, van Lier JE. "Photodynamic therapeutics: basic principles and clinical applications." *Drug Discov Today* 4 (1999): 507-517.
- Tseng S, Bargo P, Durkin A, Kollias N. "Chromophore concentrations, absorption and scattering properties of human skin in-vivo." *Optics Express* 17 (2009): 14599-14617.
- Tuchin V. *Tissue Optics: Light Scattering Methods and Instruments for Medical Diagnostics*. 2nd edition, p 165-175. SPIE Press, 2007.
- Whitton JT, Everall JD. "The thickness of the epidermis." *British Journal of dermatology* , 1973: 467-476.
- Wilson BC, Patterson MS. "The physics, biophysics and technology of photodynamic therapy." *Phys. Med. Biol* 53 (2008): R61–R109.
- Zonios G, Dimou A. "Modeling diffuse reflectance from semi-infinite turbid media: application to the study of skin optical properties." *Optics Express* 14 (2006): 8661-8674.

## 5.2 VALUE OF THE EPIDERMAL ABSORPTION WORK

In this chapter the range of values for the epidermal absorption coefficient obtained by measurements (Chapter 4) were combined with the computer model (Chapter 3) to illustrate the effect of epidermal absorption through the application of PDT treatment of a cancerous tumour. The principles can however be applied to any skin related laser treatment. In laser treatment planning both the thickness and the absorption coefficient of the epidermis are important parameters that must be taken into account. Darker skin phototypes may require up to 50% longer treatment time (374 s) than lighter skin phototypes (235 s) to deliver the same dose 200  $\mu\text{m}$  into the skin.

For individualised treatment, the ideal situation would be to do a diffuse reflectance measurement on the patient before beginning treatment to determine the absorption coefficient for the treatment location. This value can then be used to adjust either the treatment time or laser power or both, depending on the application.

In the next chapter the objectives set out in the beginning will be evaluated in the context of the results achieved in this thesis.

## CHAPTER 6: CONCLUSIONS AND WAY FORWARD

This chapter provides a summary of the important findings of the thesis followed by a comparison between the original objectives and the results of the thesis. The limitations and areas for further research will be discussed as well as the relevance of the work to the broader community.

### 6.1 BRIEF SUMMARY OF THE MAJOR FINDINGS AND CONTRIBUTIONS OF THE WORK IN THE THESIS

A layered structure computer model to predict the laser fluence rate inside skin was *developed, verified and validated* with optical measurements on skin simulating phantoms (Chapter 3). Optical properties from literature may be used, but the absorption coefficients expected for the different skin phototypes were not available in the open literature.

The diffuse reflectance probe (DRP) system together with the software algorithms developed was able to provide values for the expected range of absorption coefficients for the skin phototypes present in the South African population (Chapter 4). Initial data analysis indicated that the melanin contribution in the algorithm should be separated into the two major melanin types (eumelanin and pheomelanin). The original work on which the DRP measurements was based did not make this distinction and only used the dominant eumelanin, which is generally appropriate for lighter skin phototypes.

Implementing the model with the measured absorption coefficients indicated (section 5.1) the effect of the different epidermal absorption values, as well as the effect of scattering in the outer skin layers. The fluence rate decreases by at least 50% in the first 0.2 mm into the skin due to scattering, irrespective of the skin phototype. For the more absorbing skin phototypes there is a further *loss of about 20% due to epidermal absorption*. With this information available, the laser treatment parameters may be adjusted to compensate, either by increasing the initial fluence rate (if the fluence rate is below the damage threshold and the laser power can be increased) or by increasing the treatment time.

### 6.2 OBJECTIVES SET OUT AND THEIR ACHIEVEMENT

The objectives set in the beginning of this thesis and how well they were accomplished is described in this section:

### **6.2.1 Objective 1: To develop a computer model that can predict the laser fluence rate some distance into skin.**

This was achieved through the following:

- A layered structure skin computer model was developed in ASAP software. (Chapters 3 and 5)
- The computer model has been successfully validated with optical measurements on skin simulating phantoms. (Chapter 3)
- The model has been applied for the determination of fluence rates inside the skin for different skin phototypes. (Chapter 5)

### **6.2.2 Objective 2: To develop a non-invasive optical measurement technique to determine the epidermal absorption coefficient of an individual.**

This was achieved through the following:

- Using a diffuse reflectance probe system (based on commercially available components), software algorithms were developed to extract the absorption coefficient of the epidermis (or outer skin layers) non-invasively for different skin phototypes. The results established that the principle can be applied, but the study needs to be repeated on a much larger population sample before the system may be usable in a clinical setting. (Chapter 4)
- The extracted data gave the first indication of the range of the epidermal absorption coefficients to be expected across the South African population. (Chapter 4)
- The contributions of eumelanin and pheomelanin were explicitly separated in the data extraction algorithm. This was a requirement for dealing with the results of individuals from Southern Asian descent in the South African population. The concept has been reported in section 4.4.1 in the paper “*Diffuse reflectance spectroscopy as a tool to measure the absorption coefficient in skin: South African skin phototypes*” (Karsten A, 2012(c)).

### **6.2.3 Objective 3: To determine the effect of skin phototype on the absorption of laser light in the epidermis.**

This was achieved through the following:

- The fluence rate loss through the epidermis was quantified using the computer model for the various South African skin phototypes. The results

indicated (as expected) that the darker skin phototypes absorb more of the laser light. For the PDT application used in this work, the darker skin phototypes absorbed 20% more light than the lighter skin phototypes.

- Once effective and safe laser skin treatment parameters have been established for a specific procedure and a specific skin phototype, the computer model may be used to predict the parameters for other skin phototypes. This ‘scaling’ effect (up or down) is wavelength dependant and the model should be applied at the specific treatment wavelength.

### **6.3 LIMITATIONS OF THE WORK**

- The planar skin model used did not take the possible effect of a wavy epidermal outer surface into account. Tests on the effect of a wavy epidermal/dermal interface showed that the results were similar when compared with the corresponding planar surface (mainly due to the small difference in the refractive index between the two layers). The effect may be larger when the wavy surface is the air-epidermis boundary (refractive index 1 and 1.5 respectively). This was not investigated in the present work, because the focus was on the effect of the epidermal absorption and a simpler model was chosen.
- The data collected on the range of epidermal absorption coefficients for the South African population during the diffuse reflectance probe measurements was insightful and sufficient for the original objective of that part of the work. In order to use the data with confidence to determine an individual’s epidermal absorption coefficient, the work needs to be expanded to a much larger sample of the population. To enhance accuracy more than three measurements should be done at each measurement point.
- The probe system used in the measurements did not allow for probing different depths into the skin. A system with multiple collecting fibres located at different distances from the emitting fibre may allow for probing at different depths or skin layers.

## **6.4 FURTHER INVESTIGATIONS IDENTIFIED**

The major issues identified in this work that need further investigation:

- The diffuse reflectance probe measurements should be refined on a much larger sample of the South African population in order to apply the technique with confidence in a clinical setting.
- The diffuse reflectance probe and computer models are only valid for ‘near dermal’ applications. For applications deeper into the skin, the effect of blood vessels should be added to the model. This may constitute the next phase of the work.
- A diffuse reflectance probe system with multiple collecting fibres should be developed to test if it will be suitable for probing deeper skin layers or at other depths.
- The exact relationship between the melanin concentration extracted chemically from skin biopsies and the absorption coefficient deduced by optical means (diffuse reflectance probe) has not been clarified. This needs further investigation as well as how these parameters relate to the diffuse reflectance probe measurements.

## **6.5 CONTRIBUTIONS OF THE WORK TO THE SCIENTIFIC COMMUNITY AND THE WIDER PUBLIC**

### **6.5.1 Contribution to the scientific community**

- The computer model is an uncomplicated planar model. The use of a wavy interface between the epidermis and dermis did not change the fluence rate data significantly and this shows that a planar model is sufficient for this application.
- The model gives a good indication of the expected fluence rate at the required depth into the skin.
- The diffuse reflectance probe measurements and analysis led to the conclusion that both eumelanin and pheomelanin contributions should be accounted for in the data extraction equations. It has a more pronounced influence on people from Asian (and potentially some African) descent, but does not influence the lighter and darker skin phototypes significantly.

- The *in vivo* diffuse reflectance measurements gave the first results of the expected range of the epidermal absorption coefficient for the South African population.

### 6.5.2 Contribution to the wider public

- The process to establish a new laser treatment technique is a lengthy one. One of the initial steps is to determine the required laser parameters (amongst other parameters) in a biochemistry laboratory on the appropriate cells in a petri dish (*in vitro*). Once success is achieved, one of the next steps is to translate this information to *in vivo* testing. Due to the scattering and absorption of the laser light through the tissue, the laboratory parameters cannot be used unaltered in the initial clinical trials. The computer model developed here has the potential to be used in bridging this gap in order to reduce the number of clinical test required in the development process.
- The non-invasive diffuse reflectance measurements, performed on a patient before treatment commences, in combination with the computer model may ensure more accurate and individualised treatment parameters.

## 6.6 CONCLUSIONS

This thesis documents the development of a layered planar computer model to predict laser fluence rate at some depth into skin. The computer model was validated and calibrated against optical measurements on skin simulating phantoms. It was shown that a planar epidermal/dermal interface is adequate for simulation purposes.

The epidermal absorption coefficients of a small sample of the South African population were measured with a diffuse reflectance probe system. These measurements were the first to be done to determine the expected range of skin phototypes of the South African population.

Given the positive results, the computer model was used to evaluate the effect of the epidermal absorption coefficient (a parameter dictated by an individual's skin phototype) to predict the adjustment in laser treatment times for different absorption coefficients. Application of the computer model to photodynamic treatment of skin cancer indicated that treatment times need to be adjusted (by as much as 50%) when comparing very fair skin phototypes with very dark skin phototypes.

## REFERENCES

- Adrian RM, Shay KP. “800 nanometer diode laser hair removal in African American patients: a clinical and histologic study.” *Journal of Cutaneous Laser Therapy* 2 (2000): 183-190.
- Agache P, Humbert P. *Measuring the skin*. ISBN 3-540-01771-2. Springer-Verlag, 2004.
- Alaluf S, Heath A, Carter N, Atkins D, Mahalingam H, Barrett K, Kolb R, Smit N. “Variation in Melanin Content and Composition in Type V and VI Photoexposed and Photoprotected Human Skin: The Dominant Role of DHI.” *Pigment Cell Res* 14 (2001): 337–347.
- Alaluf S, Atkins D, Barrett K, Blount M, Carter N, Heath A. “Ethnic Variation in Melanin Content and Composition in Photoexposed and Photoprotected Human Skin.” *Pigment Cell Res* 15 (2002(a)): 112-118.
- Alaluf S, Atkins D, Barrett K, Blount M, Carter N, Heath A. “The Impact of Epidermal Melanin on Objective Measurements of Human Skin Colour.” *Pigment Cell Res* 15 (2002(b)): 119-126.
- Amelink A, Sterenborg H, Bard M, Burgers S. “In vivo measurement of the local optical properties of tissue by use of differential path-length spectroscopy.” *Opt. Lett.* 29 (2004): 1087-1089.
- Anderson RR, Parrish JA. “The optics of human skin.” *J Invest Dermatol* 77 (1981): 13-19.
- Bashkatov AN, Genina EA, Kochubey VI, Tuchin VV. “Optical properties of human skin, subcutaneous and mucous tissues in the wavelength range from 400 to 2000 nm.” *J. Phys. D: Appl. Phys.* 38 (2005): 2543-2555.
- Battle E, Hobbs L. “Laser-assisted hair removal for darker skin types.” *Dermatologic Therapy* 17 (2004): 177–183.
- Baxamua BN. *Skin Tone Chart*. 2012. <http://www.buzzle.com/articles/skin-tone-chart.html> (accessed August 28, 2012).
- Bouchier-Hayes L, Lartigue L, Newmeyer DD. “Mitochondria: pharmacological manipulation of cell death.” *J Clin Invest* 115 (2005): 2640–2647.
- Breault Research. “ASAP Technical guide: Radiometric analysis.” <http://www.breault.com>. Breault Research. 2007. (accessed June 17, 2008).
- Breault Research. “The ASAP Primer.” <http://www.breault.com>. Breault Research. 2006. <http://www.breault.com/k-base.php> (accessed October 24, 2006).
- Brown SB, Brown EA, Walker I. “The present and future role of photodynamic therapy in cancer treatment.” *Lancet Oncol* 5 (2004): 497–508.
- Calzavara-Pinton PG, Venturini M, Sala R. “Photodynamic therapy: update 2006 Part 1: Photochemistry and photobiology.” *JEADV* 21 (2007): 293-302.
- Cansa. *Statistics - National cancer registry*. 2001. [http://www.cansa.org.za/cgi-bin/giga.cgi?cmd=cause\\_dir\\_news&cat=821&cause\\_id=1056&limit=all&page=0&sort=D](http://www.cansa.org.za/cgi-bin/giga.cgi?cmd=cause_dir_news&cat=821&cause_id=1056&limit=all&page=0&sort=D) (accessed March 14, 2012).
- Castano AP, Demidova TN, Hamblin MR. “Mechanism in photodynamic therapy: part one – photosensitizers, photochemistry and cellular location.” *Photodiagnosis and Phototherapy* 1 (2004): 279-293.

- Cheong WF, Prah SA, Welch AJ. "A Review of the Optical Properties of Biological Tissues." *IEEE J. Quantum Electronics* 26 (1990): 2166-2185.
- Choukeife JE, L'Huillier JP. "Measurements of Scattering Effects within Tissue-like Media at two Wavelengths of 632.8 nm and 680 nm." *Lasers Med Sci* 14 (1999): 286–296.
- Coleman T, Li Y. "On the Convergence of Reflective Newton Methods for Large-Scale Nonlinear Minimization Subject to Bounds." *Mathematical Programming* 67 (1994): 189-224.
- Coleman T, Li Y. "An Interior Trust Region Approach for Nonlinear Minimization Subject to Bounds." *SIAM Journal on Optimization* 6 (1996): 418-445.
- Costin GE, Hearing VJ. "Human skin pigmentation: Melanocytes modulate skin color in response to stress." *FASEB J* 21 (2007): 976-994.
- Dam JS, Dalgaard P, Fabricius PE, Andersson-Engels S. "Multiple polynomial regression method for determination of biomedical optical properties from integrating sphere measurements." *Applied Optics* 39 (2000(a)): 1202-1209.
- Dam JS. *Optical analysis of biological media - continuous wave techniques*. ISBN 91-628-4546-2. Lund Reports on Atomic Physics LRAP-265, 2000(b).
- Das BB, Liu F, Alfano RR. "Time-resolved fluorescence and photon migration studies in biomedical and model random media." *Rep. Prog Phys* 60 (1997): 227-292.
- Dimofte A, Finlay JC, Zhu TC. "A method for determination of the absorption and scattering properties interstitially in turbid media." *Phys. Med. Biol.* 50 (2005): 2291–2311.
- Doornbos R, Lang R, Aalders M, Cross F, Sterenborg H. "The determination of in vivo human tissue optical properties and absolute chromophore concentrations using spatially resolved steady-state diffuse reflectance spectroscopy." *Phys. Med. Biol* 44 (1999): 967-981.
- Doronin A, Meglinski I. "Online object oriented Monte Carlo computational tool for the needs of biomedical optics." *Biomedical Optics Express* 2 (2011): 2461-2469.
- Drakaki E, Psycharakis S, Makropoulou M, Serafetinides AA. "Optical properties and chromophore concentration measurements in tissue-like phantoms." *Optics Communications* 254 (2005): 40–51.
- Fabrizio M, Del Bianco S, Ismaelli A, Zaccanti G. *Scattering and Absorption Properties of diffusive Media*. SPIE Press, 2010.
- Farrel TJ, Patterson MS. "A diffuse theory model of spatially resolved, steady-state diffuse reflectance for the noninvasive determination of tissue optical properties in vivo." *Med. Phys.* 19 (1992): 879-888.
- Firbank M, Delpy DT. "A design for a stable and reproducible phantom for use in near infrared imaging and spectroscopy." *Phys. Med. Biol.* 38 (1993): 847-853.
- Fitzpatrick TB. "The validity and practicality of sunreactive skin type-I through type-VI." *Arch Dermatol* 124 (1988): 869–871.
- Flock S, Jacques S, Wilson B, Star W, van Gemert M. "Optical Properties of Intralipid: A phantom medium for light propagation studies." *Lasers in Surgery and Medicine* 2 (1992): 510-519.
- Fu D, Ye T, Grichnik J, Hong L, Simon J, Warren S. "Probing skin pigmentation changes with transient absorption imaging of eumelanin and pheomelanin." *Journal of Biomedical Optics* 13, no. 5 (2008): 054036.

- González FJ, Martínez-Escanamé M, Muñoz RI, Torres-Álvarez B, Moncada B. “Diffuse reflectance spectrophotometry for skin phototype determination.” *Skin Research and Technology* 16 (2010): 397-400.
- Graaff R, Dassel ACM, Koelink MH, de Mul FFM, Aarnoudse JG, Zijlstra WG. “Optical properties of human dermis in vitro and in vivo.” *Appl Opt* 32 (1993): 435-447.
- Grossweiner LI. “PDT light dosimetry revisited.” *Journal of Photochemistry and Photobiology B: Biology* 38 (1997): 258-268.
- Hecht E, Zajac A. *Optics*. Addison-Wesley, 1974.
- Heney L, Greenstein J. “Diffuse radiation in the galaxy.” *Astrophys. Journal* 93 (1941): 70-83.
- Holcomb PS. “Under the skin.” *Laser+Photonik* 5 (2006): 56-58.
- Hopper C. “Photodynamic therapy: a clinical reality in the treatment of cancer.” *THE LANCET Oncology* 1 (2000): 212-219.
- IEEE. *What is Biophotonics?* 2004.  
<http://photonicsociety.org/newsletters/apr04/biophoto.html> (accessed March 12, 2012).
- Ishimaru A. “Diffusion of light in turbid material.” *Applied Optics* 28, no. 12 (1989): 2210-2215.
- Jacques SL, Prahl SA. *Introduction to Biomedical Optics*. 1998(a).  
<http://omlc.ogi.edu/classroom/ece532/class3/index.html> (accessed May 15, 2012).
- Jacques SL, Prahl SA. *Steady-state Monte Carlo: A minimal program, "mc321.c"*. 1998(b).  
<http://omlc.ogi.edu/classroom/ece532/class4/ssmc/index.html> (accessed May 16, 2012).
- Jacques S. *Oregon Medical Laser Centre website*. 2001.  
<http://omlc.ogi.edu/spectra/melanin/index.html> (accessed November 24, 2011).
- Jacques SL. “Modeling tissue optics using Monte Carlo modeling: a tutorial.” Edited by Roach WP, Thomas RJ Jacques SL. *Optical Interactions with Tissue and Cells XIX, SPIE Vol. 6854*. SPIE, 2008(a). 1605-7422.
- Jacques S, Pogue BW. “Tutorial on diffuse light transport.” *Journal of Biomedical Optics* 13 (2008(b)): 1-19.
- Jacques SL. “How tissue optics affect dosimetry of photodynamic therapy.” *Journal of Biomedical Optics* 15, no. 5 (2010): 051608-1.
- Johns M, Giller CA, German DC, Liu H. “Determination of reduced scattering coefficient of biological tissue from a needle-like probe.” *Optics Express* 13 (2005): 4828-4842.
- Karsten AE, Singh A, Ndhundhum IM. “Resin phantoms as skin simulating layers.” *SA Institute of Physics Conference, St George Hotel, Pretoria, 12-15 July 2011*. SAIP <http://hdl.handle.net/10204/5665>, 2011. 1-6.
- Karsten AE, Singh A, Braun MW. “Experimental verification and validation of a computer model for light–tissue interaction.” *Lasers Med Sci* 27 (2012(a)): 79–86.
- Karsten A, Singh A, Karsten P, Braun M. “Diffuse reflectance spectroscopy as a tool to measure the absorption coefficient in skin: system calibration.” *Lasers in Medical Science* DOI 10.1007/s10103-012-1079-2 (2012(b)).

- Karsten A, Singh A, Karsten P, Braun M. "Diffuse reflectance spectroscopy as a tool to measure the absorption coefficient in skin: South African skin phototypes." *Photochemistry & Photobiology*, 2012(c): DOI: 10.1111/j.1751-1097.2012.01220.
- Kessel D, Lou Y. "Mitochondrial photodamage and PDT-induced apoptosis." *J Photochem Photobiol B* 42 (1998): 89-95.
- Kollias N. "The Physical Basis of Skin Color and its Evaluation." *Clinics in Dermatology* 13 (1995): 361-367.
- Kurtz SK, Kozikowski S, Wolfram LJ. "Optical constants of solid melanins determined from reflection measurements in the visible spectrum." *J Invest Dermatol* 87 (1986).
- Labsphere. *A Guide to Integrating Sphere Theory and Applications*. 2012. <http://www.photonicsonline.com/doc.mvc/Tech-Guide-A-Guide-To-Integrating-Sphere-Theo-0001> (accessed May 16, 2012).
- Lanigan S. "Incidence of side effects after laser hair removal." *J Am Acad Dermatol* 49 (2003): 882-886.
- Laser Institute of America. *ANSI Z136.1 - 2007 for Safe Use of Lasers*. Laser Institute of America, 2007.
- Lepselter J, Elman M. "Biological and clinical aspects in laser hair removal." *Journal of Dermatological Treatment* 15 (2004): 72-83.
- Lim SRP, Lanigan SW. "A review of the adverse effects of laser hair removal." *Lasers Medical Science* 21 (2006): 121-125.
- Liu Y, Hong L, Wakamatsu K, Ito S, Adhyaru B, Cheng CY, Bowers CR, and Simon JD. "Comparison of structural and chemical properties of black and red human hair melanosomes." *Photochem. Photobiol* 81 (2005): 135-144.
- Maduray K, Karsten A, Odhav B, Nyokong T. "In vitro toxicity testing of zinc tetrasulfophthalocyanines in fibroblast and keratinocyte cells for the treatment of melanoma cancer by photodynamic therapy." *Journal of Photochemistry and Photobiology B: Biology* 103 (2011): 98-104.
- Mang TS. "Lasers and light sources for PDT: past present and future." *Photodiagnosis and Photodynamic Therapy* 1 (2004): 43-48.
- Marchesini R, Bono A, Carrara M. "In vivo characterization of melanin in melanocytic lesions: spectroscopic study on 1671 pigmented skin lesions." *Journal of Biomedical Optics* 14 (2009): 014027.
- Martelli F, Del Bianco S, Ismaelli A, Zaccanti G. *Light Propagation through Biological Tissue and Other Diffusive Media*. ISBN 978-0-8194-7658-6. SPIE Press, 2010.
- MD Anderson Cancer Centre. *Skin Cancer*. 2009. <http://health.usnews.com/health-conditions/cancer/skin-cancer> (accessed May 16, 2012).
- Meglinsky IV, Matcher SJ. "Modelling the sampling volume for skin blood oxygenation measurements." *Med Biol Eng Comput* 39 (2001): 44-50.
- Meglinski IV, Matcher SJ. "Quantitative assessment of skin layers absorption and skin reflectance spectra simulation in the visible and near-infrared spectral regions." *Physiol. Meas.* 23 (2002): 741-753.
- Michel B, Beck TJ. "Raytracing in Medical Applications." *Laser+Photonik* 5 (2005): 38-40.

- Michielsen K, De Raedt H, Przeslawski J, Garcia N. “Computer simulation of time-resolved optical imaging of objects hidden in turbid media.” *Physics Reports* 304 (1998): 89-144.
- Mqoqi N, Kellett P, Sitas F, Jula M. *Incidence Of Histologically Diagnosed Cancer In South Africa, 1998 – 1999*. 2004. <http://www.cansa.org.za/unique/cansa/files/stats98.pdf> (accessed May 14, 2012).
- Mustafa FH, Jaafar MS, Ismai AH, Omar AF, Timimi ZA, Houssein HA. “Red Diode Laser in the Treatment Epidermal Diseases in PDT.” *World Academy of Science, Engineering and Technology* 70 (2010): 780-783.
- Mustafa FH, Jaafar MS, Ismail AH. “Control Light Delivery in PDT by Taking Account the Optical Properties of Hair Density on the Skin Surface.” *Modern Applied Science* 5, no. 2 (2011): 149-155.
- National Cancer Institute. *Learning about skin cancer*. 2011. <http://www.genome.gov/10000184> (accessed January 15, 2012).
- Nilsson AM, Stureson KC, Liu DL, Andersson-Engels S. “Changes in spectral shape of tissue optical properties in conjunction with laser-induced thermotherapy.” *Appl. Opt.* 37 (1998): 1256-1267.
- Nombona N, Maduray K, Antunes E, Karsten A, Nyokong T. “Synthesis of phthalocyanine conjugates with gold nanoparticles and liposomes for photodynamic therapy.” *Journal of Photochemistry and Photobiology B: Biology* 107 (2011): 35–44.
- Overton G, Anderson S, Belforte D, Hausken T. “Annual review and forecast.” *Laser Focus World* 47 (2011): 40-60.
- Peng Q, Juzeniene A, Chen J, O'Svaasand L, Warloe T, Giercksky K, Moan J. “Lasers in Medicine.” *Rep Prog Phys* 71 (2008): 1-28 (doi:10.1088/0034-4885/71/5/056701).
- Pfefer TJ, Matchette LS, Bennett CL, Gall JA, Wilke JN, Durkin AJ, Ediger M. “Reflectance-based determination of optical properties in highly attenuating tissue.” *Journal of Biomedical Optics* 8 (2003): 206–215.
- Pickering JW, Prah SA, van Wieringen N, Beek JF, Sterenborg HJCM, van Gemert MJC. “Double integrating-sphere system for measuring the optical properties of tissue.” *Appl. Opt* 32 (1993): 399-410.
- Pogue B W, Patterson MS. “Review of tissue simulating phantoms for optical spectroscopy, imaging and dosimetry.” *Journal of Biomedical Optics* 11, no. 4 (2006): 041102-1 – 041102-16.
- Prah SA, Keijzer M, Jacques SL, Welch AJ. “A Monte Carlo Model of Light Propagation in Tissue.” In *SPIE Institute Series Vol. IS 5*, 102-111. SPIE, 1989.
- Prah S. *Oregon Medical Laser Centre website - Optical Absorption of Hemoglobin*. 1999. <http://omlc.ogi.edu/spectra/hemoglobin/index.html> (accessed November 24, 2011).
- Prah S. *Oregon Medical Laser Centre website*. 2007(a). <http://omlc.ogi.edu/software/> (accessed December 13, 2011).
- Prah S. *Monte Carlo Simulations*. 2007(b). <http://omlc.ogi.edu/software/mc/> (accessed August 28, 2012).
- Reif R, A’Amar O, Bigio I. “Analytical model of light reflectance for extraction of the optical properties in small volumes of turbid media.” *Applied Optics* 46 (2007): 7317-7328.

- Reif R, Amorosino MS, Calabro KW, A' Amar O, Singh SK, Bigioa IJ. "Analysis of changes in reflectance measurements on biological tissues subjected to different probe pressures." *Journal of Biomedical Optics* 13 (2008): 010502-1-3.
- Robertson CA, Hawkins Evans D, Abrahamse H. "Photodynamic therapy (PDT): A short review on cellular mechanisms and cancer research applications for PDT." *Journal of Photochemistry and Photobiology B: Biology* 96 (2009): 1–8.
- Salomatina E, Jiang B, Novak J, Yaroslavsky AN. "Optical properties of normal and cancerous human skin in the visible and near-infrared spectral range." *Journal of Biomedical Optics* 11, no. 6 (2006): 064026-1.
- Scheuplein RJ. "A survey of some fundamental aspects of the absorption and reflection of light by tissue." *Journal of the Society of Cosmetic Chemists* 15 (1964): 111-122.
- Schuitmaker J, Baas P, van Leengoed H, van der Meulen F, Star W, van Zandwijk N. "Photodynamic therapy: a promising new modality for the treatment of cancer." *Journal of Photochemistry and Photobiology B: Biology* 34 (1996): 3-12.
- Sekkat N, van den Bergh H, Nyokong T, Lange N. "Like a Bolt from the Blue: Phthalocyanines." *Biomedical Optics Molecule* 17 (2012): 98-144.
- Sharman WM, Allen CM, van Lier JE. "Photodynamic therapeutics: basic principles and clinical applications." *Drug Discov Today* 4 (1999): 507-517.
- Simpson R, Kohl M, Essenpreis M, Cope M. "Near-infrared optical properties of ex vivo human skin and subcutaneous tissues measured using the Monte Carlo inversion technique." *Phys. Med. Biol* 43 (1998(a)): 2465–2478.
- Simpson R, Laufer J, Kohl M, Essenpreis M, Cope M. "Measurement of skin optical properties." *BORL: Skin optical properties*. University Colledge London. 1998(b). [http://www.medphys.ucl.ac.uk/research/borg/research/NIR\\_topics/skin/skinoptprop.htm](http://www.medphys.ucl.ac.uk/research/borg/research/NIR_topics/skin/skinoptprop.htm) (accessed July 30, 2012).
- Singh A, Karsten AE, Dam, JS. "Robustness and accuracy of the calibration model for the determination of the optical properties of chicken skin." *International Conference of the World Association of Laser Therapy*. Sun City: Medimond, 2008. 165-169.
- Singh A, Karsten AE, Mputle I, Chetty A and Naidoo K. "Determination of the optical properties of PNIPAAm gels used in biological applications." *European Conference on Biomedical Optics, Munich, 2009*. SPIE 7373, doi:10.1117/12.831882 , 2009. 107.
- Singh A, Karsten AE. "Comparison of the accuracy of the calibration model on the double and single integrating sphere systems." *Proc. 4th International Symposium on Photoelectronic Detection and Imaging (ISPDI 2011)*. SPIE, <http://dx.doi.org/10.1117/12.899879>, 2011. 81924U-1-7.
- Splinter R, Hooper BA. *An Introduction to Biomedical Optics*. CRC Press, Taylor & Francis group, 2007.
- Star WM, Marijnissen JPA, van Gemmert MJC. "Light dosimetry in optical phantoms and in tissues: I. Multiple flux and transport theory." *Phys. Med. Biol.* 3, no. 4 (1988): 437-454.
- Star WM. "Light dosimetry in vivo." *Phys. Med. Biol* 42 (1997): 763–787.
- Stevenson M. "Optical software: which program is right for me?" *Institute of Physics and IOP Publishing Ltd*, 2006.
- Stevenson MA. *Human Skin and Tissue Phantoms in Optical Software: Engineering Design*

- and Future Medical Applications*. The University of Arizona, <http://hdl.handle.net/10150/146219>, 2009.
- Störriing M. *Computer vision and human skin colour*. Ph.D. dissertation, Aalborg University, Denmark, URL: <http://www.cvmt.dk/~mst>, 2004.
- Szabo G, Gerald AB, Pathak MA, Fitzpatrick-TB. “Racial differences in the fate of melanosomes in human epidermis.” *Nature* 222 (1969): 1081-1084.
- Tseng S, Bargo P, Durkin A, Kollias N. “Chromophore concentrations, absorption and scattering properties of human skin in-vivo.” *Optics Express* 17 (2009): 14599-14617.
- Tuchin V. *Tissue Optics: Light Scattering Methods and Instruments for Medical Diagnostics*. First. SPIE Press, 2000.
- Tuchin V. *Tissue Optics: Light Scattering Methods and Instruments for Medical Diagnostics*. 2nd edition, p 165-175. SPIE Press, 2007.
- van Gemert MJC, Jacques SL, Sterenborg HJCM, Star WM. “Skin optics.” *IEEE Trans Biomed Eng* 36 (1989): 1146-1154.
- van Staveren HJ, Moes CJM, van Marie J, Prahl SA, van Gemert MJC. “Light scattering in Intralipid-10% in the wavelength range of 400-1100 nm.” *Applied Optics* 31 (1991): 4507-4514.
- Vo-Dinh T. *Biomedical Photonics Handbook*. ISBN 0-8493-1116-0. CRC Press, 2003.
- Wang Q, Yang H, Agrawal A, Wang NS, Pfefer TJ. “Measurement of internal tissue optical properties at ultraviolet and visible wavelengths: Development and implementation of a fiberoptic-based system.” *Optics Express* 16 (2008): 8685-8703.
- Welch A, van Gemert MJC. *Optical-Thermal Response of Laser-Irradiated Tissue*. 2nd. Springer, 2011.
- Whitton JT, Everall JD. “The thickness of the epidermis.” *British Journal of dermatology*, 1973: 467-476.
- Wilson BC, Jacques SL. “Optical reflection and transmission of tissues: Principles and application.” *IEEE Journal of Quantum Electronics* 26, no. 12 (1990): 2186-2199.
- Wilson BC, Patterson MS. “The physics, biophysics and technology of photodynamic therapy.” *Phys. Med. Biol* 53 (2008): R61–R109.
- Wu J, Partovi F, Field MS, Rava RP. “Diffuse reflectance from turbid media: an analytical model of photon migration.” *Applied Optics* 32 (1993): 1115-1121.
- Yoon T, Lei T, Yamaguchi Y, Batzer J, Wolber R, Hearing V. “Reconstruction of 3-dimensional human skin of various ethnic origins as an in vitro model for studies of skin pigmentation.” *Analytical Biochemistry* 316 (2003): 260-269.
- Zhang R, Verkuysse W, Choi B, Viator JA, Jung B, Svaasand LO, Aguilar G, Nelson JS. “Determination of human skin optical properties from spectrophotometric measurements based on optimization by genetic algorithms.” *Journal of Biomedical Optics* 2 (2005): 024030-1.
- Zhu TC, Finlay JC. “Prostate PDT dosimetry.” *Photodiagnosis and Phototherapy* 3 (2006): 234-246.
- Zonios G, Bykowski J, Kollias N. “Skin melanin, haemoglobin, and light scattering properties can be quantitatively assessed in vivo using diffuse reflectance spectroscopy.” *J. Invest. Dermatol* 117 (2001): 1452-1457.

- Zonios G, Dimou A. "Modeling diffuse reflectance from semi-infinite turbid media: application to the study of skin optical properties." *Optics Express* 14 (2006): 8661-8674.
- Zonios G, Bassukas I, Dimou A. "Comparative evaluation of two simple diffuse reflectance models for biological tissue applications." *Applied Optics* 47 (2008(a)): 4965-4973.
- Zonios G, Dimou A. "Melanin optical properties provide evidence for chemical and structural disorder in vivo." *Optics Express* 16 (2008(b)): 8263-8268.
- Zonios G, Dimou A, Bassukas I, Galaris D, Tsolakidis A, Kaxiras E. "Melanin absorption spectroscopy: new method for noninvasive skin investigation and melanoma detection." *Journal of Biomedical Optics* 13 (2008(c)): 014017-1.

## APPENDIX III: SOURCE CODE FOR THE ASAP COMPUTER MODEL

```
!!++
!! Tumor with macros.INR
!!
!! Description: A skin model is illuminated with a 676nm light source.
!!           The energy absorbed in the slab volume is tracked using the
!!           VOXELS command. Model consists of epidermis, dermis and
!!           tumor embedded in dermis. SCC tumour data is used. The optical
!!           properties used is data published by Solamatmina, Journal of
!!           Biomedical Optics 11(6), 064026 November/December 2006
!!           Note!!!!
!!           The units use by Solamatmina is in mm-1, but
!!           when Tuchin reference it, they mistakenly used
!!           the same values but with units of cm-1.
!!
!!
!!           MACRO OUTPUT ANALYSIS CALCULATES THE ABS AND TRANS THROUGH THE LAYERS
!!
!!MACRO: OUTPUT_ANALYSIS
!! Functions: 1. Output analysis result to .txt file for post processing
!!
OUTPUT_ANALYSIS { 1
$ECHO NONE
$IO OUTPUT #1.TXT -FILE(10)
    $SCR 10
FILENAME = #1.TXT
NUMBER OF RAYS =\NRAYS.\
EPIDERMIS THICKNESS (MM) = \EPIDERMISTHICKNESS.\
TOTAL FLUX REFLECTED = \REFLECTED.\
TOTAL FLUX TRANSMITTED=\TRANSMITTED.\
SLICE THICKNESS=\SLICE_THICKNESS.\
EPIDERMIS MU_A=\E_MUA.\
EPIDERMIS MU_S=\E_MUS.\

SLICE DEPTH (MM) FLUX ABSORBED IN SLICE (mW) FLUX TRANSMITTED IN SLICE (mW)
$IO OUTPUT CLOSE
$ECHO ALL

FTRANS_SLICE=1-REFLECTED          !! VARIABLE DEFINED
$DO 1 (EVAL_ZSLICE)
{
    DISPLAY VOXEL_ABS ?          !!DO ANALYSIS FOR EACH SLICE
    RETURN

$GRAB 'File header:' 2 1 D_SLICE  !!D_SLICE is the variable/register to
!!store the depth of each slice
$GRAB 'Average' 0 1 VOX_FLUX_AVE
$GRAB 'Integral =' 0 1 VOX_FLUX_INT
FLUX_SLICE1=VOX_FLUX_AVE*SLICE_THICKNESS*SLICE_AREA
```

```

FTRANS_SLICE=FTRANS_SLICE-FLUX_SLICE1      !!FLUX TRANSMITTED THROUGH SLICE
$ECHO NONE

$SIO OUTPUT #1.TXT +FILE(10)      !! ALL SUCCESSIVE ITERATIONS '+' ADD DATA
!!TO EXISTING DATA IN FILE

$SCR 1
\D_SLICE. \          \FLUX_SLICE1^ \          \FTRANS_SLICE^\
$SIO OUTPUT CLOSE
}
}
Skin model file name>

!!-----
!!MAIN
!!-----
SYSTEM NEW                                !!COMMANDS TO REINITIALIZE DATA
STORAGE
RESET
BEAMS INCOHERENT GEOMETRIC

!!DEFINE RAY SPLIT AND SCATTER CHARACTERISTICS
    SPLIT 100 MONTECARLO                    !!DETERMINES THE NUMBER OF TIMES A
!!SINGLE RAY CAN BE SPLIT AND HOW
    LEVEL 100 ALL                            !!DETERMINES THE NUMBER OF TIMES A
!!RAY CAN SCATTER FROM A SINGLE SURFACE

FRESNEL AVE

!!SET SYSTEM UNITS
    UNITS MM 'mW'                            !!SETS DISTANCE MEASUREMENT UNITS
!!TO MM AND CREATES THE mW LABEL FOR ENERGY VALUES

!!SET SOURCE WAVELENGTH
    WAVELENGTH 676 NM                        !!SETS WAVELENGTH TO 676NM FOR
TRACE

!!DEFINE COATINGS
    COATING
        0 0 'ABSORB'                            !!ABSORBING COATING
        0 1 'TRANSMIT'                          !!CREATES A COMPLETELY TRANSMITTING
!!(ZERO LOSS) COATING FOR SURFACES
!! DEFINE VARIABLES THAT MAY CHANGE
NRAYS=2001
ZSLICE=309
E_MUA=5.000
EPIDERMISTHICKNESS=0.09
EVAL_ZSLICE=ZSLICE
E_MUS=22.4      !!G=0.8

!!CREATE SCATTER AND ABSORPTION MODELS FOR TISSUE AND TUMOR
!! USE DATA FROM ARTICLE AND RSM @676 NM from Solamatmina
    MODEL !! g      us      ua      F

```

```

VOLUM .80 E_MUS`E_MUA 1 !!EPIDERMIS SCATTER AND ABSORPTION MODEL
VOLUM .80 13.9`0.15 1 !!DERMIS SCATTER AND ABSORPTION MODEL
VOLUME .80 8.55`0.11 1 !!TUMOR SCATTER AND ABSORPTION MODEL USE SCC

!!CREATE MEDIA FOR TISSUE AND TUMOR USE n FROM RSM
MEDIA
  1.50 SCATTER 1 'EPIDERMIS' !!APPLIES TISSUE CATTER AND
!!ABSORPTION MODEL TO MEDIA WITH INDEX OF REFRACTION OF 1.50
  1.40 SCATTER 2 'DERMIS' !!APPLIES TISSUE SCATTER AND
!!ABSORPTION MODEL TO MEDIA WITH INDEX OF REFRACTION OF 1.40
  1.40 SCATTER 3 'TUMOR' !!APPLIES TUMOR SCATTER AND
!!ABSORPTION MODEL TO MEDIA WITH INDEX OF REFRACTION OF 1.40

!!VARIABLES FOR BUILDING GEOMETRY
!!THICKNESSES OF LAYERS AS IN RSM ASSUME SIMMILAR OPTICAL PROPERTIES FOR
!!DERMIS AND HYPODERMIS
HWEPIIDERMIS=20 !!HALF-WIDTH OF EPIDERMIS SURFACE IN MM
HWDERMIS=20 !!HALF-WIDTH OF TISSUE SURFACE IN MM
DERMISTHICKNESS=3 !!TISSUE THICKNESS IN MM
HWTUMOR=5 !!HALF-WIDTH OF TUMOR SURFACE IN MM
TUMORTHICKNESS=2 !!TUMOR THICKNESS IN MM
EPIDERMISLOCATION=0 !!LOCATION OF EPIDERMIS SURFACE ALONG THE Z AXIS
DERMISLOCATION=EPIDERMISTHICKNESS !! DERMIS BEGINS WHERE EPIDERMIS ENDS
TUMORLOCATION=0.2 !!LOCATION OF TUMOR SURFACE ALONG THE Z AXIS

!!EPIDERMIS SLAB GEOMETRY
ENT OBJ
PLANE Z (EPIDERMISLOCATION) RECT (HWEPIIDERMIS) 'EPIDERMIS.SURFACE'
INTERFACE COATING BARE AIR EPIDERMIS
REDEFINE COLOR 10
PLANE X (HWEPIIDERMIS) RECT (HWEPIIDERMIS) (EPIDERMISTHICKNESS/2)
'EPIDERMIS.EDGE1'
INTERFACE COATING ABSORB AIR EPIDERMIS
SHIFT Z (EPIDERMISTHICKNESS/2)
REDEFINE COLOR 10
PLANE X -(HWEPIIDERMIS) RECT (HWEPIIDERMIS) (EPIDERMISTHICKNESS/2)
'EPIDERMIS.EDGE2'
INTERFACE COATING ABSORB AIR EPIDERMIS
SHIFT Z (EPIDERMISTHICKNESS/2)
REDEFINE COLOR 10
PLANE Y (HWEPIIDERMIS) RECT (EPIDERMISTHICKNESS/2) (HWEPIIDERMIS)
'EPIDERMIS.EDGE3'
INTERFACE COATING ABSORB AIR EPIDERMIS
SHIFT Z (EPIDERMISTHICKNESS/2)
REDEFINE COLOR 10
PLANE Y -(HWEPIIDERMIS) RECT (EPIDERMISTHICKNESS/2) (HWEPIIDERMIS)
'EPIDERMIS.EDGE4'
INTERFACE COATING ABSORB AIR EPIDERMIS
SHIFT Z (EPIDERMISTHICKNESS/2)
REDEFINE COLOR 10
PLANE Z (EPIDERMISTHICKNESS) RECT (HWEPIIDERMIS) 'EPIDERMIS.BACK'
INTERFACE COATING BARE EPIDERMIS DERMIS
REDEFINE COLOR 10

```

```

RETURN
!!DERMIS SLAB GEOMETRY
ENT OBJ
PLANE Z (DERMISLOCATION) RECT (HWDERMIS) 'DERMIS.SURFACE'
INTERFACE COATING BARE EPIDERMIS DERMIS
REDEFINE COLOR 14
PLANE X (HWDERMIS) RECT (HWDERMIS)
((DERMISLOCATION+DERMISTHICKNESS)/2) 'DERMIS.EDGE1'
INTERFACE COATING ABSORB AIR DERMIS
SHIFT Z ((DERMISLOCATION+DERMISTHICKNESS)/2)
REDEFINE COLOR 14
PLANE X -(HWDERMIS) RECT (HWDERMIS)
((DERMISLOCATION+DERMISTHICKNESS)/2) 'DERMIS.EDGE2'
INTERFACE COATING ABSORB AIR DERMIS
SHIFT Z ((DERMISLOCATION+DERMISTHICKNESS)/2)
REDEFINE COLOR 14
PLANE Y (HWDERMIS) RECT ((DERMISLOCATION+DERMISTHICKNESS)/2)
(HWDERMIS) 'DERMIS.EDGE3'
INTERFACE COATING ABSORB AIR DERMIS
SHIFT Z ((DERMISLOCATION+DERMISTHICKNESS)/2)
REDEFINE COLOR 14
PLANE Y -(HWDERMIS) RECT ((DERMISLOCATION+DERMISTHICKNESS)/2)
(HWDERMIS) 'DERMIS.EDGE4'
INTERFACE COATING ABSORB AIR DERMIS
SHIFT Z ((DERMISLOCATION+DERMISTHICKNESS)/2)
REDEFINE COLOR 14
PLANE Z ((DERMISLOCATION+DERMISTHICKNESS)) RECT (HWDERMIS)
'DERMIS.BACK'
INTERFACE COATING BARE DERMIS AIR
REDEFINE COLOR 14
RETURN

!!TUMOR SLAB GEOMETRY CYLINDRICAL
ENT OBJ
PLANE Z (TUMORLOCATION) ELLIPSE (HWTUMOR) 'TUMOR.SURFACE'
INTERFACE COATING BARE TUMOR DERMIS
REDEFINE COLOR 14
TUBE Z (TUMORLOCATION) (HWTUMOR) (HWTUMOR)
(TUMORTHICKNESS+TUMORLOCATION) (HWTUMOR) (HWTUMOR) 0 0 'TUMOR.RING'
INTERFACE COATING BARE TUMOR DERMIS
REDEFINE COLOR 14
PLANE Z (TUMORLOCATION+TUMORTHICKNESS) ELLIPSE (HWTUMOR) 'TUMOR.BACK'
INTERFACE COATING BARE DERMIS TUMOR
REDEFINE COLOR 14
RETURN

!! SET UP A DETECTOR PLANE TO EVALUATE THE FLUENCE THROUGH THE LAST PLANE
ENT OBJECT
PLANE Z (DERMISTHICKNESS+EPIDERMISTHICKNESS+0.2) ELLIPSE 20 20
'DETECTOR'
INTERFACE 0 0 !!DEFINE INTERFACE TO BE 100% ABSORPTIVE
REDEFINE COLOR 50
RETURN

```

```

!! SET UP ELLIPSOID DETECTOR TO MEASURE ALL THE BACSCATTERED LIGHT LEAVING
!!THE SAMPLE IN -Z
SURFACE; ELLIPSOID 3@20 3@0 -Z
OBJECT 'DETECTOR.REFLECT'; INTERFACE 0 0 AIR AIR

!! VIEW GEOMETRY
WINDOW Y Z
PLOT FACETS 5 5 0
$VIEW

!! DEFINE LIGHT SOURCE
GRID ELLIP Z -3.734 -4@6 2@(NRAYS) RANDOM 1
SOURCE DIRECTION 0 0 1
FLUX TOTAL 1

!!DEFINE VOXEL EVALUATION SYSTEM
!!ZSLICE=22    !! ALREADY DEFINIED EARLIER
VOX_X1=-(HWDERMIS)
VOX_X2=(HWDERMIS)
VOX_Y1=-(HWDERMIS)
VOX_Y2=(HWDERMIS)
VOX_Z1=0
VOX_Z2=(DERMISTHICKNESS+EPIDERMISTHICKNESS)

SLICE_AREA=(VOX_X2-VOX_X1)*(VOX_Y2-VOX_Y1)
SLICE_THICKNESS=(VOX_Z2-VOX_Z1)/ZSLICE

!! ABSORPTION EVALUATIONS
VOXELS ABSORB (VOX_X1) (VOX_X2) (VOX_Y1) (VOX_Y2) (VOX_Z1) (VOX_Z2) 2@200
(ZSLICE)

PLOT FACETS 5 5 0 OVERLAY    !!OVERLAY OVER GEOMETRY PLOT
TRACE
STATS
$COPY 9 VOXEL_ABS.DIS
$VIEW
&VIEW VOXEL_ABS.DIS

!!ANALYSIS
STATS
CONSIDER ONLY DETECTOR.REFLECT    !!ONLY EVALUATE RAYS REACHING REFLECTION
!!DETECTOR
STATS
$GRAB 'TOTAL' 0 2 REFLECTED

CONSIDER ALL    !!ONLY EVALUATE RAYS REACHING !!TRANSMISSION DETECTOR
CONSIDER ONLY DETECTOR
STATS
$GRAB 'TOTAL' 0 2 TRANSMITTED
$REG REFLECTED
$REG TRANSMITTED
$OUTPUT_ANALYSIS A1"

```